EFFECTS OF TRANSPORT PROPERTIES AND FLAME UNSTEADINESS ON NITROGEN OXIDES EMISSIONS FROM LAMINAR HYDROGEN JET DIFFUSION FLAMES

by

DOYOUB PARK

B.S. University of Kyung-Il, 2000

A thesis submitted in partial fulfillment of the requirements
for the degree of Master of Science
in the Department of Mechanical, Materials and Aerospace Engineering
in the College of Engineering and Computer Science
at the University of Central Florida
Orlando, Florida

Summer Term
2005

ABSTRACT

Experimental studies on the coupled effects of transport properties and unsteady fluid dynamics have been conducted on laminar, acoustically forced, hydrogen jet diffusion flames diluted by argon and helium. The primary purpose of this research is to determine how the fuel Lewis number and the flow unsteadiness play a combined role in maximum flame temperature and affect NO_x emission from jet diffusion flame. The fuel Lewis number is varied by increasing/decreasing the mole fraction of diluents in the fuel stream. Therefore, maximum flame temperatures and then NO_x emission levels were expected to differ for Ar- and He-diluted flames.

In an investigation of unsteady flames, two different frequencies (10 and 100 Hz) were applied to observe a behavior of NO_x emission levels and flame lengths by changes of unsteady fluid dynamics and transport properties.

Dedicated to my grandmother, Hakhee Kim, parents, Soonam Park and Sookhwa Suk, two sisters, Sunju and Younju Park, wife, Hayoung Lee and daughter, Serim Park

ACKNOWLEDGMENTS

I have been blessed to be guided by great teachers throughout the completion of my master thesis. I would like to express my deepest heartfelt gratitude to all those who supported me.

Foremost, I take this opportunity to sincerely thank my advisor Dr. Ruey-Hung Chen for his support and cooperation. I am grateful to Dr. Fang Xu and Dr. Marcos Chaos for their support and interest in my academic endeavors as the members of committee.

I especially thank Dr. Marcos Chaos for his continued advice with generosity throughout my years as a student. Working with him has allowed me to be knowledgeable in the field of engineering and his technical assistance was essential to achieve this study. I also thank Dr. Louis Turek for his support regarding LDV experiment.

I express by deep gratitude to my friends and people in my church for their encouragement and love. Finally, I would like to greatly appreciate the love and encouragement that I have received from my family, my wife's family and my wife throughout my academic endeavors that I desire to achieve throughout my lifetime.

TABLE OF CONTENTS

LIST OF FIGURES

LIST OF TABLES

LIST OF NOMENCLATURE

a	Buoyancy Acceleration
A_b	Thermocouple Bead Surface Area
C_p	Specific Heat
D	Mass Diffusivity
D_a	Binary Diffusivity of Air
d_b	Thermocouple Bead Diameter
d_f	Burner Exit Diameter
Da	Damkohler Number
E_A	Activation Energy
$EINO_x$	NO_x Emission Index
EI_{NOx}	NO_x Emission Index
EI_{NO}	Nitric Oxide Emission Index
g	Gravitational Acceleration
h	Convection Heat Transfer Coefficient
k	Thermal Conductivity
LDV	Laser Doppler Velocimetry
Le_f	Fuel Mixture Lewis Number

Le	Lewis Number
L_f	Flame Length
$L_{f,Ar}$	Flame Length of Ar Flame
$L_{f,He}$	Flame Length of He Flame
L_{sp}	Separation Distance
$NO_{x,Ar}$	NO_x Emission Level of Ar flame
$NO_{x,He}$	NO_x Emission Level of He flame
PLIF	Planar Laser-Induced Fluorescence
ppm	Part per Million
Pr	Prnadtl Number
Q_f	Volumetric Flowrate of Fuel Mixture
R	Universal Gas Constant
Re_d	Reynolds Number
S	Stoichiometric Volume Ratio of Air to Fuel and Inert Mixture
T_a	Absolute Flame Temperature
T_{ad}	Adiabatic Flame Temperature
T_f	Maximum Flame Temperature
T_{film}	Gas Film Temperature
T_g	Gas Temperature
T_o	Ambient Temperature
T_{TC}	Thermocouple Temperature
T_∞	Room Temperature

$\bar{u}$	Fuel Jet Mean Velocity
U_f	Fuel Mixture Jet Velocity
U_G	Global Fuel jet Velocity during Sinusoidal Oscillation Cycle
u'	Velocity Fluctuation
u'_{ext}	Velocity Fluctuation for Flame Extinction Limit of He Flame
V	Speaker Voltage
V_{ext}	Speaker Voltage for Flame Extinction Limit of He Flame
[ ]	Concentration of Species

Greek

α	Thermal Diffusivity
ε	Emissivity
μ	Viscosity Coefficient
ν	Kinematic Viscosity
ρ_f	Fuel Mixture Density
τ_f	Flame Residence Time
Φ	Equivalent Ratio
φ	Phase Angle

CHAPTER 1: INTRODUCTION

Nitrogen oxides emissions ($NO_x \equiv NO + NO_2$) from practical combustion systems have been major environmental issues in the recent decade. The principal sources in NO_x (nitrogen oxides) production were automobiles and power generation plants that use hydrocarbon fuels (i.e. coal and oil) (Glassman, 1996). The appearance of many recent conferences on NO_x emission proves that research on this pollutant is of interest due to environmental concerns related to ambient ozone levels, acid rain and depletion of ozone in the stratosphere (Turns, 1995). The Clean Act Amendments of 1990 have enormously contributed to intensive awareness of NO_x control, owing to their programs to accomplish ambient air quality standards for ozone.

The presence of complicated effects of fluid mechanics and kinetics interaction on NO_x formation is a topic of research interest. Although the chemical processes are similar in premixed and non-premixed flames, more attention has been focused on NO_x pollutant formation in non-premixed combustion systems (Turns, 1996). NO_x emissions from fuels that are not of N_2-bound fuels (i.e. ammonia, pyridine and many other amines) are governed by three major chemical formations that are the thermal, or Zeldovich; the prompt, or Fenimore; and the N_2O-intermediate mechanism respectively. In non-premixed (diffusion) combustion of hydrocarbons, the first two mechanisms are

relatively significant and responsible for the majority of NO_x formed. Many experimental studies have examined the combustion of hydrogen (H_2) fuel due to its inherent benefit that it does not contain carbon (C) atoms resulting in bringing less complication of NO_x formation by its dependency only on the thermal (Zeldovich) mechanism. Moreover, due to the need to clearly understand interaction between fluid dynamics and chemistry in turbulent diffusion flames, the H_2 jet diffusion flame provides an important tool for such purposes.

NO_x formation by the Zeldovich mechanism is strongly temperature dependent and is confined only to high temperature regions. It involves the thermal fixation of atmospheric nitrogen by oxygen atoms (O). The thermal NO_x formation rate is:

$$\frac{d[NO]}{dt} = 2 \times 10^4 [O][N_2] \exp\left(\frac{-E_A}{R \cdot T_a}\right) \tag{1}$$

where [ ] denotes concentration of a selected species in moles/cm^3, R is the universal gas constant, E_A is the activation energy and T_a is the absolute temperature (Glassman, 1996). The activation energy, E_A for this thermal mechanism is 76,500 J/mole, approximately twice that of combustion reactions that are typically around 40,000 J/mole for hydrocarbon fuels. Consequently, one may say the NO formation rate is remarkably smaller than combustion (i.e. heat release reaction) rate. This leads to much smaller NO concentration than that of combustion products. Fenimore NO_x formation mechanism is not temperature sensitive and occurs at a time scale typically far smaller than the

combustion reaction time scale. This is why it is also called the "prompt" mechanism.

It was noted that the portion of NO_x formed by the Fenimore mechanism in laminar diffusion flames is usually very small in hydrocarbon combustion except for flames that are under intensified strain rate or unsteadiness in turbulence (Drake *et. al.*, 1991). Fenimore (1971) found that other than the Zoldovich mechanism, the "prompt" mechanism plays a role in producing NO. He also found that the prompt mechanism does not appear in flames of non-hydrocarbon fuels. The general scheme of the Fenimore mechanism is that hydrocarbon radicals react with molecular nitrogen to form amines or cyano compounds. The key steps are as follows:

$$CH + N_2 \rightarrow HCN + N$$

$$C_2 + N_2 \rightarrow 2CN$$

The hydrogen cyanide, HCN, formed in the reaction above finally contributes to produce NO through a multi-step chain sequence (Turns, 1995), and the cyanogen radical, CN, could also yield NO by an attack of oxygen or oxygen atom.

Fuel-dilution has been investigated with various conditions in flow field to examine its effect on NO_x emission. Due to the increase of heat capacity by an increase of dilution levels (20%, 40% and 60% dilution in this study), maximum flame temperatures and also NO_x emission levels are expected to become lower as the dilution level increases. Adding flue gas or inert species (in this study He and Ar) may possibly increase or decrease thermal and mass transport properties of the fuel which could cause

a change in the flame temperature and affected the thermal NO_x production rate. By varying the degree of dilution, Le_f of the fuel can be varied. Lewis number (Le) is defined as the ratio of the thermal diffusivity of the bulk mixture to the mass (i.e. species) diffusivity of the relevant reactant ($Le = \alpha / D$). The effect of fuel Lewis number (Le_f for the fuel-inert mixture) on a flame temperature can be explained in the following manner. For $Le_f < 1$, mass diffusivity is larger than thermal diffusivity. For a steady state one-dimensional case, the mass flux going into the flame zone has to be balanced by the thermal flux flowing out of the flame zone. The flux can be represented by the thermal/mass diffusivity times the temperature/concentration gradient. Therefore, since the thermal diffusivity is lower than the mass diffusivity, the temperature gradient has to increase in order to increase the thermal flux which leads to a higher flame temperature. The opposite also holds true for $Le_f > 1$. In other words, for $Le_f < 1$, the gradient of the temperature is larger than that of the fuel concentration within the flame for the balance between thermal enthalpy flowing out of and the chemical enthalpy (fuel mass) flowing into the reaction zone. Therefore, the maximum temperature (T_f) along the diffusion flame surface exceeds the adiabatic flame temperature (T_{ad}). T_{ad} is the theoretical value of the maximum flame temperature which can be obtained by assuming $Le_f = 1$ and no heat loss of any form. However, for flames with $Le_f > 1$, the contrary holds, and the maximum flame temperature (T_f) is expected to be lower than T_{ad}. The fuel Le_f can be varied by diluting a fuel with different diluents (e.q. He, Ar, CO_2 and N_2) and different levels of dilution. Chen *et. al.* (1997) diluted H_2, CH_4 and C_3H_8 with inert gases He and Ar to vary the Le_f of fuels in their Burke-Schumann flame study.

This experimental study is an extension of previous work done on Burke-Schumann type flames under steady (Chen *et. al.*, 1997) and unsteady conditions (Chaos, 2003). Although Le_f has been understood as an important factor on Burke-Schumann type flames (Law and Chung, 1982; Chung and Law, 1984; Chen *et. al.*, 1997; Chaos, 2003), its role on turbulent jet flames (Gabriel *et. al.,* 2000) was found to be not as pronounced as it was on laminar Burke-Schumann type flame. Perhaps inherent unsteadiness of the turbulent mixing on the flame causes the diminished Le_f effect. Therefore, a study regarding flame unsteadiness and vortex-interaction is of great importance for understanding the effect of fuel Le_f on NO_x emission from perturbed Burke-Schumann (laminar) diffusion flames.

In this study, laminar H_2 flame diluted by He or Ar are investigated systematically. The flames were acoustically forced at two frequencies (i.e. 10 and 100 Hz) and amplitudes by using a speaker. Three major fuel dilution levels (i.e. 20%, 40% and 60%) were adopted in order to vary the thermal and mass transport properties of the fuel mixture in order to observe the coupled the effect of Le_f along with flame unsteadiness.

CHAPTER 2: LITERATURE REVIEW

In general, combustion has been categorized in two regimes: premixed and non-premixed combustion. Non-premixed flames are frequently called diffusion flames. The discussion below is mainly limited to these types of flames since they are relevant to the experimental work presented herein.

2.1 Diffusion Flame Theory

Diffusion flames were investigated theoretically and experimentally by Burke and Schumann (1928). The coflow diffusion flame studied by Burke and Schumann is shown in Figure 2.1 below. They made the following assumptions which laid foundations for early studies of diffusion flames:

A. The velocity of the gas and air up the tube in the region of the flame is constant.
B. The coefficient of interdiffusion of the fuel and oxidizer streams is constant.
C. The interdiffusion is entirely radial (i.e. axial diffusion is neglected).
D. Mixing of the fuel and oxidizer streams occurs by diffusion only.

E. The coaxial gradient is smaller than the radial gradient.

F. Lewis number is unity.

G. Fuel and oxidizer react in stoichiometric proportions at the flame. Chemical kinetics are assumed to be infinitely fast, resulting in the flame being represented as an infinitesimally thin sheet. (Flame-Sheet approximation)

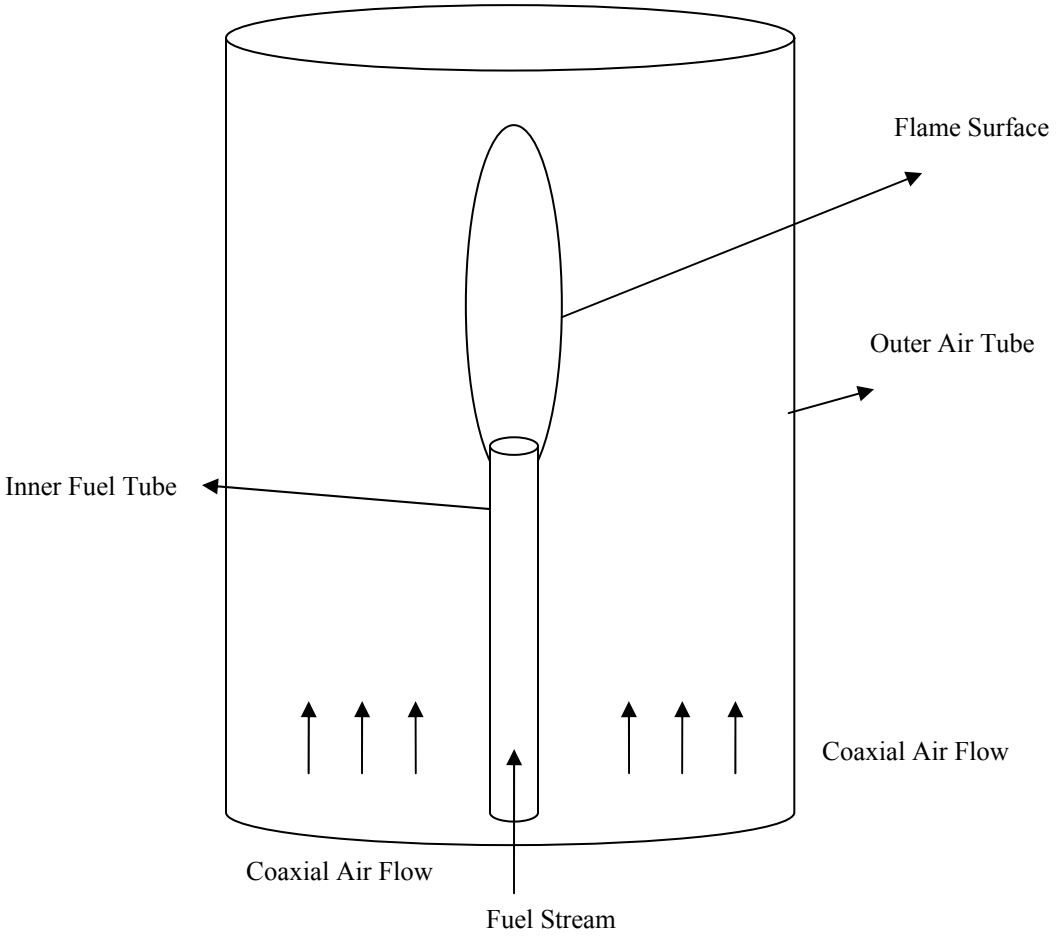

Figure 2.1: Schematic of Burke-Schumann flame.

Owing to the fundamental significance of the study above, some of their experimental findings will be reviewed here. In Equation (3) of Burke and Schumann (1928), they inferred that the flame length (L_f) would not be affected by the size of burner tube if velocities of fuel and air were kept constant. Applying variation of pressure did not show any effect on the flame height if all other factors (i.e. velocity, dimensions of burner, diffusion coefficient, concentration of fuel, oxidizer, etc.) are kept constant (Burke and Schumann, 1928).

2.2 Nitrogen Oxides Emission

A review on NO_x formation and emission from atmospheric pressure turbulent diffusion flames is available in the literature (Turns, 1995) and mainly describes the issue of NO_x emission index scaling with respect to physical quantities such as the nozzle exit diameter (d_f), initial jet velocity (U_f), fuel types, Damkohler number and Reynolds number. The relevant parameters also presented in this review are NO formations-chemical pathways, O-atom concentration, temperatures, flame strain and radiation loss.

To this author's knowledge, Chen *et. al.* (1997) were the first investigators to systemically document the effect of dilution on NO_x emissions from laminar jet diffusion flames of H_2, CH_4 and C_3H_8. They quantified the NO_x emission levels along with varying degree of dilution of He and Ar from 20% up to 60%. They used He and Ar as diluents since these two diluents have identical volumetric heat capacities along with different

mass diffusivities, and these might be expected to provide prominent comparison and contrast in terms of flame temperatures affected by Le_f. As mentioned in Chapter 1, the effect of Le_f was significant to vary a maximum flame temperature in their study. Their result of H_2 mixtures (i.e. with He or Ar in the fuel stream) exhibits that increasing dilution level from 20% to 60% considerably increases the maximum flame temperatures from 2,160K to 2,410K (by about 250K) for the H_2-Ar flame and slightly decreases from 2,293K to 2,243K (by about 50K) for the H_2-He flame. With this finding, it may be concluded that the dilution effect perhaps is suppressed and dominated by the effect of Le_f whose corresponding values were 1.324 to 0.679 for the H_2-Ar flame and 0.962 to 1.013 for the H_2-He flame as dilution level increases from 20% to 60%. In their study, it can be noted that regardless of the type of fuels (such as hydrocarbon or non-hydorcarbon), flames with the same degree of dilution of He or Ar, that produce lower Le_f yield higher flame maximum temperatures and higher NO_x emission levels.

Chen and Driscoll (1990) quantified the effects of coaxial air and other mixing parameters (viz. coaxial air, Reynolds number and Damkohler number that is defined as the ratio of flow mixing time to chemical reaction time) on NO emission levels for turbulent jet diffusion flames such as H_2-air and CH_4-air. This study revealed that the forcing coaxial air into the flame reduced NO_x emission index up to six times more than without coaxial air substituted. Likewise, adding swirl into the flame exhibited an analogous trend to adding coaxial air. The reason is that it significantly reduces the L_f (i.e. the decrease of a reaction zone volume in a H_2-air flame) and also the local residence time for NO_x formation by adding coaxial air. Contrary to the result of the H_2-air flame, it

was found that the addition of coaxial air had almost negligible effect on the EINOX (see Equation (2) below) levels of the CH_4-air flame. They suggested the two possible factors for the reason why the CH_4-air flame did not scale as well as the H_2-air did by the equation (see Equation (2)). One is that almost 70% of the overall NO_x is from "prompt" mechanism (and which did not depend on thermal NO_x formation. The other factor is that flame strain may have affected the CH_4-air flame more intensively due to the greater chemical reaction rate of the flame:

$$EINOX = \frac{c \cdot L_f^{\,3}}{\rho_f \cdot U_f \cdot d_f^{\,2}} \tag{2}$$

where c is a constant proportional to $d(NO)/dt$, d_f is a burner exit diameter and ρ_f is a fuel density.

As an extension study of the previous work of Chen and Driscoll (1990), Driscoll *et. al.* (1992) experimentally studied the effects of residence time (denoted by L_f/U_f) and Damkohler number (defined as the ratio of species mixing time to chemical reaction time) on NO_x emission index for H_2, CH_4 and C_3H_8 flames respectively. They found that as the concentration of He increased in order to decrease the Damkohler number, the measured NO_x emission index exceeded that of the equilibrium theory up to a factor of 24. In the case of a propane flame, it was noted that the larger Reynolds number provided less residence time (L_f/U_f) for soot formation and the flame color which turned from yellow into blue. Therefore, this decreased radiant loss fraction rates and increased the

flame temperature and NO_x. In other words, although addition of coaxial air with high Reynolds number evidently reduced the L_f resulting less NO_x formed, there was compensation of counterpart that the increased flame temperature by reduction of radiant heat loss fraction with less soot formation.

Gabriel *et. al.* (2000) continued the investigation of the early work of Chen and Driscoll (1990) and Driscoll *et. al.* (1992). They quantitatively defined the effects of transport properties and non-dimensionalized parameters (viz. Lewis and Damkohler number) on the NO_x emission index of H_2-diluents (i.e. He and Ar) turbulent jet diffusion flame which eliminated complexity of the radiative cooling, prompt NO_x formation and buoyancy effects. It was noted that the effect of Le_f on turbulent diffusion flame was less pronounced than that on the Burke-Schumann flame of Chen *et. al.* (1997). As the dilution level of the H_2-Ar flame increased, the measured NO_x levels and the flame temperatures increased for the B-S flame whereas the opposite was true for the turbulent jet diffusion flame (Gabriel *et. al.*, 2000). It was also determined that with the increase of the level of dilution, the Ar-diluted H_2 flames surpassed the He-diluted H_2 flames in producing higher NO_x emission index. This is probably owing to the fact that as the degree of dilutions increases, Le_f, for the He-diluted flames remains around unity (i.e. 0.962 to 1.013) whereas that of the Ar-diluted flames changes its value from greater than unity to smaller than unity (i.e. from 1.324 to 0.679).

Samaniego *et. al.* (1998) studied nitric oxide formation in Ar-diluted natural gas-oxygen (instead of air) diffusion flame and investigated experimentally with Ar or He dilution to vary the adiabatic flame temperature from 2,100 to 3,000K. Although it

apparently seems that there will not be any NO_x formed from combustion of natural gas and oxygen, it is noted that natural gas contains N_2 (from 1 to 10%) and commercially available oxygen also contains traces amount of N_2 (from 0 to 5%). It was verified that above the Ar dilution level of approximately 50% NO levels varied gradually with dilution whereas the dilution level is below 50%, NO increases drastically with decreasing dilution. This is due to the transition of NO formation mechanism within the flame from prompt and N_2O-path NO at high dilution (low adiabatic flame temperature) to thermal NO at low dilution (high adiabatic flame temperature). They found that peak temperature and peak NO mole fraction diminish with increasing dilution and strain rate with radiative losses. It was concluded that at low flame temperature, NO is mostly generated by the prompt and nitrous oxide (N_2O) mechanisms while at high flame temperature, NO is primarily governed by the Zeldovich (viz. thermal) mechanism.

One recent experimental study on CH_4 laminar diffusion and counterflow flames, (Feese and Turns, 1998) was performed by substituting N_2 inert either on fuel-side or air-side of the flame. The experimental result observed indicated that the substitution of N_2 on the fuel-side contributed to somewhat higher NO_x formation and that on the air-side. This may be conjectured from the fact that N_2 dilution on the fuel-side rather than the air-side presumably influences the thermal and transport properties of the mixture (CH_4-N_2) rendering its Le_f lower and resulting in a higher temperature and NO_x emissions.

Rørtveit *et. al.* (2002) scrutinized effects on NO_x formation of laminar H_2 counterflow flame with N_2, He and CO_2 dilution experimentally and numerically. The experimental and computational results of temperatures and NO concentrations (i.e.

measured and calculated) showed good agreement in the lower temperature regime (where T_f below about 1,900K). However, as the flame temperature increases, the calculated value of the NO concentration was up to twice as high as the measured one. It was found that CO_2 lowered the flame temperature more than the others. This is because CO_2 contains the highest heat capacity among the three diluents. In addition, adding water and increasing strain rate lowered the NO concentration noticeably.

Although not analogous to the type of burner studied in this research, Nishioka *et. al.* (1994) addressed numerical research of NO emission characteristics of CH_4-air Bunsen-type burner with the geometry of counterflow flame. They selected the hydrocarbon flame with the burner since it is known that the flame on such burner is the double flame. The double flame has a structure which is a bright inner cone where the rich premixed hydrocarbon-air flame produces CO and H_2 as the main intermediate products and an outer portion surrounding the cone where the diffusion flame of intermediate products burns with surrounding air. It was shown that the C_2 chemistry adopted for kinetics calculation was appropriate to describe reactions in the flame due to the almost perfectly accurate reproduction of the calculations for experimentally observed the double flame structure. In the analysis of one dimensional premixed Bunsen flame, as the equivalent ratio Φ increased and reached larger than 1.2, it was found that the role of the Fenimore mechanism became more important than the Zeldovich mechanism and keeps dominant source of NO production. On the other hand, for counterflow of rich-premixed flame with air, it is interesting that when Φ exceeds the value 2.9 (fuel rich case), the Fenimore mechanism became dominant over thermal mechanism for NO_x

formation. For the injection velocity (denoted by u) between 5 to 15 cm/s with the experimental condition that the separation distance, L_{sp}, between the nozzles was fixed, they reported several observations. One is that at 5 cm/s, the thermal mechanism produces more NO than the Fenimore mechanism. However, at 15 cm/s, NO production by the Fenimore mechanism begins exceeding that by the thermal mechanism. Nishioka *et. al.* (1994) concluded that the total emission index of NO of double flame is rather insensitive to the equivalence ratio, Φ. It was also concluded that as the injection velocity increases from 5 to 180 cm/s, thermal NO formation decreased rapidly while the Fenimore NO formation increases first and then decreases gradually in terms of a slope of the plots.

To the author's knowledge, an early attempt by Takeno and Nishioka (1993) to evaluate NO_x emission index for counterflow turbulent diffusion flames after defining universal quantities such as the mass fraction rate per unit flame surface area or L_f first introduced the integral equation for the NO emission index (EI_{NO}). The emission index is defined as the rates of the mass production rate of NO per unit flame surface area to the fuel mass injection rate per unit flame surface area. They also quantitatively demonstrated that the calculated numerical values EI_{NOx} are of the same order of magnitude as those observed in turbulent jet diffusion flames by Driscoll *et. al.* (1992)

Li and Williams (1999) studied CH_4-air two-staged counterflow combustion to help understand how the manner reduces emissions of NO_x from gas turbines. The structure of two-staged counterflow flame is that first premixed CH_4-air from the nozzle of the fuel side partially burns (first stage) and then the mixture reacts with air from the

nozzle of the oxidizer side (second stage). They utilized partially premixed fuel with Φ varying from 1.5 to 3.0 and substituted diluents in air (oxidizer) stream with water, CO_2 and N_2. They employed CH_4 since it is the simplest chemical structure in the hydrocarbon fuels and it can provide a certain starting point to research other hydrocarbon fuels. Also, methane is the principal component of natural gas which is getting attention as a main gas-turbine fuel and as one of the fuels in dual-duel diesel engines. They reported that as for an effect of dilution, the water as a diluent on the reducing NO emission index was the most effective agent, and the second most effective one was CO_2 agreeing with the results of Rørtveit *et. al.* (2002). On the other hand, N_2 and Ar were somewhat less effective in reducing NO emission than water and CO_2. In order to determine the effectiveness of agents in reducing the flame temperature, they investigated the change in the thermal enthalpy per unit mass of the agent between the air stream temperature and the flame temperature. Upon this change of enthalpy, it is noted that the thermal effect of water is the largest while those of CO_2 and N_2 are about 50% of water (as the enthalpy change of water between 300K to 2,000K is defined as 100%) and that of Ar is only about 20% of that of water. In addition, they also found that adding CO_2 is almost twice as effective as N_2 in reducing NO_x probably due to the additional possible chemical effect of CO_2 on reducing prompt NO_x. Furthermore, Li and Williams (1999) experimentally revealed that the addition of water or CO_2 is even more effective in reducing NO_x when Φ is large. This may be due to the fact that if water vapor is added in the oxidizer stream to increase the concentration of water in flame zone, it would reduce the NO_x emission by removing some CH radicals which reacts with N_2 to form HCN and then NO.

It is also of interest to understand NO_2 formation. The NO_2 can be formed two different routes such as combustion-formed and probe-formed. NO_2 can form during sampling hot combustion gas. The mechanism of probe-formed NO_2 has been found to be due to oxidation NO of by HO_2 radicals during the rapid cooling process. Hori (1986) experimentally studied the mechanism of nitrogen dioxide (NO_2) formation in a combustion system of two different flow fields. The flow fields were propane-fueled laboratory swirl burner and a simplified flow field consisting of double concentric jets which simulated the mixing region of hot combustion gas with coflowing cold air. It was proved that in the double concentric jets burner, the amount of NO_2 formed increased with increasing cooling rate of the combustion gas and initial combustion gas temperature, and also the ratio of NO_2/NO_x increased with decreasing initial NO concentration.

2.3 Lewis Number Effect

Early work on Lewis number on laminar diffusion flames includes that of Law and Chung (1982) and Chung and Law (1984). They analytically studied the effect of the Lewis number on flame structure and temperature for a variety of flow configurations (one-dimensional counterflow flames and jet diffusion flames) assuming no flame radiation. In their study, it was found that if the Lewis number, $Le > 1$, the system tended to reduce the flame temperature from its adiabatic value. The opposite holds for $Le < 1$. For $Le > 1$, thermal diffusivity is lager than mass diffusivity resulting in a smaller

temperature gradient than mass gradient and therefore, the lower flame temperature is expected than the case of $Le < 1$. In conclusion, Lewis number is an important factor affecting flame temperature, extinction and NO_x formation (Law and Chung, 1982).

2.4 Unsteady/Vortex-Interacted Flame

Lewis *et. al.* (1988) experimentally studied the structure of a diffusion flame imbedded in an unsteady vortical flow by employing a laminar co-flowing jet diffusion flame. It was found that on the centerline at the base of the flame, higher strain rate was observed on the centerline of the flame base than elsewhere in the OH image by planar laser-induced fluorescence measurement. They demonstrated the evolution of the flame in the unsteady flow field (i.e. periodic vertical motion induced by acoustic excitation of fuel stream) and local extinction of the flame. They concluded that relatively high local strain rates generated by the vortical motion led to the flame extinction.

Im *et. al.* (1999) numerically investigated effects of unsteady strain rate on chemical response of methane-air counterflow diffusion flames. They reported that the maximum CO concentration was insensitive to the variation in the scalar dissipation rate which is characteristic flow time scale (see Equation (7) in Im *et. al.*, 1999), and the emission indices for NO_x exhibited a monotonic decay with an increase in impulse frequency. For the scalar dissipation rates due to the relatively short residence time (~100 s^{-1}) and low temperature (less than 1,900K), they found that the Zeldovich and N_2O paths

represented only a few percent of the total NO production. Consequently, the NO considered in their study was mainly prompt NO. In conclusion, in the matter of sensitive response of NO_x formation, they suggested that a low-frequency velocity fluctuation is preferred as to pollutant control.

Santoro *et. al.* (2002) explored the recent study NO formation in methane diffusion flame affected by employing vortex-interaction on flow field. Their experimental data indicated that the peak flame temperature and CO and CO_2 mass fractions are not strongly dependent on the vortex-interaction while the peak NO mass fraction in the CH_4 flames is higher than the steady case by a factor of 2. From their experimental study, it should be noted that the peak mass fraction of thermal NO is strongly related to the timescale of unsteady interaction; however, that of prompt NO tended to be nearly independent. Their conclusion described the fact that during the vortex interaction, the peak mass fraction of prompt NO_x was found to depend only on scalar dissipation rate for both of the states with steady or vortex-perturbed. However, the peak mass fraction of thermal NO_x was affected by CO, CO_2 and peak temperature inclusive of the scalar dissipation rate.

Chaos (2003) studied the effect of transport properties with the interaction of fluid dynamics and combustion in acoustically forced laminar hydrogen jet diffusion flames. This experiment is one of the few studies that presents quantitative OH planar laser-induced fluorescence measurements in laminar jet diffusion flames. He conducted the experiment using PLIF technique to measure two-dimensional OH and temperature fields which revealed significant roles of transport property (i.e. fuel Le_f) and unsteadiness (i.e.

curvature). His research concerned the NO_x level (ppm) from the unsteady H_2-He and H_2-Ar flames by coupling the levels and two-dimensional temperature data by PLIF since NO_x formation rate of any flames have a strong dependence on flame temperatures. The temperature data of H_2-He and H_2-Ar unsteady flames showed that regardless of Le_f, unsteady H_2-He flames always produced higher maximum temperatures than that of H_2-Ar diluted flames. This result was different from the trends observed in the steady state H_2-He and H_2-Ar flames conducted during his research. He reported that depending on the Le_f of the fuel mixture, the stretch and compression imposed on the flame by the speaker pulsation affect the flame temperature differently. In the study, although Le_f effects were present in the low and the high frequency flames (10 and 100Hz), the effect was more prominent in the high frequency flames (Chaos, 2003). A flame temperature of unsteady flames with $Le_f \geq 1$ increased when compressed (i.e. reaction zone thickness increases) and decreased when stretched (i.e. reaction zone thickness decreases). On the other hand, a flame temperature of the flames with $Le_f < 1$ decreased when compressed and increased when stretched.

CHAPTER 3: EXPERIMENTAL SETUP

This research work studied laminar flames interacting with unsteady fluid dynamics generated by a loudspeaker. This was done to study the effect turbulence has on flames since turbulent diffusion flames are encountered in most of the practical devices currently operated.

A laminar diffusion flame was generated by H_2 diluted with He or Ar exiting from a straight vertical circular steel tube surrounded by coflowing air. The levels of dilution and the values of Le_f studied for the fuel mixtures are tabulated in Table 3.1. The value of Le_f and the degree of dilutions are similar to those in Chen *et. al.* (1997). The Le_f used in this study is calculated from transport properties from Dandy (2003). As mentioned, by varying the degree and the type of dilution, the value of Le_f is varied. The values of adiabatic flame temperature T_{ad} are also listed in Table 3.1. These adiabatic flame temperatures were calculated using CHEMKIN (Kee *et. al.*, 2000).

Table 3.1: Fuel Lewis number and adiabatic temperature for H_2-He and H_2-Ar flame

Degree of Dilution*	Fuel Lewis Numbers, Le_f		T_{ad} (K) with He dilution**	T_{ad} (K) with Ar dilution**
	H_2-He	H_2-Ar		
20%	0.998	1.389	2323	2223
40%	1.012	1.012	2226	2226
60%	1.035	0.718	2041	2041

*Degree of dilution by volume
** Adiabatic flame temperature calculated by CHEMKIN (Kee *et. al.*, 2000)
Every Lewis number is calculated by a website (http://navier.engr.colostate.edu/tools/diffus.html, Dandy, 2003)

3.1 Diffusion Flame Burner Setup and Peripheral Apparatus for Pulsation

The burner used in this research is shown in Figure 3.1. The inside and outside diameters of the stainless steel fuel tube are 4.6 and 6.5 mm, respectively. The inside diameter of the transparent plexiglass air tube is 88.5 mm. The ratio of the inside diameters of the fuel tube and the air tubes is 0.077. The mean velocities of the fuel and the air streams were always kept 30 cm/s (for all the experiments described here). This gives a Reynolds number, based on the inside diameter of the fuel tube (4.6 mm), of less than 70 (i.e. ranging from 12 for the 60% He-diluted flame to 62 for the 60% Ar-diluted flame). Solid glass beads (Fisher Scientific, 1 mm in diameter) and stainless steel screens were utilized to ensure uniform air velocities in the coflowing air stream. The plexiglass

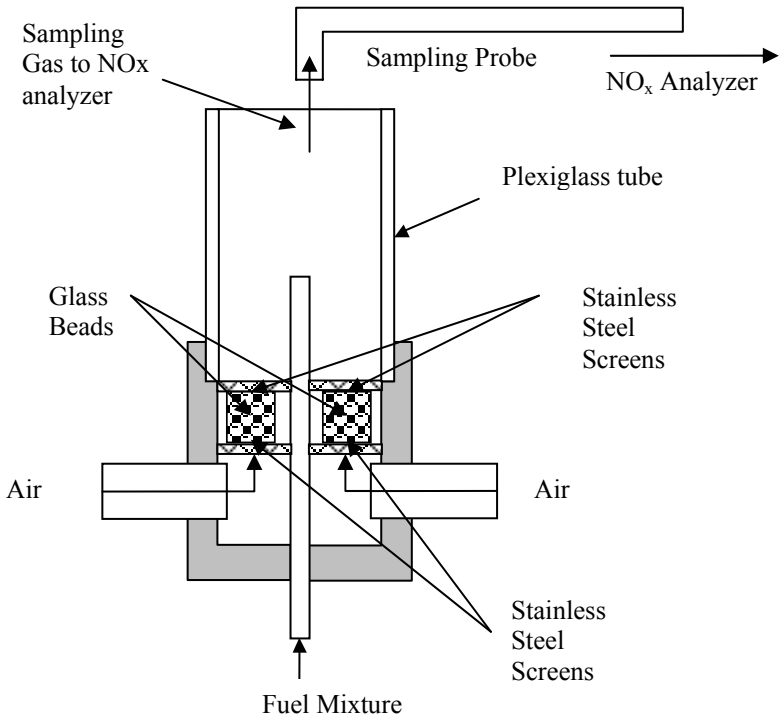

Figure 3.1: Laminar coflowing diffusion flame burner.

air tube was used to ensure to produce a Burke-Schumann flame and to protect combustion products (i.e. NO_x) from possible interference of any room air entrainment and to allow optical access.

A quartz probe, 3.82 mm in the inlet diameter, (see Figure 3.2) was employed for the NO_x products sampling instead of the water-cooled stainless steel probe previously used (Chen *et. al.,* 1997). The temperature of the quartz probe was monitored during the course of the experiments and found to remain below 80^{o}C, a temperature sufficiently

low to avoid undesirable formation of NO_x at the tip of probe. The probe to sample combustion product was positioned at least two maximum flame lengths downstream from the jet exit for all fuel-inert mixtures as discussed by Drake *et. al.* (1987). This was

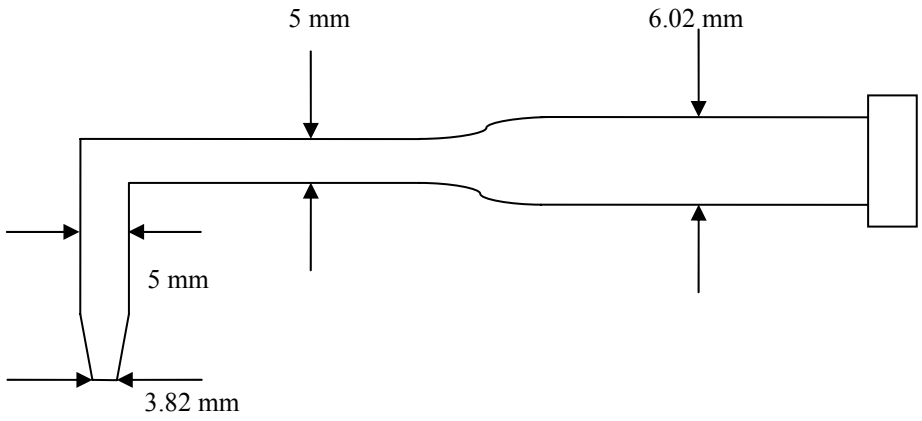

Figure 3.2: Schematic of sampling quartz probe.

done due to the fact that the NO_x concentration along the radial direction was found to be uniform. Drake *et al*. (1987) also discuss that the use of quartz as opposed to stainless steel does not lead to any difference in the NO_x data obtained since probe reactions (including NO to NO_2 conversion) are negligible. The sampling probe was located at the exit of the plexiglass air tube along the centerline directly above the fuel jet for all data runs. In Figure 3.3, a water trap (Schrader Bellows, BB4) was mounted on the sampling tube after the probe to ensure the sample read by the NO_x analyzer was dry as NO_2 is

known to be soluble in water. The sampled combustion gasses were passed to a chemiluminescence NO_x analyzer (Thermo-Environmental Model 42-H) which measured the concentration of NO directly.

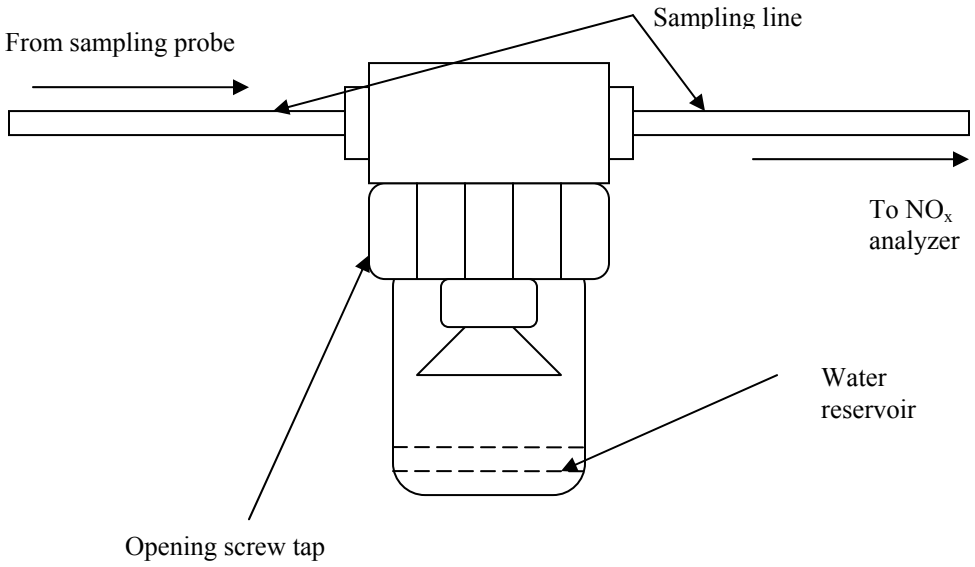

Figure 3.3: Schematic of water trap

The method of measuring NO and NO_2 is that the sampled NO is drawn into the NO_x analyzer, and after it reaches the reaction chamber, it mixes with ozone which is generated by internal ozonator. This reaction produces a characteristic luminescence with intensity proportional to the concentration of NO. To measure the NO_x ($NO + NO_2$) concentration, NO_2 must be transformed to NO prior to reaching the reaction chamber by a stainless steel converter heated to approximately 625 °C. Finally, the converted

molecules along with the original NO molecules react with ozone again, and then total NO_x can be obtained.

The NO_x analyzer was calibrated prior to each experimental run with standard NO and NO_2calibration gasses with concentration of 87.1 (± 0.9%) and 71.0 (± 3%) ppm, respectively. The schematic of the laminar flame burner apparatus along with the data collection peripherals used is presented in Figure 3.4. The tube which supplied the fuel-inert mixture was passed through a plexiglas plenum to which a 50 watt, 203.2 mm diameter polypropylene woofer speaker (Radio Shack, Cat. Model No. 40-1024A) was attached with a frequency response from 35 Hz up to 3000 Hz. In Figure 3.4, it is described that the speaker was lined with a 40 A latex rubber sheet (Durometer) 0.203 mm thickness to generate artificial unsteady flow by momentum transferred from the speaker through the latex sheet.

The dimensions of plenum cavity were 263.5 x 263.5 x 5.56 mm. The sinusoidal wave was generated by a synthesized function generator (Stanford Research Systems (SRS) DS335 3.1 MHz). The signal was amplified using a power amplifier (Optimus MPA-125 100 watt) furnished a double amplification (i.e. twice of the amplitude made by the function generator) of the original voltage of the sinusoidal signal generated by the function generator.

To control and measure flowrates of fuel and air, MKS mass flow controllers were employed with accuracy of ± 1% of full scale and repeatability ± 0.2% of their full scale. Also, for the control of diluents, Omega FMA 1700 & 1800 mass flowmeters were operated with accuracies ± 1.5% of full scale.

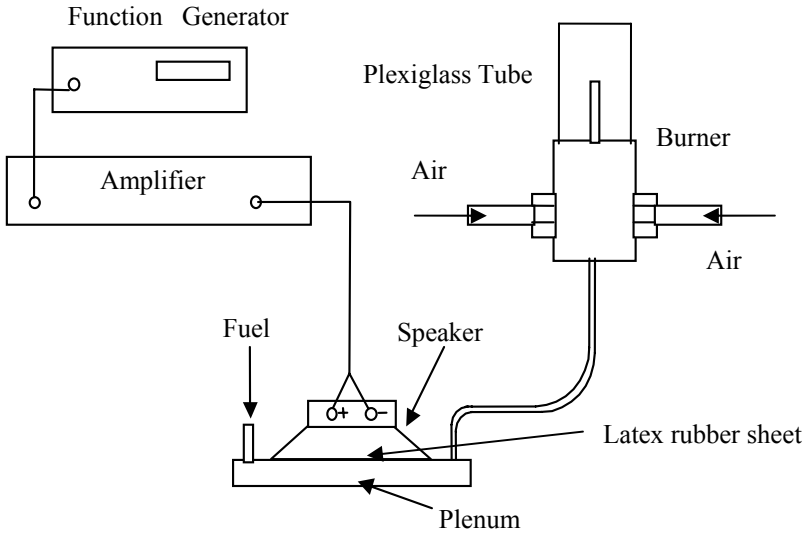

Figure 3.4: Apparatus of laminar flame burner with peripheral.

Since the velocities of air and fuel were kept equal (i.e. 30 cm/s) to avoid any shear instabilities and flame flicker, it should be noted that the only flame strain induced in flames were due to the vortices generated in the fuel stream by the loudspeaker (Chaos, 2003). Flowrates supplied to the burner for each specific dilution level are tabulated in Table 3.2, and the experimental values of the speaker voltages (i.e. the maximum peak to peak voltages) for extinction limit of pulsed flames are shown in Table 3.3. The values of voltages at flame extinction limit were measured by increasing the amplitude of sinusoidal wave until a flame extinguished. The same range of voltages applied to each dilution level of He- and Ar-diluted flames to compare trend of NO_x formation trend. The extinction limit of maximum measurement voltages was always based upon that from He-

diluted flame since it always extinguished at the lower voltage than that of Ar-diluted flame for all the degree of dilutions as also reported in Chaos (2003).

Table 3.2: Laminar flame burner flowrates

Dilution Level	H_2 (cm^3/min)	Diluents (cm^3/min)	Air Coflow (L/min)
20%	239	60	50.6
40%	179	120	50.6
60%	120	179	50.6

The mean velocity at fuel tube port is 30 cm/s

Table 3.3: Imposed voltages for flame extinction of H_2-Ar and H_2-He unsteady flames measured at the speaker

Frequency (Hz)	H_2-He diluted flame			H_2-Ar diluted flame		
	20%	40%	60%	20%	40%	60%
	Voltage for Flame Extinction Limit V_{ext} (volt)			Voltage for Flame Extinction Limit V_{ext} (volt)		
10	0.8	0.7	0.6	2.2	3.4	3.8
100	32	28	28	---	---	---

3.2 Thermocouple Temperature Measurement

Temperatures were measured with a fine wire R-type (Pt – Pt/13 % Rh) thermocouple with a bead diameter size of 76.2 μm (0.003 in), approximately. Radial temperature profiles of He- and Ar-diluted H_2 steady flames were obtained every 2 mm above the burner in order to compare with previous work and fully characterize these baseline flames so that the effects of Le_f as well as dilution on flame temperature could be obtained. The thermocouple was mounted on a computer controlled traversing table. Radial temperature profiles were taken with a thermocouple traversing speed rate of 263 μm/sec and readings were performed from 1 mm to 15 mm above the burner. Measurements were obtained over a radial length of 12.65 mm. Thermocouple voltages were read by a computer-based data-acquisition multimeter (Hewlett Packard Model 34401 A). The voltage-measuring multimeter was controlled with the help of LabView, a software package from National Instruments. LabView is a graphical user interface that can be used to create "virtual" instruments to acquire, analyze and display data. Thermocouple data was taken at 5Hz, therefore, for each radial run, a total number of 240 data points were sampled (i.e. 263 μm/sec = 3.799 sec/mm multiplied by 5Hz = 19 samples per mm).

Uncorrected TC temperature data was corrected for radiation losses following the procedures of Bradley and Matthews (1968). Values of emissivity, ε, for the R-type thermocouple employed in this study were based upon the early work Glawe and Shepard (1954) and are tabulated in Table 3.4 and Table 3.5. Thermodynamic gas properties used

for radiation correction of a measured flame temperature were those of the stoichiometric combustion products and were calculated using software located on a website (Dandy, 2003) which is based upon the CHEMKIN database (Kee *et. al*., 2000). These values of the thermodynamic properties are tabulated in Table 3.4 and Table 3.5 for the He and Ar dilution cases, respectively. In addition, the thermodynamic properties of the unburned fuel mixtures are listed in Table 3.6. Combustion products in Table 3.4 and Table 3.5 for 20% to 60% dilution levels are as follows:

A. Chemical reaction of 20% dilution case

$$2\left(H_2+\frac{20}{80}Diluent\right)+\left(O_2+\frac{79}{21}N_2\right)\rightarrow 2H_2O+\frac{79}{21}N_2+\frac{40}{80}Diluent$$

B. Chemical reaction of 40% dilution case

$$2\left(H_2+\frac{40}{60}Diluent\right)+\left(O_2+\frac{79}{21}N_2\right)\rightarrow 2H_2O+\frac{79}{21}N_2+\frac{80}{60}Diluent$$

C. Chemical reaction of 60% dilution case

$$2\left(H_2+\frac{60}{40}Diluent\right)+\left(O_2+\frac{79}{21}N_2\right)\rightarrow 2H_2O+\frac{79}{21}N_2+\frac{120}{40}Diluent$$

Table 3.4: Thermodynamic properties of combustion product* (H_2-He diluted flame)

T (K)	ρ (kg/m^3)	v (m^2/s)	K (W/m K)	C_p (J/kg K)	Emissivity
20% dilution					
1400	0.19936	2.59850E-04	0.13145	1619.8	0.18991
1600	0.17444	3.26930E-04	0.14804	1663.0	0.20410
1800	0.15506	3.99959E-04	0.16402	1699.3	0.21828
2000	0.13955	4.78649E-04	0.17939	1729.7	0.23247
2200	0.12687	5.62760E-04	0.19419	1755.1	0.26085
40% dilution					
1400	0.18004	2.91687E-04	0.14760	1701.0	0.18991
1600	0.15753	3.66830E-04	0.16535	1743.3	0.20410
1800	0.14003	4.48640E-04	0.18246	1778.7	0.21828
2000	0.12603	5.36800E-04	0.19892	1808.4	0.23247
2200	0.11457	6.31050E-04	0.21479	1833.2	0.26085
60% dilution					
1400	0.15242	3.51439E-04	0.17507	1852.8	0.18991
1600	0.13337	4.41700E-04	0.19484	1893.3	0.20410
1800	0.11855	5.39950E-04	0.21387	1927.2	0.21828
2000	0.10669	6.45830E-04	0.23221	1955.6	0.23247
2200	0.09699	7.59030E-04	0.24992	1979.3	0.26085

Every thermodynamic property is calculated by a website (http://navier.engr.colostate.edu/tools/diffus.html, Dandy, 2003)

*Refer the chemical reaction formula above

Table 3.5: Thermodynamic properties of combustion product* (H_2-Ar diluted flame)

T (K)	P (kg/m^3)	v (m^2/s)	k (W/m K)	C_p (J/kg K)	Emissivity
20% dilution					
1400	0.22435	2.36350E-04	0.11501	1439.4	0.18991
1600	0.19630	2.97150E-04	0.12986	1477.8	0.20410
1800	0.17449	3.63290E-04	0.14415	1510.1	0.21828
2000	0.15704	4.34540E-04	0.15790	1537.1	0.23247
2200	0.14277	5.10670E-04	0.17112	1559.6	0.26085
40% dilution					
1400	0.23884	2.31400E-04	0.10727	1282.2	0.18991
1600	0.20898	2.90570E-04	0.12083	1314.1	0.20410
1800	0.18576	3.54890E-04	0.13387	1340.8	0.21828
2000	0.16719	4.24130E-04	0.14641	1363.2	0.23247
2200	0.15199	4.98100E-04	0.15847	1381.9	0.26085
60% dilution					
1400	0.25955	2.24660E-04	0.09650	1088.1	0.18991
1600	0.22711	2.81650E-04	0.10827	1111.8	0.20410
1800	0.20187	3.43540E-04	0.11958	1131.7	0.21828
2000	0.18169	4.10120E-04	0.13045	1148.4	0.23247
2200	0.16517	4.81190E-04	0.14090	1162.3	0.26085

Every thermodynamic property is calculated by a website (http://navier.engr.colostate.edu/tools/diffus.html, Dandy, 2003)
*Refer the chemical reaction formula above

Table 3.6: Thermodynamic properties of unburned H_2-He and H_2-Ar diluted mixture

Dilution Level	ρ (kg/m^3)	v (m^2/s)	k (W/m K)	C_p (J/kg K)	α (cm^2/s)	D (cm^2/s)
H_2-He diluted mixture						
20%	0.098689	1.1239 E-04	0.17704	11293	1.5884	1.59
40%	0.11494	1.1511 E-04	0.16882	9121.6	1.6103	1.59
60%	0.13119	1.1719 E-04	0.16175	7487.8	1.6467	1.59
H_2-Ar diluted mixture						
20%	0.39268	4.5574 E-05	0.12766	2838.3	1.1454	0.82
40%	0.70292	2.9842 E-05	0.087497	1491.5	0.83456	0.82
60%	1.0132	2.1975 E-05	0.058128	969.53	0.59176	0.82

Every thermodynamic property is calculated by a website (http://navier.engr.colostate.edu/tools/diffus.html, Dandy, 2003)
Temperature and pressure were 298K (room temperature) and 1 atm

A radiation correction to the thermocouple temperature can be obtained by assuming a steady state heat balance between the radiant and convective heat transfer modes:

$$h \cdot A_b (T_g - T_{TC}) = \sigma \cdot \varepsilon \cdot A_b ({T_{TC}}^4 - {T_\infty}^4) \qquad (3)$$

Rearranging this:

$$T_g = \frac{\sigma \cdot \varepsilon}{h}\left(T_{TC}{}^4 - T_\infty{}^4\right) + T_{TC} \tag{4}$$

where A_b is a bead surface area, T_g is a gas temperature, T_{TC} is a thermocouple temperature, T_∞ is a room temperature, ε is emissivity, σ is Stefan-Boltzmann constant, and h is a heat transfer coefficient. To find T_g, it is necessary to know a relationship of h and Nusselt number which is defined as:

$$Nu_d = \frac{h \cdot d_b}{k} \tag{5}$$

where d_b is a thermocouple bead diameter and k is thermal conductivity. With this relationship, the Nusselt number as function of Reynolds and Prandtl number can be obtained from an equation developed by Churchill and Bernstein (1977). The equation they recommended is for cross-flow to a wire:

$$Nu_d = 0.42 \cdot \mathrm{Pr}^{0.2} + 0.57 \cdot \mathrm{Pr}^{\frac{1}{3}} \cdot \mathrm{Re}_d{}^{\frac{1}{2}} \tag{6}$$

where Pr is Prandtl number ($=\mu C_p/k$) and Re_d is Reynolds number ($=d_b U_f/v$) where μ is the gas viscosity coefficient, C_p is the gas specific heat, U_f is the gas jet velocity, d_b is a bead diameter, v is kinematic viscosity.

All gas properties require to be evaluated at the film temperature T_{film}:

$$T_{film} = \frac{T_g + T_{TC}}{2} \tag{7}$$

Gas properties of the stoichiometric combustion products were used. The density, kinematic viscosity, thermal conductivity and heat capacity of this mixture were calculated over a temperature range of 1,400K to 2,200K using software located on a website (Dandy, 2003).

Since the heat balance equation expresses the gas temperature T_g, in terms of the convective heat transfer coefficient *h* (which is dependent on the gas properties) which are again dependent on T_g, iteration procedure was required to calculate the radiation corrected gas temperature. This correction procedure was performed in an Excel spreadsheet using the equations above. An initial guessed gas temperature was introduced to calculate the film temperature T_{film} where all gas properties were evaluated. The guessed gas temperature was substituted repetitively until the guessed gas temperature and the calculated gas temperature with all the properties become converged.

3.3 Experimental Uncertainty

Although attention in every experimental process has been taken to avoid possible errors and undesirable results, there was an uncertainty discovered throughout the NO_x

sampling. The NO_x emission levels (i.e. ppm) obtained from the NO_x chemiluminescence analyzer using two different water vapor removing methods (i.e. Schrader Bellows BB4 water trap and Fisher Scientific silica gel desiccant reagent S684 10) showed considerable difference in the NO_2 reading. It was concluded that using the desiccant leads to considerable trapping and dissociation of NO_2 by the water and heat accumulated in the desiccant leading to lower NO_2 readings. Several experiments were carried out using both water trap and desiccant as well as experiments without any water trapping device. The water trap was shown to produce the best and most reliable readings and all data reported herein uses this method

The experimental uncertainty of the thermocouple temperature measurement is ± 21K. It is evaluated that the tolerance lies within ± 1% of the range of the maximum temperature, approximately 2100K, which the thermocouple can measure up to.

CHAPTER 4: RESULTS AND DISCUSSION

In this chapter, the results from NO_x emission, a visual flame length, L_f, and flame temperatures are presented for both steady and unsteady flames. The data will be supported by previous measurements performed on the burner used in this study (Chaos, 2003). An attempt of some comparisons to correlate with previous studies was made and its results will be discussed.

4.1 Flame Lengths of Steady State H_2-Ar and H_2-He Flames

Visual flame lengths are plotted in Figure 4.1. The L_f increases relatively monotonically and proportionally to increase of U_f, jet exit velocity. The present results in this study qualitatively agree with those of Chen *et. al.* (1997). In Figure 4.1, it is shown that as dilution level increases (regardless of diluents), the L_f decreases. Therefore, the size of reaction zone decreases since the air flowrate remains unchanged for the diluted flames. For the relatively low velocities (i.e. from 2 cm/s to 8 cm/s), however, it is noted that streamwise (axial) diffusion is important, and it is also defined that Burke-Schumann assumptions may be no longer valid (Chen *et al*., 1997). This regime (i.e. velocities less that 10 cm/s) is outside the scope of this study.

As predicted in Roper (1997) and Roper *et. al.* (1977), it was found that the flame

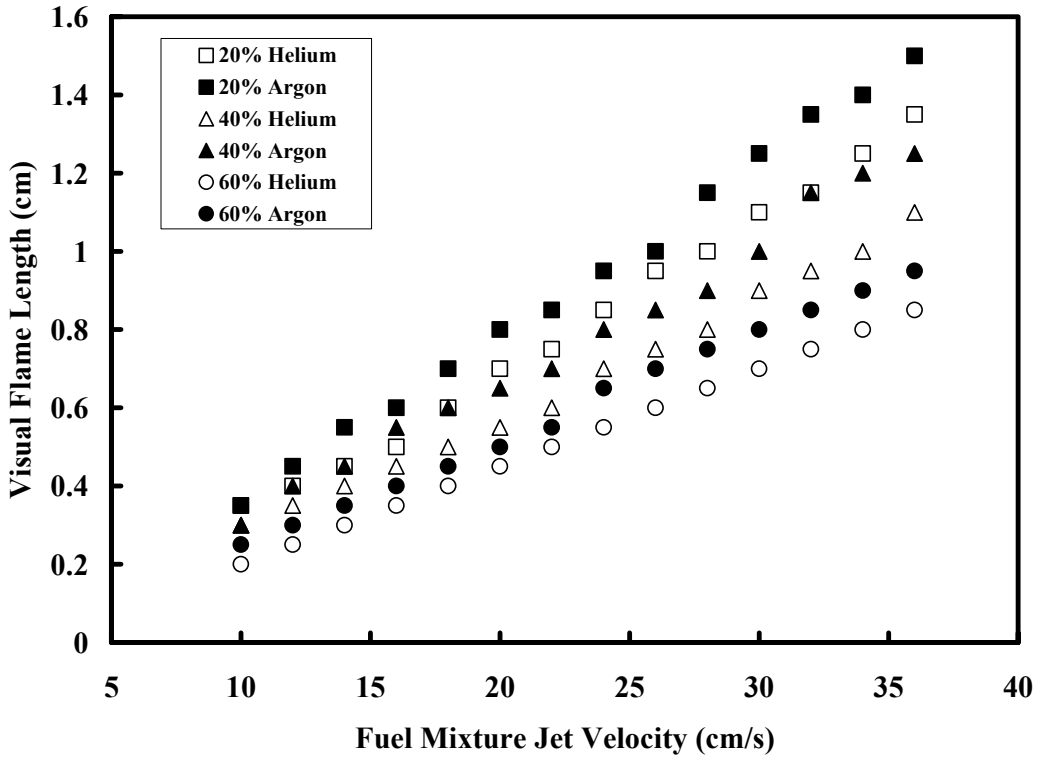

Figure 4.1: Flame lengths vs fuel jet velocity of H_2-Ar and -He diluted flames at various dilution levels.

Length, L_f, of laminar diffusion flames increased as the volumetric flowrate, Q_f, increased. In the case of circular burner port, it was observed that L_f is independent of either the flame is buoyancy or momentum-dominated. The theoretical Equation (8) indicates how Q_f affects L_f by Roper *et. al.* (1997), and the flame lengths based upon the equation were also obtained in Chen *et. al.* (1997):

$$L_f = \frac{Q_f}{4 \cdot \pi \cdot D_o}\left[\ln\left(1+\frac{1}{S}\right)^{-1}\right] \cdot \left(\frac{T_o}{T_f}\right)^{0.67} \tag{8}$$

where S is the stoichiometric volume ratio of air to fuel and inert

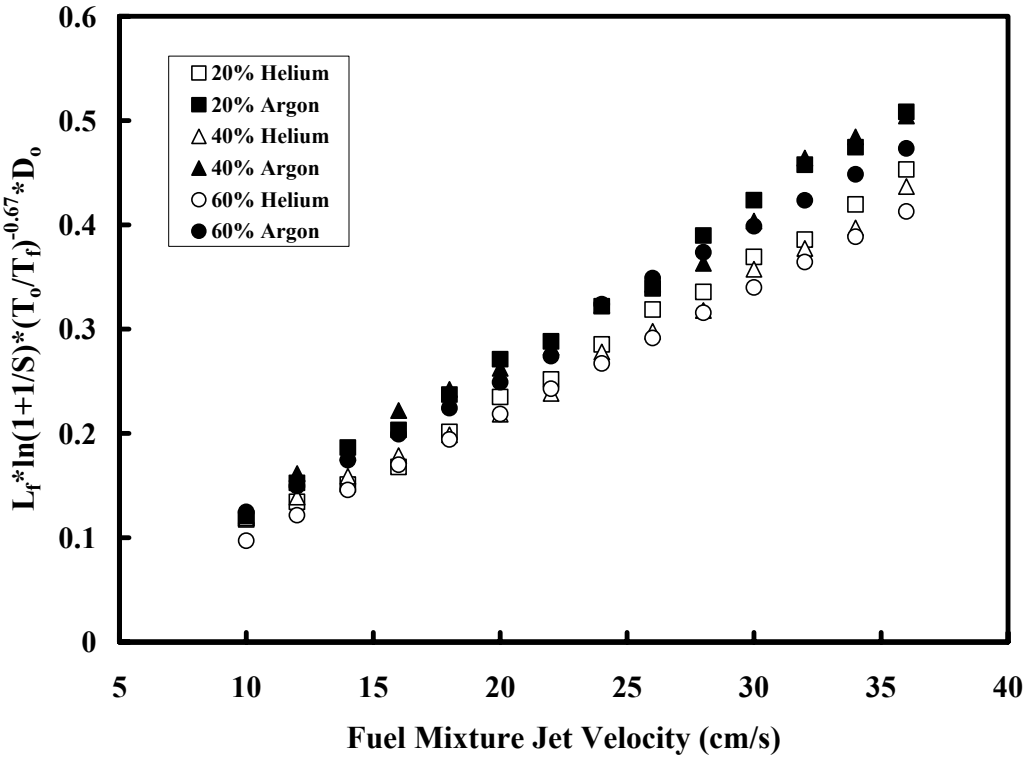

Figure 4.2: Scaling relationship of flame length of H_2-Ar and -He diluted flames based upon Roper *et. al.* (1977).

mixture, Q_f is volumetric flowrate of fuel mixture, D_o is binary mass diffusivity of air, T_f

is maximum flame temperature and T_o is a ambient temperature. The results regarding L_f scaling relationship in this study are plotted in Figure 4.2. As seen in Figure 4.2, the plot demonstrates that the slopes are nearly constant. This is mainly due to the reason that Roper and his coworkers assumed that diffusivity is constant throughout the regions of the flame.

4.2 Flame Temperatures of Steady State H_2-Ar and H_2-He Flames

The primary reason that He and Ar as diluting gases were utilized in this study is that they both have the same volumetric heat capacities which lead to identical adiabatic flame temperatures as calculated and shown in Table 3.1. In addition, Helium is an attractive species to use as a diluent since it has relatively high thermal conductivity (k, W/m K) (see Table 3.6 for how thermal conductivities of H_2-He and H_2-Ar mixture are). By means of temperature measurement for 20% He- and Ar-diluted flames, it was revealed that Le_f effect on this study is less pronounced than it was in the studies (Chen *et. al.*, 1997; Chaos, 2003) since the flame temperature for the H_2-Ar diluted flame was expected to be lower than that of the H_2-He diluted flame as observed in those studies and, yet the H_2-Ar diluted flame was higher than that of the H_2-He diluted flame. This is contrary to the data of Chen *et. al.* (1997) and Chaos (2003).

It was also noted that the effects of Le_f are only observed in the 40% and 60% Ar- and He-diluted flames and shows qualitatively match with Chaos (2003) with a fuel mean

velocity of 30 cm/s. The thermocouple data of the flame temperatures for the 40% and 60% Ar- and He-diluted flames from Chaos (2003) were tabulated in Table 4.1 with those in the present study. The maximum temperatures of the He- and Ar-diluted flames were 2,077K vs 2,155K for 40% dilution and 1,904K vs 1,844K for the 60% dilution from Chaos (2003). However, those for the present study were 1,986K vs

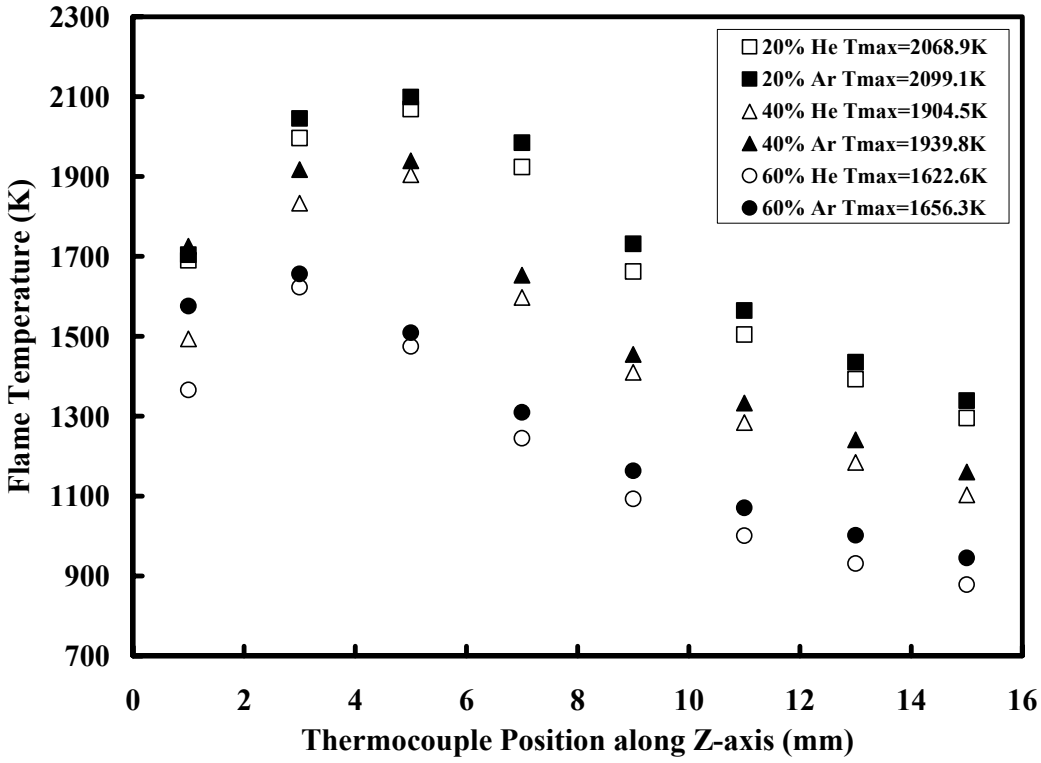

Figure 4.3: Radiation-corrected temperature of H_2-Ar and -He diluted flames for fuel mean velocity 18 cm/s.

2,034K for the 40% dilution and 1,708K vs 1,774K for the 60% dilution. The difference

of the maximum flame temperatures differ by 78K vs 48K for the 40% dilution and 60K vs 66K for the 60% dilution in Chaos (2003) and the present study, respectively. The results for the temperature measurement for 18 and 30 cm/s in this study are showed a qualitative agreement in the matter of propensity of temperature behavior, and they are drawn in Figures 4.3 and 4.4. The radial temperature profile of thermocouple

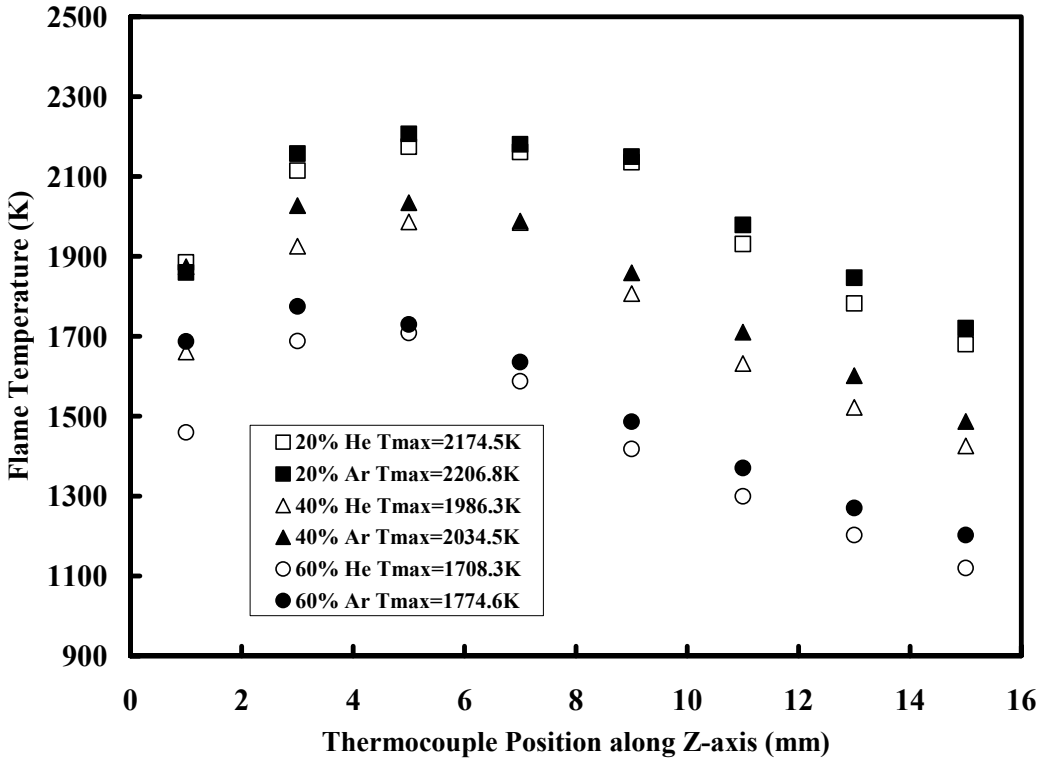

Figure 4.4: Radiation-corrected temperature of H_2-Ar and -He diluted flames for fuel mean velocity 30 cm/s.

Table 4.1: Summary and comparison of previous and present studies with radiation corrected temperatures

Diluent	H_2-He diluted flame			H_2-Ar diluted flame		
Dilution Level	20%	40%	60%	20%	40%	60%
Le_f[(a)]	0.998	1.012	1.035	1.389	1.012	0.718
T_{ad}[(b)] (K)	2323	2226	2041	2323	2226	2041
Maximum Flame Temperature T_f, (K)						
Chen *et. al.* (1997)	2293	2251	2243	2160	2281	2410
Gabriel *et. al.* (2000)	2228	2007	1842	2189	2022	1968
Chaos (2003)	2300	2077	1844	2251	2155	1904
Chaos (2003)[(c)]	2276	2080	1880	2267	2139	1969
Kothawala (2003)	----	1946	1718	----	1977	1835
This Study	2174	1986	1708	2206	2034	1774

(a) Fuel mixture Lewis number calculated from a website (http://navier.engr.colostate.edu/tools/diffus.html, Dandy, 2003)
(b) An adiabatic flame temperature, Tad, calculated using CHEMKIN (Kee *et. al.,* 1999)
(c) Temperature data based upon PLIF measurement (Planar Laser-Induced Fluorescence) while the rest based upon thermocouple measurement

Table 4.2: Maximum radiation-corrected temperatures based upon radial temperature profiles along positions of z-axis for 18 cm/s fuel jet velocity in the steady state

	H_2-He diluted flame			H_2-Ar diluted flame		
	20%	40%	60%	20%	40%	60%
Position along Z	Maximum Flame Temperature T_f, (K)					
1 mm	1690.2	1493.9	1365.5	1704	1725.4	1575.5
3 mm	1996.5	1833.3	1622.6	2045.5	1917.1	1656.3
5 mm	2068.9	1904.5	1474.2	2099.1	1939.8	1509
7 mm	1923.9	1597.5	1244.5	1984.5	1653	1309.4
9 mm	1662	1409.8	1092.8	1731.7	1454.9	1163
11 mm	1504.4	1284	1000.8	1564.5	1332.9	1070.4
13 mm	1392.3	1184.5	930.9	1435	1240.8	1001.9
15 mm	1295.4	1102.7	878.1	1338.7	1160.2	944.8

Table 4.3: Maximum radiation-corrected temperatures based upon radial temperature profiles along positions of z-axis for 30 cm/s fuel jet velocity in the steady state

	H_2-He diluted flame			H_2-Ar diluted flame		
	20%	40%	60%	20%	40%	60%
Position along Z	Maximum Flame Temperature T_f, (K)					
1 mm	1885.2	1660.9	1459.2	1859.6	1874.4	1687.1
3 mm	2114.6	1925.3	1687.9	2157.1	2027.3	1774.6
5 mm	2174.5	1986.3	1708.3	2206.8	2034.5	1729.5
7 mm	2161.4	1984.8	1587.6	2180.5	1988.3	1635.4
9 mm	2135.4	1806.9	1417.8	2149.6	1859.3	1486.3
11 mm	1931.3	1631.8	1299.2	1978.5	1710.6	1370.4
13 mm	1782	1522.3	1202.2	1846.4	1601.5	1270.2
15 mm	1680.1	1425.5	1119.7	1720.4	1486.5	1202

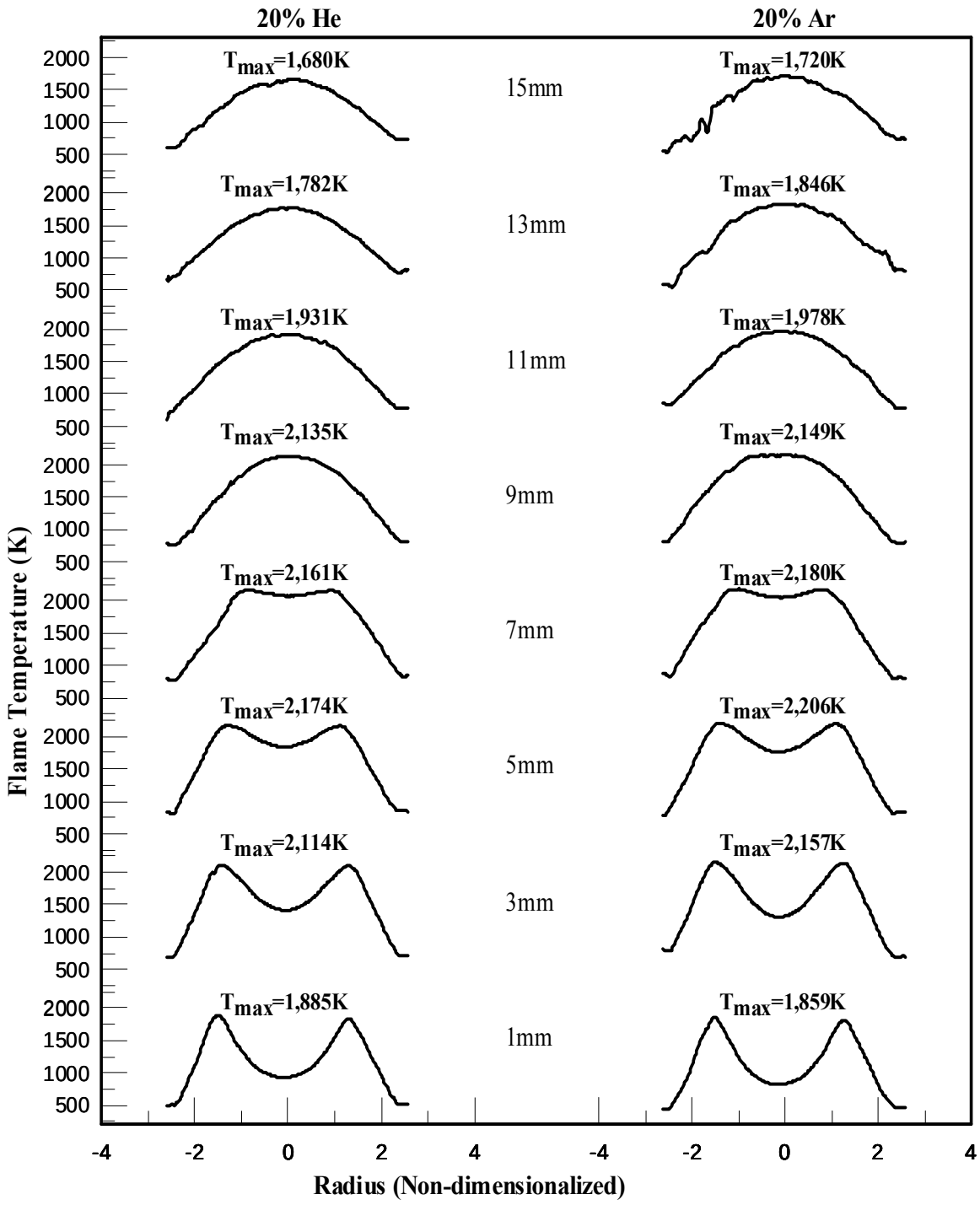

Figure 4.5: Radiation-corrected radial temperature profiles for 20% H_2-Ar and -He diluted flames.

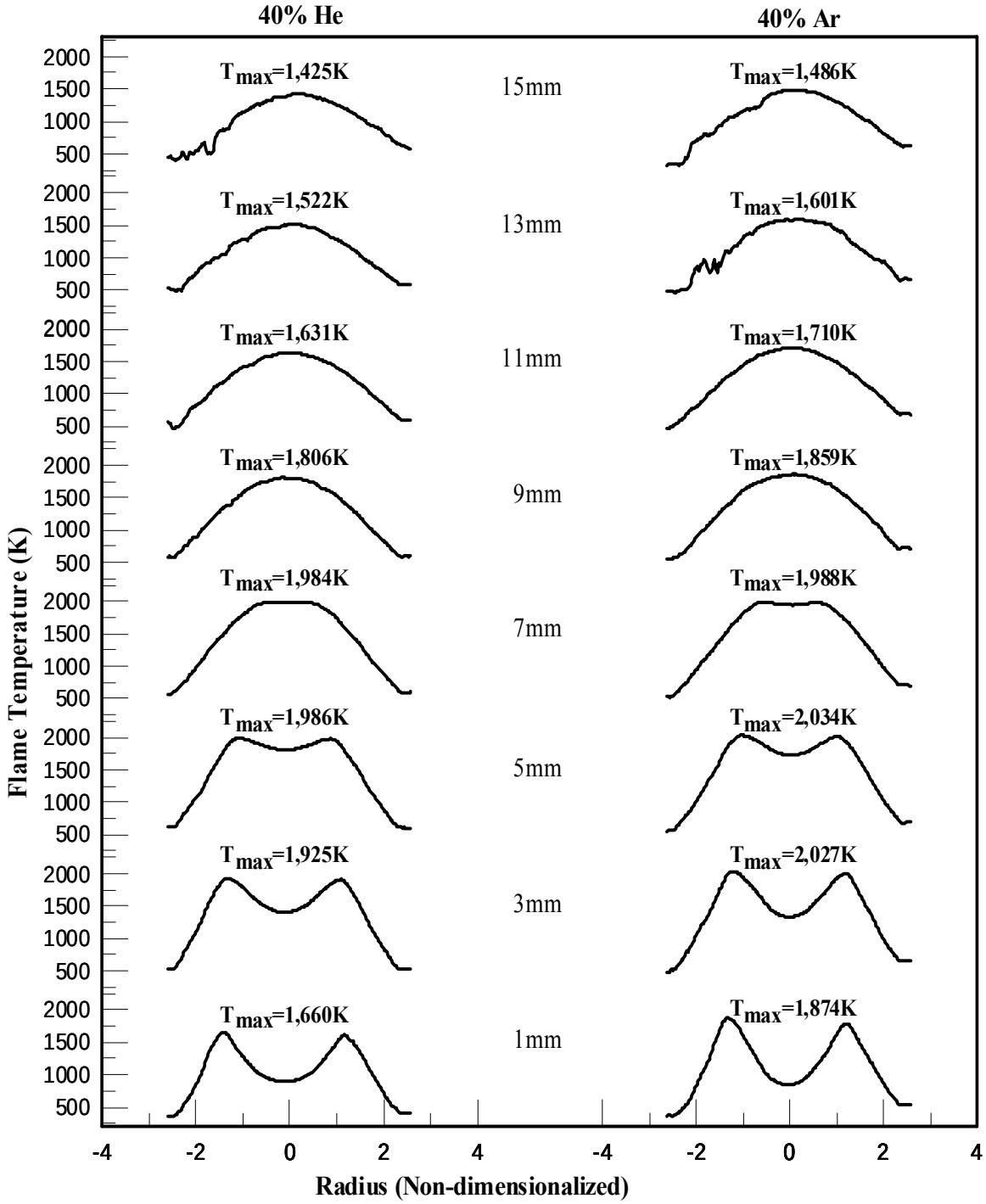

Figure 4.6: Radiation-corrected radial temperature profiles for 40% H_2-Ar and -He diluted flames.

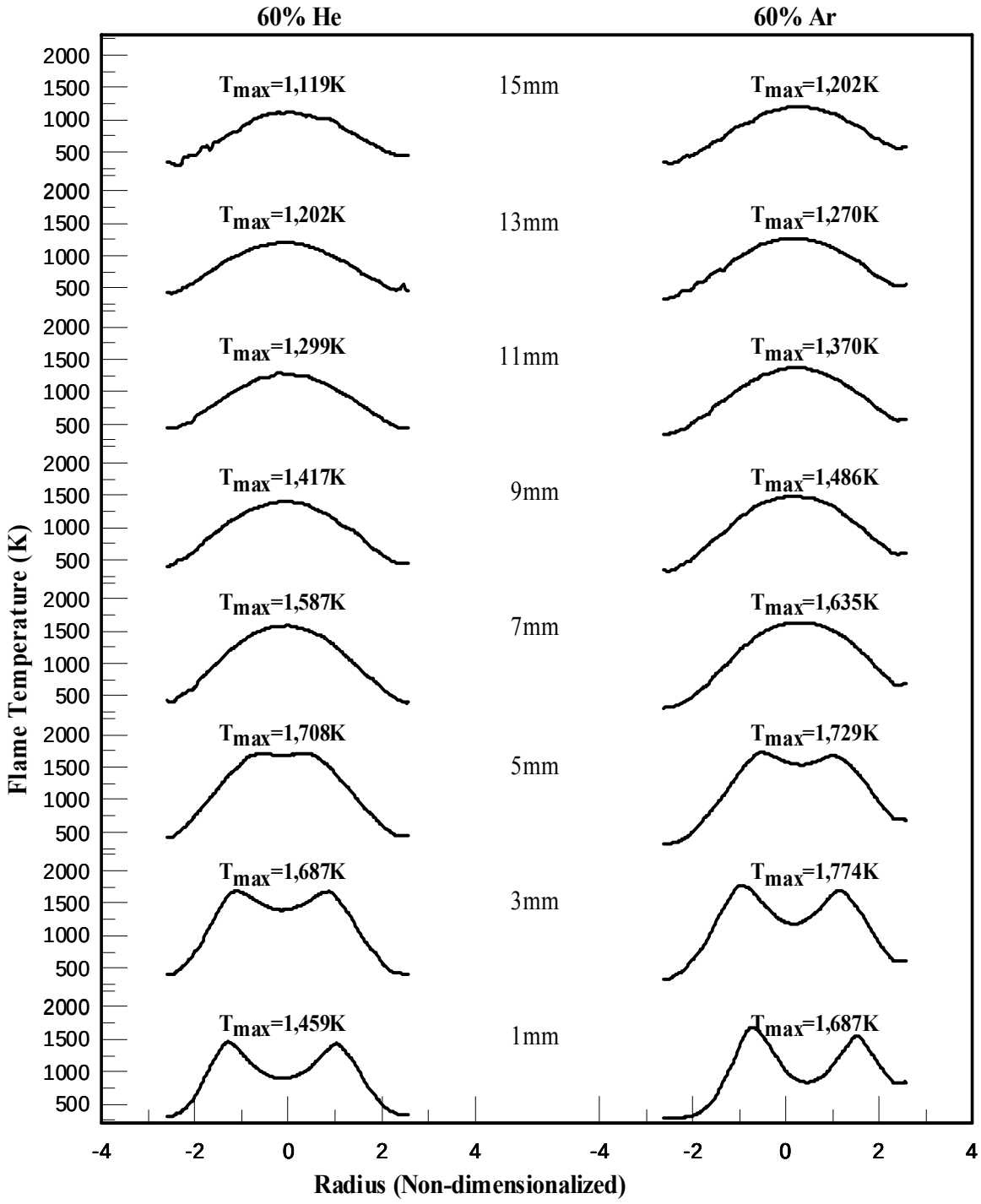

Figure 4.7: Radiation-corrected radial temperature profiles for 60% H_2-Ar and -He diluted flames.

measurement is presented for 20%, 40% and 60% dilutions in Figures 4.5, 4.6 and 4.7, and the maximum temperatures on each position along the z-axis for 18 cm/s are tabulated in Table 4.2, and those for 30 cm/s are in Table 4.3. In Table 4.2 and Table 4.3, the maximum flame temperature of radial temperature profile always occurs at the position, approximate 5 mm above of burner port except the case of the 60% Ar-diluted flame at jet velocity 30 cm/s and the 60% dilution of Ar- and He-diluted flames at 18 cm/s (see Table 4.2 and Table 4.3). After that point, all of the temperature along the z-axis decreased monotonically as thermocouple approached downstream to the flame tip. For all the dilution cases, it was expected that the flame temperature of both diluents would be identical or at least similar since their specific heats are equal (20.8 J/mol K). However, it was experimentally observed that the maximum temperatures in the 40% He- and Ar-diluted flames were 1,986K and 2,034K, respectively. This temperature difference may be attributable to the Le_f effect since the heat capacity of the two diluents is identical (Chaos, 2003). Nevertheless, the temperature difference of the 40% dilution case in his study was 78K (Ar-diluted flame was higher) and however, the difference in this study was 48K. As can be seen in Table 4.1, all the radiation-corrected temperature data of the studies presented in the table for the 40% dilution vary by about 1.33%(15K) to 3.75%(78K) for the all the 40% cases among the studies. Consequently, it is noted that the temperatures measured for the 40% dilutions in this study qualitatively agree to the temperatures in the other studies in Table 4.1 (i.e. the temperature of 40% Ar-diluted flame is always higher than He-diluted flame). The pertinent explanation which may be suggested regarding the temperature deviation between the 40% Ar- and He-diluted

flames with $Le_f \approx 1$ (i.e. as mentioned above) is that heat and mass diffuse simultaneously with almost identical rate of diffusivity if gradients of heat and mass are the same. It was found that in the steady case, the 40% He-diluted flame had a wider temperature profile than the 40% Ar-diluted flame by OH profile image of Chaos (2003). Thus, thermal gradient of Ar-diluted flame is relatively smaller than that of He-diluted flame (Chaos, 2003). An additional supporting idea to substantiate the aforementioned statement is that

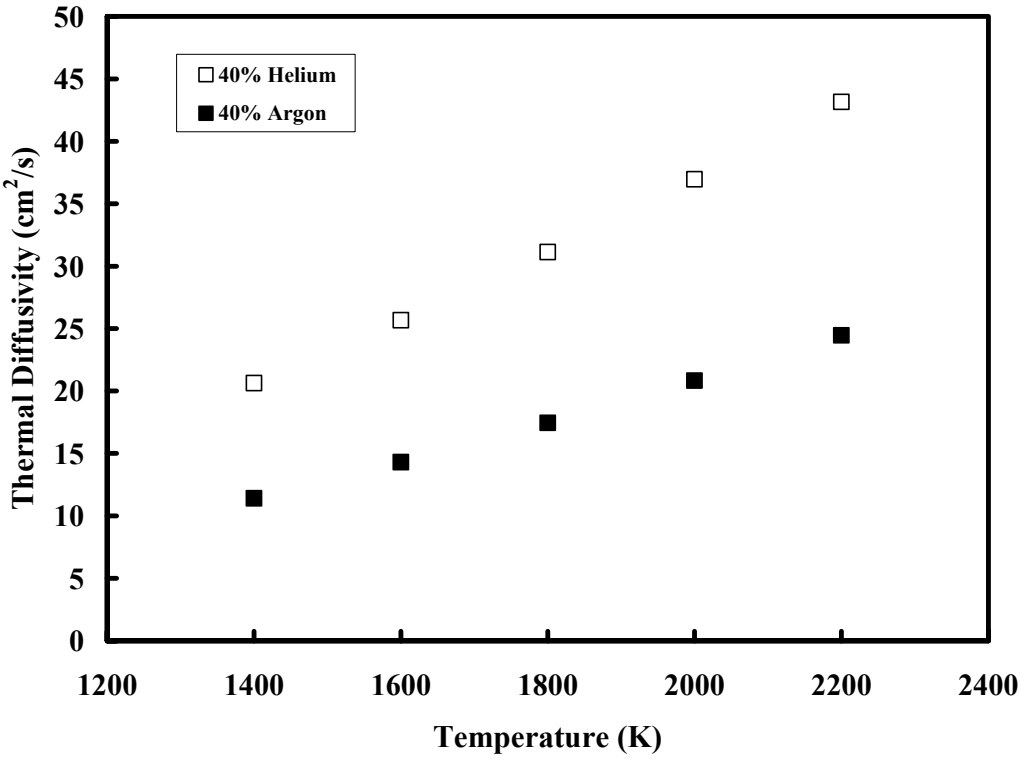

Figure 4.8: Thermal diffusivity of 40% H_2-Ar and -He diluted mixtures with a range of temperature.

thermal diffusivity, α, of the 40% Ar-diluted flame is always lower than that of the 40% He flame within a range of temperature, shown in Figure 4.8. If it is assumed that the heat flux leaving the flame is the same for the 40% H_2-Ar and H_2-He flames, then it is obvious that the maximum flame temperature of the 40% Ar-diluted flame is higher than that of the 40% He-diluted flame to compensate for the smaller gradient as well as the smaller thermal diffusivity (Chaos, 2003).

In the case of Samaniego *et. al.* (1998), counter-flow of methane with 47.5% Ar- and He-diluted flames (Le_f number 1.006 for the Ar-diluted flame and 0.806 for the He-diluted flame) in a mole fraction showed that peak temperature of He was lower on the order of 300K. This could be attributable to major difference in thermal diffusivity, α, (0.176 cm^2/s for Ar and 1.55 cm^2/s for He evaluated at 273K) as suggested in their study, although Le_f for the 47.5% Ar-diluted flame is higher than that of the 47.5% He-diluted flame, it is expected to reduce the flame peak temperature. The difference is almost a factor of 9 which possibly promotes cooling of flame temperature. As for a difference in kinematic viscosity, ν, Samaniego *et. al.* (1998) also implied that a potential role of the difference may also affect local flame property.

In the cases of the 60% He- and Ar-diluted flames from Table 4.1 similar to the case of the 40% diluted flames, the trend of the flame temperatures can be determined that a higher value of Le_f yields a lower maximum flame temperature and the opposite holds. This trend corresponds to the effects of Le_f number for the 60% He- and Ar-diluted flames, and this trend is in qualitative agreement over all the studies presented in Table 4.1. However, the temperature results of the 60% He- and Ar-diluted flames from Chen *et.*

al. (1997) and this study are not consistent for the temperature measurements of both 18 and 30 cm/s (i.e. fuel mixture mean velocity). It is noted that as the degree of dilution increases from 20% to 60%, the maximum temperatures corresponding to each case of dilution always declines (Chaos, 2003; Gabriel *et. al.*, 2000; Kothawala, 2003 in Table 4.1). For the 60% Ar- and He-diluted flames, the difference of the maximum flame temperatures for all the studies vary from the minimum value (1,904K - 1,844K = 60K) by Chaos (2003) to the maximum value (2,410K - 2,243K = 167K) by Chen *et. al.* (1997). From Table 4.1, it is obvious that as the dilution level increases from 20% to 60%, the temperatures of the H_2-He diluted flames in Chen *et. al.* (1997) do not vary much. This is somewhat counterintuitive since the effect of the heat capacity could be present and would lower the flame temperatures considerably. For coflow flames (Chen *et. al.*, 1997; Kothawala, 2003; Chaos, 2003), it is also expected to have effects of convective heat transfer which would further lower the flame temperature. However, this would not be seen in counterflow flames.

According to Figures 4.3 and 4.4, the maximum flame temperatures of the 20% He- and Ar-diluted flames differ (i.e. the temperature of the Ar-diluted flame is higher than He-diluted flame for both of 18 cm/s and 30 cm/s cases) by approximately 30K for 18 cm/s and 32K for 30 cm/s (for the temperature data of 18 cm/s, see Table 4.3). In the 20% He- and Ar-diluted flames, the major effect of Le_f is relatively less pronounced compared to the effects of the 40% and 60% dilution cases. In fact, due to the degree of dilution, it was expected that the maximum flame temperature for Ar-diluted flame would be lower than that of He-diluted flame since Le_f for Ar-diluted flame is nearly 1.3 times

greater than He-diluted flame. However, if Le_f is larger than unity, thermal diffusion from the flame zone into incoming flow of fuel mixture may preheat the incoming fuel mixture before the fuel diffuses into the reaction zone. Then, even though the value of Le_f for the Ar-diluted flame is higher than that of the He-diluted flame, the gradient of flame temperature is smaller than that of the He-diluted flame. This may cause more intensive burning of the reactants at the flame reaction zone which leads to a higher flame temperature and less loss of flame temperature caused by the temperature difference between incoming mixture and burning reactants. Furthermore, the higher thermal conductivity, k, of 20% He-diluted mixture which causes heat loss through the thermal conduction from flame zone to the burner port which may further reduce flame temperature (as also discussed in Rørtveit *et. al.*, 2002). When reducing the maximum flame temperature, it is also possible to consider the above effect in addition to the fact that Ar-diluted flame always has larger L_f than He-diluted flame since H_2 diffuses radially more in He dilution than in Ar dilution due to the large difference in density (Chaos, 2003). Therefore, H_2-He diluted flame does not need a longer distance for a fuel to be consumed than Ar flame needs which may lead to less accumulation of heat in the entire flame surface and also lead to less NO_x formation.

4.3 NO_x Emission Levels of Steady State H_2-Ar and H_2-He Flames

As introduced early in Chapter 1, the primary route of NO_x formation in the flame

investigated in this study is the Zeldovich mechanism, which is less significant in a hydrocarbon flame compared to the case of a hydrogen flame. If the complexity of NO_x mechanism can be removed and simplified using the hydrogen flame, the major effort to understand the prompt formation can be focused solely upon the behavior of the maximum flame temperature to determine whether it shows the Le_f effect or other thermodynamic properties of the fuel mixture. Figure 4.9 indicates how the maximum flame temperature is related to NO_x formation of all of the dilution levels with

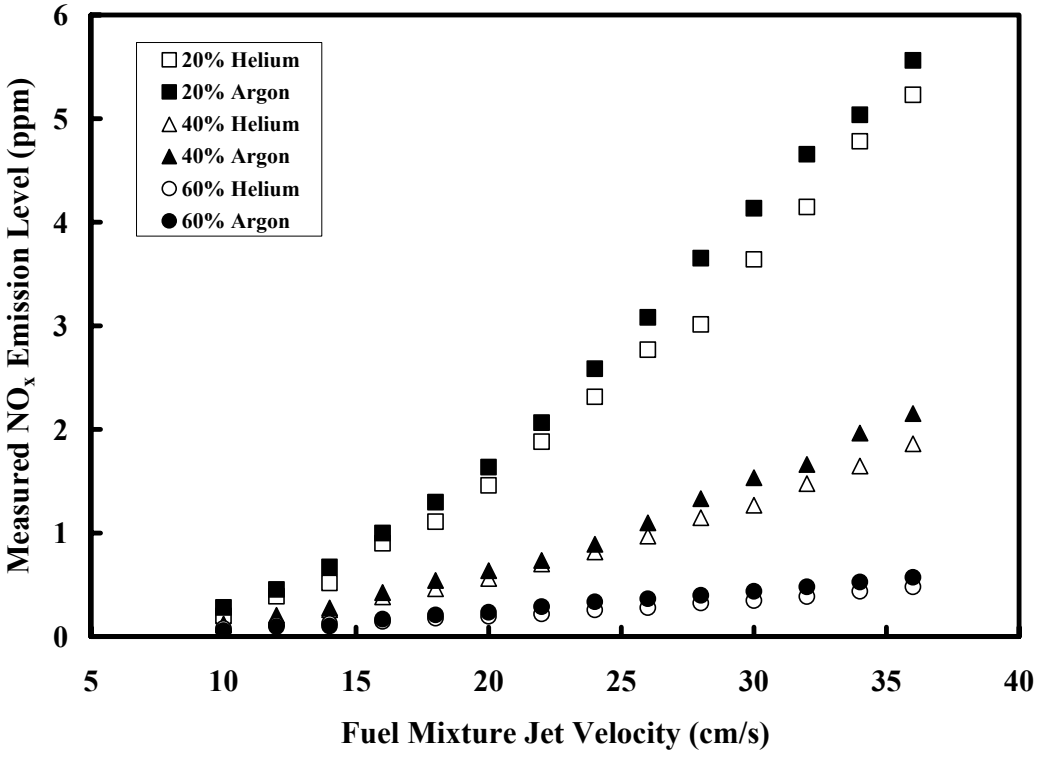

Figure 4.9: NO_x emission level vs fuel mixture jet velocity of H_2-Ar and -He diluted flames.

both diluents presented in Section 4.2. The increase of the NO_x emission levels along the jet velocity from 10 to 36 cm/s is monotonic. For the sake of avoiding experimental uncertainty, the velocities below 10 cm/s were not included in this investigation due to uncertainty in the emission level below 0.1ppm. The measurement accuracy of the NO_x analyzer was 0.1ppm since it was 1% of the full scale (i.e. measurement range) which was 0-10ppm. Therefore, any NO_x levels above 0.1ppm can be considered as valid except the values of NO_x level (0.057ppm at 10 cm/s for 60% Ar-diluted flame and 0.079ppm at 10 cm/s for 60% He-diluted flame).

In the low velocity regimes (i.e. less than 10 cm/s) the axial diffusion becomes important on the mass velocity which makes Burke-Schumann assumption invalidated. In the 40% mole fraction of He and Ar, the difference of NO_x levels is less evident at the low velocity (i.e. around 10 cm/s) whereas it become diverged as the jet velocity increases. This should be the fact that the two diluents have different transport properties and density. In Figure 4.9, the difference of the NO_x levels of the 40% Ar- and He-diluted flames vary by 0.006ppm (i.e. about 5.6%) at the lowest velocity (i.e. 10 cm/s) and 0.291 (i.e. about 15.6%) ppm at the highest velocity (i.e. 36 cm/s) from the data of the 40% Ar- and He-diluted flames. It is also noticed that the difference of the NO_x levels increased from 18 to 30 cm/s by 0.807ppm for He-diluted flame and 0.991ppm for Ar-diluted flame and the difference of the maximum temperatures is by about 81K and 95K for He and Ar, respectively. This would be able to be explained by the consideration of temperature difference in the 40% He- and Ar- diluted flames in Section 4.2.

With the case of 60% dilution, the NO_x formation by the Le_f effect in varying a

flame temperature is most clarified since higher Le_f leads to a lower flame temperature. The values of Le_f and the maximum flame temperatures of 60% Ar- and He-diluted flames are 1.035 vs 1,708K for He and 0.718 vs 1,774K for Ar. Throughout the velocity range selected (i.e. 10 to 36 cm/s) for 60% cases of dilution, NO_x level for the Ar-diluted flame is always higher than that of the He-diluted flame. The flame maximum temperatures 1,844K vs 1,904K for 60% He- and Ar-diluted flames (Chaos, 2003) and 1,718K vs 1,835K for 60% He- and Ar-diluted flames (Kothawala, 2003) are in agreement of the trend observed in the present study. The possible reason for this trend may not be limited to the effect of transport properties. The characteristic of flame residence time which increases along L_f may play some role in varying NO_x level (a flame temperature). In Section 4.1, an increase of L_f is principally attributable to an increase of volumetric flow rate, Q_f, early defined by Roper (1997).

It is noted that greater L_f leads to greater flame residence time τ_f and the values of τ_f are in Table 4.4. This is due to the fact that the flame residence time, $\tau_{f,}$ is often defined as the time required for a stoichiometirc amount of oxidizer (i.e. in this study, always air) to react with a fuel or a fuel mixture. If the former statement holds true, it is evident that if the L_f increases along the volumetric flowrate given, the flame residence time also follows the increase of L_f due to demands of both an increase in the required amount of a stoichiometric oxidizer for complete combustion and an increase of sufficient fuel consumed in the combustion. This would lead to higher NO_x formation rate since the NO_x emissions are based upon an integral effect of the overall accumulated temperature throughout the entire flame regime.

Table 4.4: Flame residence time including buoyancy acceleration with fuel jet velocity for H_2-Ar and H_2-He diluted flame

Jet Velocity (cm/s)	H_2-He diluted flame			H_2-Ar diluted flame		
	20% dilution	40% dilution	60% dilution	20% dilution	40% dilution	60% dilution
	Flame Residence Time τ_f* (sec)			Flame Residence Time τ_f* (sec)		
10	0.019281	0.017397	0.013080	0.019267	0.017375	0.015370
12	0.019683	0.017965	0.014117	0.021370	0.019746	0.016145
14	0.020028	0.018448	0.014962	0.023113	0.020088	0.016791
16	0.020329	0.018863	0.015669	0.023219	0.021872	0.017340
18	0.021982	0.019226	0.016273	0.024618	0.022044	0.017814
20	0.023412	0.019545	0.016796	0.025845	0.022197	0.018228
22	0.023487	0.019829	0.017254	0.025806	0.022335	0.018594
24	0.024683	0.021297	0.017661	0.026851	0.023615	0.020172
26	0.025752	0.021466	0.018024	0.026775	0.023676	0.020399
28	0.025722	0.021619	0.018351	0.028648	0.023731	0.020605
30	0.026538	0.022790	0.018646	0.029430	0.024776	0.020792
32	0.026593	0.022877	0.018916	0.030148	0.026653	0.020964
34	0.027416	0.022957	0.019162	0.029975	0.026595	0.021122
36	0.028175	0.023931	0.019388	0.030625	0.026540	0.021267

τ_f* values are calculated by Equations (10) to (13) below including Equation (9) for buoyancy acceleration

In a laminar flame case, greater L_f should lead to higher temperature and eventually higher NO_x emission. Therefore, the flame lengths of the entire dilution levels (i.e. three different degrees of dilutions per each diluent) investigated in this study, it is noted that Ar-diluted flame always has greater L_f than He-diluted flame based upon the range of the velocity regime. For instance, at the highest velocity (36 cm/s), the flame lengths of Ar- and He-diluted flames were 1.5cm vs 1.35cm for the 20% dilution case, 1.25cm vs 1.1cm for the 40% dilution case and 0.95cm vs 0.85cm for the 60% dilution case respectively. This propensity can be explained by the fact that L_f tends to be directly correlated to a flame maximum temperature on a flame, and the maximum flame temperature is attributable to stimulating an increase of buoyancy acceleration according to Equation (9):

$$a = g \cdot \left(1 - \frac{T_o}{T_f} \right) \tag{9}$$

where a is buoyancy acceleration, g is the gravitational acceleration, T_o is an ambient temperature (=298K) and T_f is a maximum flame temperature as tabulated in Table 4.1. The mathematical definition of flame residence time containing a consideration of an effect of buoyancy acceleration is also presented into the following:

$$d\tau_f = \frac{dz}{U} \tag{10}$$

$$U = \sqrt{U_f{}^2 + 2 \cdot a \cdot z} \tag{11}$$

$$\tau_f = \int_0^{L_f} \frac{dz}{\left(U_f{}^2 + 2 \cdot a \cdot z\right)^{\frac{1}{2}}} \tag{12}$$

$$\tau_f = \frac{\sqrt{2 \cdot a \cdot L_f + U_f{}^2}}{a} - \frac{U_f}{a} \tag{13}$$

Equation (13) was obtained by integrating Equation (12) and simplifying it as previously obtained by Chen *et. al.* (1997). The buoyancy-accelerated mass velocity leads to higher flame residence time which is not likely to keep a constant value along the selected range of velocity.

Figure 4.10 indicates how NO_x formation with flame residence time ($\tau_f \sim$ Da) behaves as the jet velocity increases (also the L_f increases). This is due to the important effect of buoyancy on a laminar diffusion flame. The Damkohler number is defined as the ratio of fluid mixing time to chemical reaction time. As can be expected from Table 4.4 and Figure 4.10, the flame residence time (also NO_x level) continuously increases along the jet velocity although it seems to be slow in the slope near the high velocity regime in the range of velocities studied (around 30 to 36 cm/s). When comparing Figures 4.9 and 4.10 with Table 4.4, it is noted that the flame residence times of Ar- and He-diluted

flames for the 20% dilution are similar (0.019sec vs 0.019sec for He and Ar) at U_f = 10 cm/s while they are different (0.028sec vs 0.030sec for He and Ar) at U_f = 36 cm/s. With this trend, the NO_x emission levels of the 20% Ar- and He-diluted flames are expected to differ as the jet velocity increases (i.e. more NO_x formation for Ar flame). This suggests that by increasing jet velocity, it is expected that the flame residence time from 20% Ar-diluted flame became longer (larger time taken) than He flame.

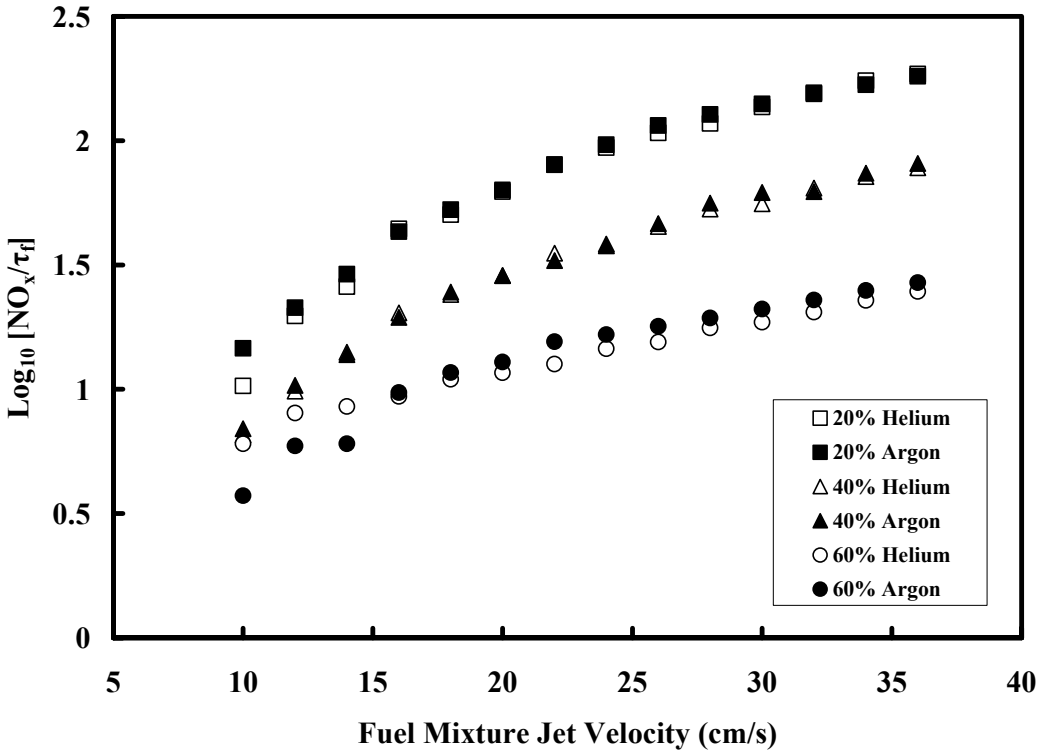

Figure 4.10: NO_x level normalized by the flame residence time vs flame jet velocity of H2-Ar and -He diluted flames.

This trend was also observed in the 40% case (see Figure 4.10 with Table 4.4).

4.4 Flame Lengths of Unsteady State H_2-Ar and H_2-He Flames

Transport properties of Ar- and He-diluted flames are expected to play such an important role in unsteady speaker-pulsed flames. By summarizing the results regarding the effective diluents in reducing NO_x emission and flame temperatures from Rørtveit *et. al*. (2002) and Li and Williams (1999)**,** it is noted that He should be more effective gas than Ar in reducing flame temperature and NO_x emission. Consequently, it is anticipated that the coupled effect of difference in Le_f of two mixtures, and the effect of a diluent should play a role in a certain manner in the unsteady flame behavior studied in this section although it was previously found that the Le_f effect on the turbulent jet diffusion flame (Gabriel *et. al.*, 2000) is relatively less evident than on the laminar diffusion flame (Chen *et. al.*, 1997).

In this study, it was found that unsteady flame lengths are linearly related to the speaker voltage, and in Chaos (2003), it was shown that the sinusoidal velocity fluctuation, u', was also proportional to the speaker voltage. Therefore, it is reasonable to assume that the radio of V/V_{ext} is equivalent to u'/u'_{ext} (where V_{ext} and u'_{ext} are the voltage and velocity fluctuation at extinction of He-diluted flame)

Note that all the flame lengths presented in Figure 4.11 through Figure 4.16 are the maximum visual flame lengths during the cycle of speaker pulsation, and also if

Table 4.5: Speaker voltages and calculated velocity fluctuation based on Chaos (2003)

20% dilution			
10Hz		100Hz	
V (volt)	u' (cm/s)	V (volt)	u' (cm/s)
0.2	7.934	4	3.778
0.3	11.900	8	7.556
0.4	15.867	12	11.334
0.5	19.834	16	15.112
0.6	23.801	20	18.890
0.7	27.768	24	22.668
0.8*	31.735**	28	26.446
----	----	32*	30.224**
40% dilution			
10Hz		100Hz	
V (volt)	u' (cm/s)	V (volt)	u' (cm/s)
0.2	7.934	4	3.778
0.3	11.900	8	7.556
0.4	15.867	12	11.334
0.5	19.834	16	15.112
0.6	23.801	20	18.890
0.7*	27.768**	24	22.668
----	----	28*	26.446**
60% dilution			
10Hz		100Hz	
V (volt)	u' (cm/s)	V (volt)	u' (cm/s)
0.2	7.934	4	3.778
0.3	11.900	8	7.556
0.4	15.867	12	11.334
0.5	19.834	16	15.112
0.6*	23.801**	20	18.890
----	----	24	22.668
----	----	28*	26.446**

The global velocity during the sinusoidal cycle is defined as $U_G = \bar{u}$ (30 cm/s) + u' (sinφ)
* indicates V_{ext} (maximum measured voltage for extinction of He-diluted flame)
** indicates u'_{ext} (velocity fluctuation corresponding to the flame extinction voltage)

flame extinction limit is mentioned, then it is always for the cases of He-diluted flame. It is noted that the flame lengths for Ar- and He-diluted flames were always longer than those values of the steady state flames. This can be observed in the Figure 4.11 through Figure 4.16. For example, for the 20% unsteady case, the flame lengths of the Ar- and He-diluted flames were 1.35cm and 1.45cm at 0.2volt at 10Hz and 1.3cm and 1.3cm at 4volt at 100Hz whereas those lengths of the steady case of the Ar- and He-diluted flames were 1.25cm and 1.1cm at the fuel jet velocity 30 cm/s. Even though the intensity of turbulence at the onset (i.e. each beginning point of measurement see Table 4.5) of oscillation in the fuel stream should be relatively weaker than that at the He-diluted flame extinction, it is obviously excited by acoustic pulsation. As a result, the excited flame would have lengthened L_f (i.e. reaction volume). From Figure 4.11 to Figure 4.16, the flame lengths of unsteady Ar- and He-diluted flames were presented with u'/u'_{ext}. These flame lengths are to correlate the consideration how velocity fluctuation responds intensity of a speaker voltage increases up to the extinction voltage limit of an unsteady flame (i.e. maximum voltages until which a flame extinguishes, see Table 4.5).

As reviewed in Section 2.4, Chaos (2003) experimentally explored the effect of Le_f and unsteadiness on He- and Ar-diluted H_2 flames with OH intensity and two dimensional temperature fields by PLIF. The importance of his study herein is that the experimental results of velocity fluctuation (denoted by u' in Chaos, 2003) by LDV measurement revealed that as a voltage (i.e. speaker strength) increased, the velocity fluctuation also increased almost linearly for two frequencies, 10 and 100Hz. These linear results of u' with an increase of a speaker voltage enable the employment his u' data into

Table 4.6: Measured speaker voltages, voltages normalized by flame extinction voltages and velocity fluctuation normalized by flame extinction velocity fluctuation

20% dilution					
	10Hz			100Hz	
V (volt)	V/V_{ext}	u'/u'_{ext}	V (volt)	V/V_{ext}	u'/u'_{ext}
0.2	0.250	0.250	4	0.125	0.125
0.3	0.375	0.375	8	0.250	0.250
0.4	0.500	0.500	12	0.375	0.375
0.5	0.625	0.625	16	0.500	0.500
0.6	0.750	0.750	20	0.625	0.625
0.7	0.875	0.875	24	0.750	0.750
0.8	1.000	1.000	28	0.875	0.875
----	----	----	32	1.000	1.000
40% dilution					
	10Hz			100Hz	
V (volt)	V/V_{ext}	u'/u'_{ext}	V (volt)	V/V_{ext}	u'/u'_{ext}
0.2	0.286	0.286	4	0.143	0.143
0.3	0.429	0.429	8	0.286	0.286
0.4	0.571	0.571	12	0.429	0.429
0.5	0.714	0.714	16	0.571	0.571
0.6	0.857	0.857	20	0.714	0.714
0.7	1.000	1.000	24	0.857	0.857
----	----	----	28	1.000	1.000
60% dilution					
	10Hz			100Hz	
V (volt)	V/V_{ext}	u'/u'_{ext}	V (volt)	V/V_{ext}	u'/u'_{ext}
0.2	0.333	0.333	4	0.143	0.143
0.3	0.500	0.500	8	0.286	0.286
0.4	0.667	0.667	12	0.429	0.429
0.5	0.833	0.833	16	0.571	0.571
0.6	1.000	1.000	20	0.714	0.714
----	----	----	24	0.857	0.857
----	----	----	28	1.000	1.000

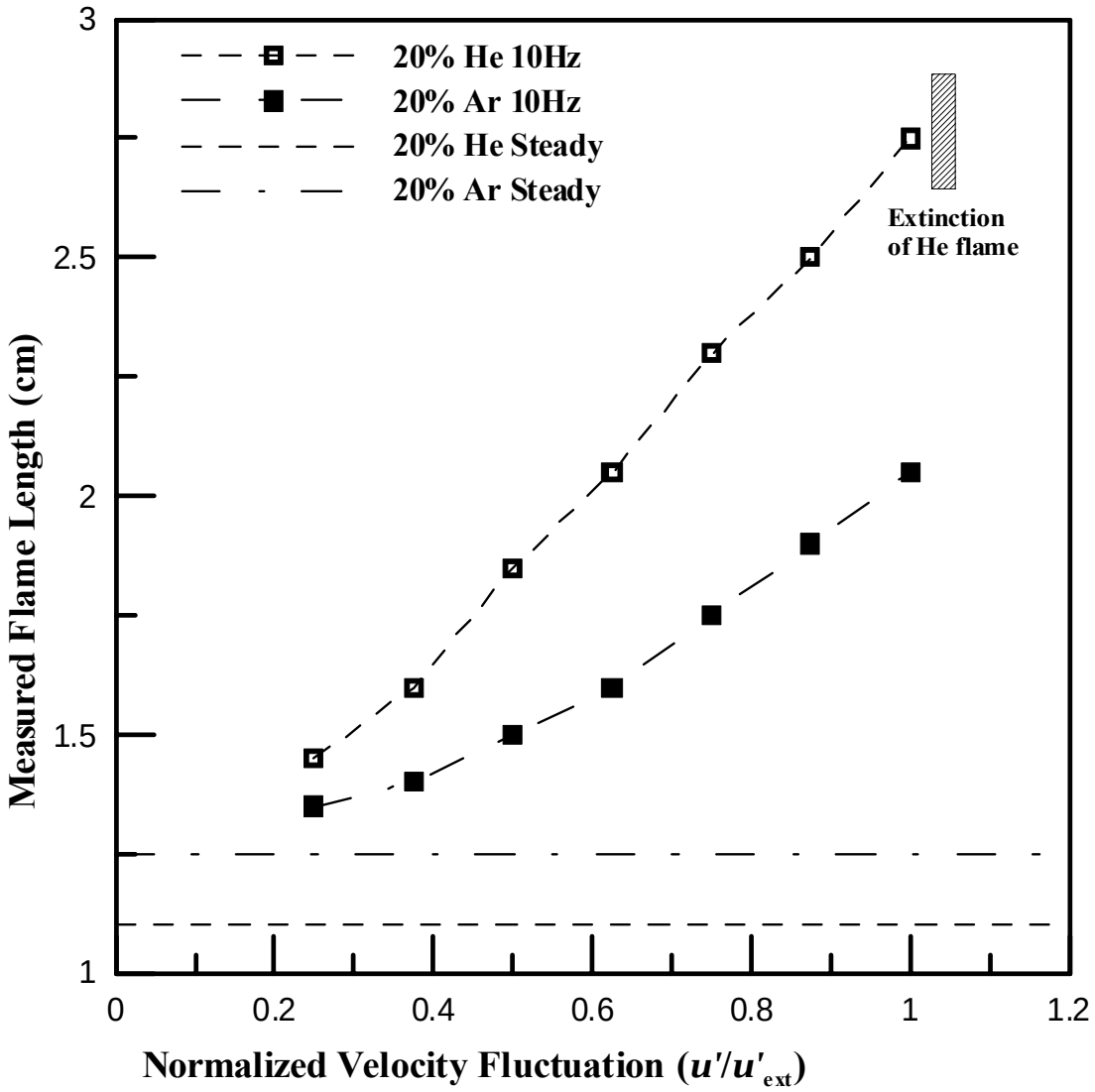

Figure 4.11: Flame length vs u'/u'_{ext} of 20% Ar- and He-diluted flames pulsed at 10Hz.

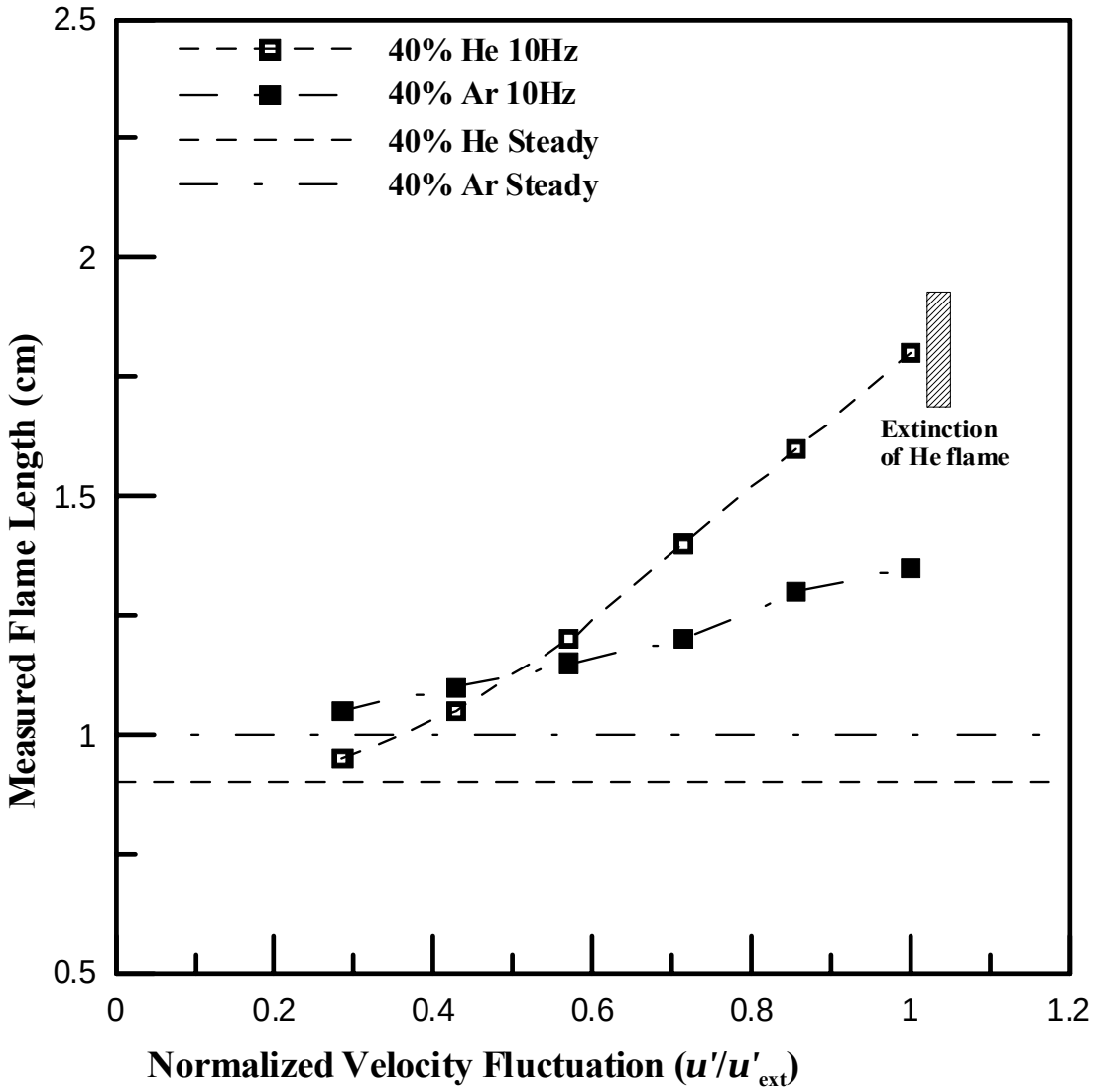

Figure 4.12: Flame length vs u'/u'_{ext} of 40% Ar- and He-diluted flames pulsed at 10Hz.

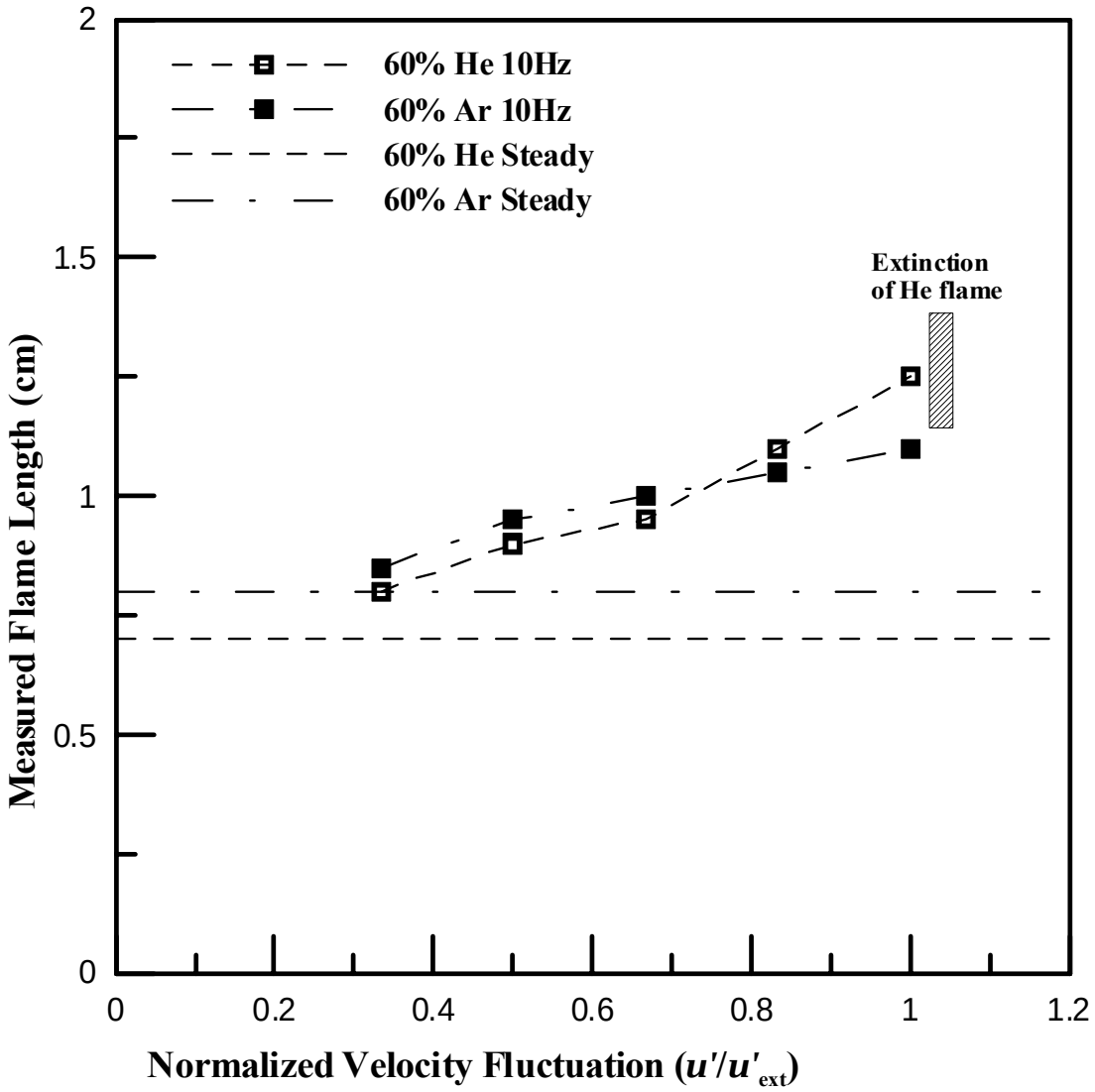

Figure 4.13: Flame length vs u'/u'_{ext} of 60% Ar- and He-diluted flames pulsed at 10Hz.

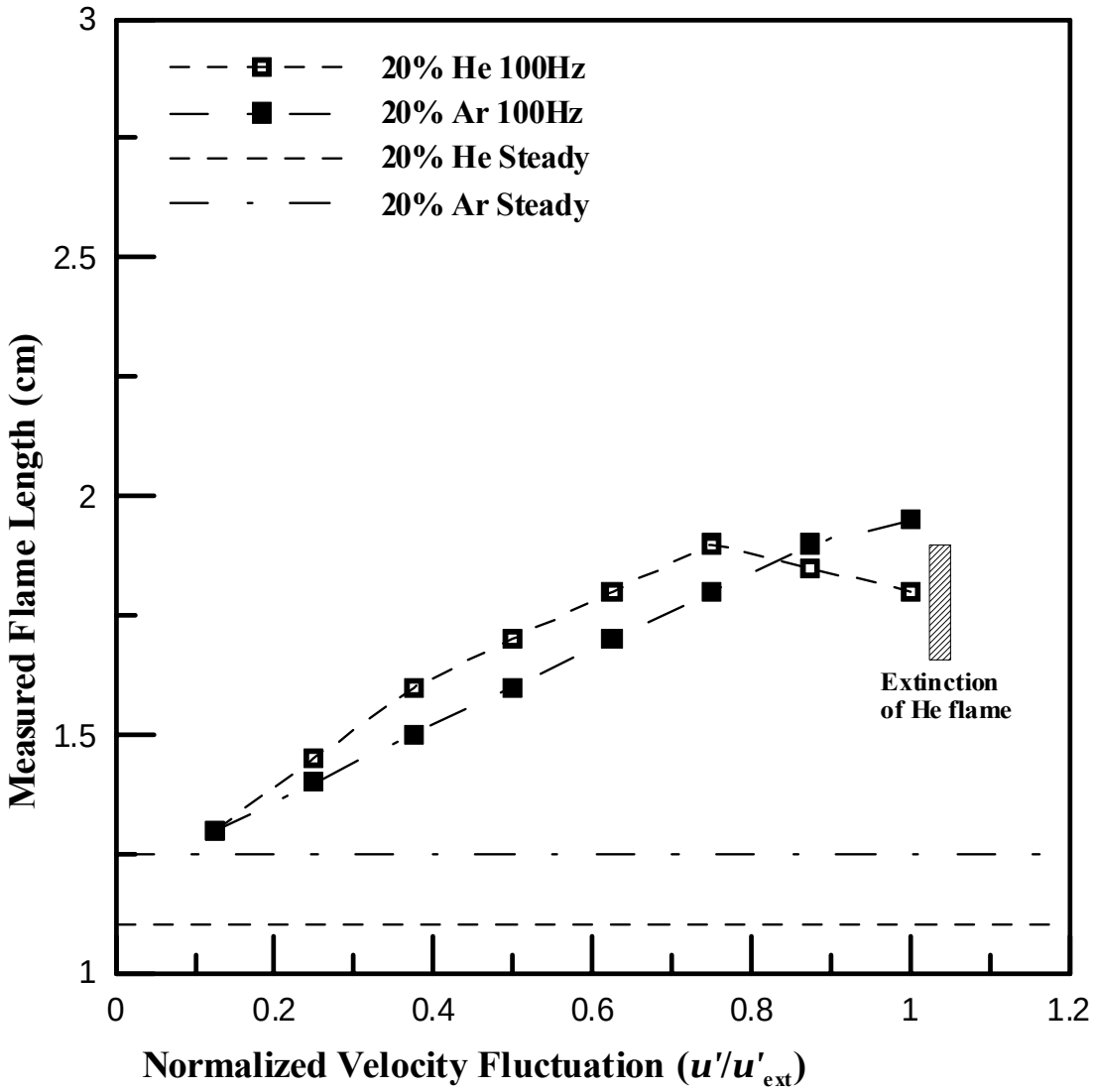

Figure 4.14: Flame length vs u'/u'_{ext} of 20% Ar- and He-diluted flames pulsed at 100Hz.

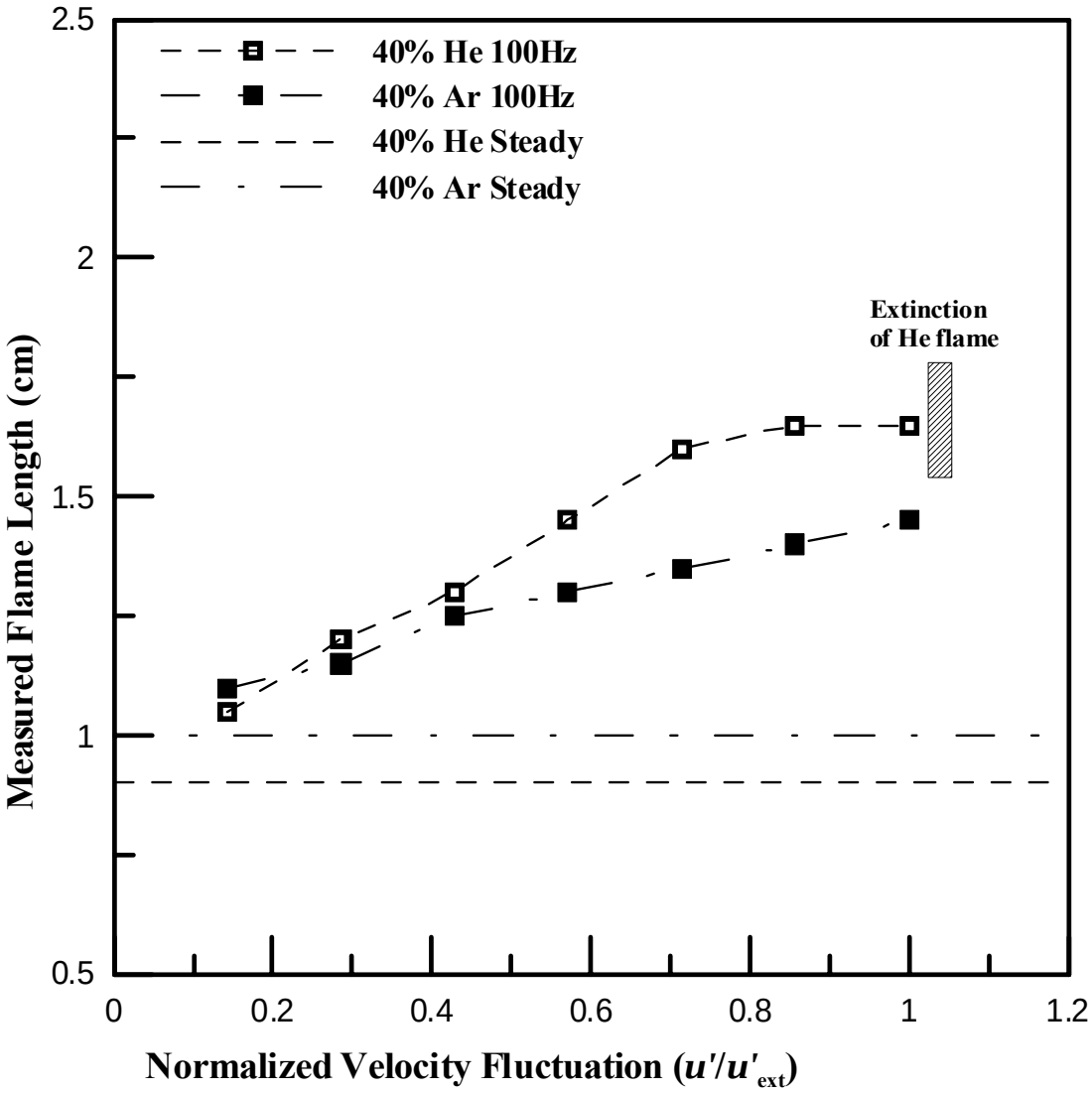

Figure 4.15: Flame length vs u'/u'_{ext} of 40% Ar- and He-diluted flames pulsed at 100Hz.

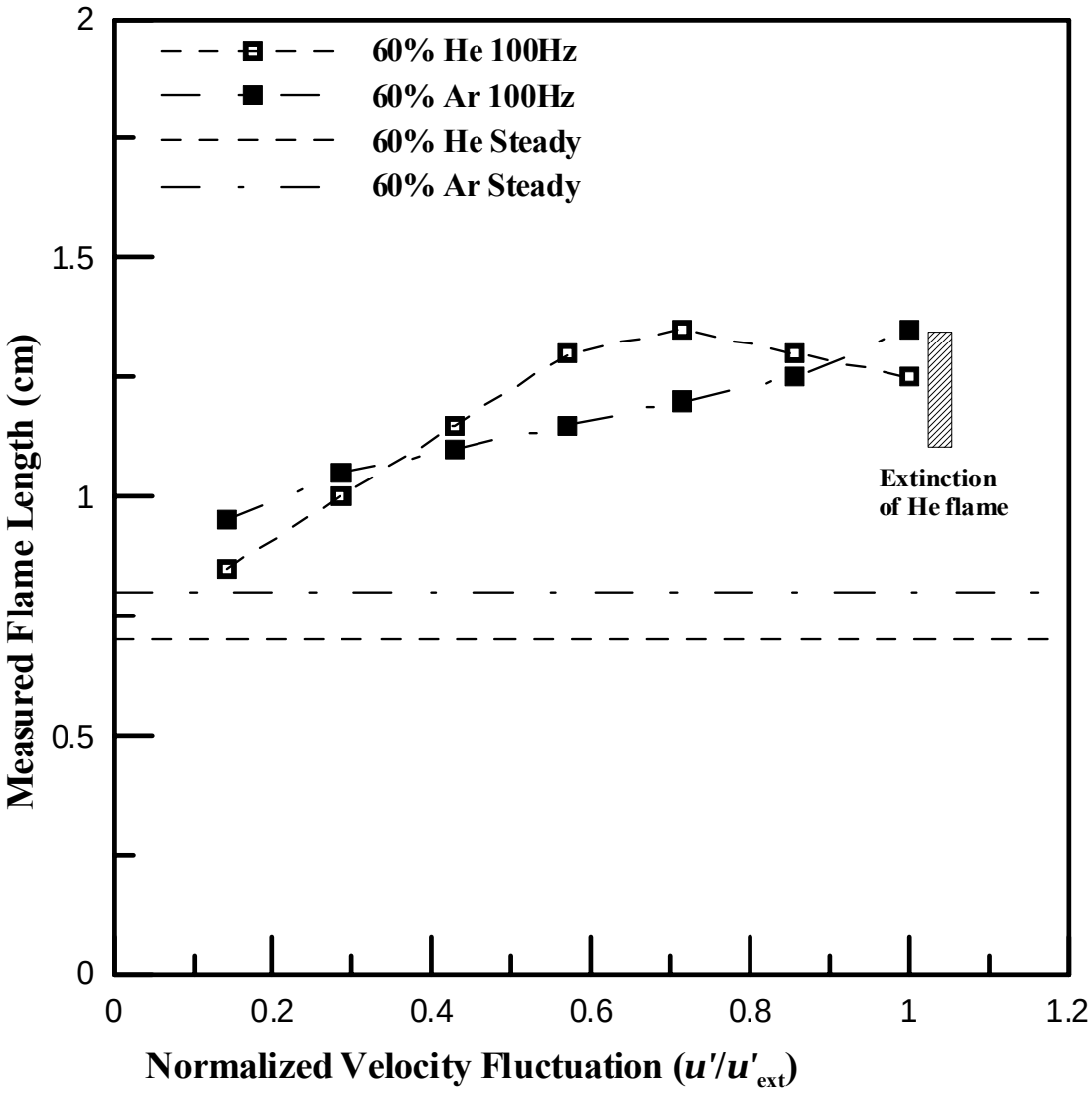

Figure 4.16: Flame length vs u'/u'_{ext} of 60% Ar- and He-diluted flames pulsed at 100Hz.

this study so that it can be used in the unsteady flame analysis. In addition, it is possible to assume that the ratio of velocity fluctuation to velocity fluctuation for He-diluted flame extinction limit should be a constant and can substitute for the ratio of a speaker voltage to a voltage for He-diluted flame extinction limit.

At the lowest velocity fluctuation for Ar- and He-diluted flames at all the dilution levels in Figures 4.11 through 4.13, it is shown that the magnitude of the L_f for the Ar-diluted flame is always greater than that of the He-diluted flame except in 20% flame case pulsed at 10Hz. This trend is similar to the observed result from the steady state flame between Ar and He dilution which means that at a dilution level, L_f for Ar-diluted flame was always higher than that of He-diluted flame. As velocity fluctuation increased, it was observed that after the onset of unsteadiness (where each value of the lowest u'/u'_{ext} is minimal for a dilution level) a He-diluted flame became more unstable, and its volume of the flame zone against the speaker pulsation bulged out more than that of the Ar-diluted flame. This should be due to the higher diffusivity of H_2-He diluted flame, the less density of H_2-He diluted flame and the lower viscosity of H_2-He diluted flame. Therefore, these would possibly make He-diluted mixture spread out wider and higher to axial and radial directions due to the variation in momentum transfer from the speaker to the He-diluted mixture. It is also reasonable to further support the preceding idea with the fact that the flame is extinguished near the maximum velocity fluctuation (at $u'/u'_{ext} = V/V_{ext} \approx 1$), which leads the flame to extinguish, and the difference of the flame lengths for the Ar and He flames significantly deviated each other primarily due to the transport properties of Ar and He considered above. The plots of the flame lengths showed

crossing-tendency for 40% and 60% at 10Hz and also the same levels at 100Hz. In Figures 4.12, 4.13, 4.15 and 4.16, the L_f of He-diluted flame is smaller than that of Ar-diluted flame at each of the smallest values of u'/u'_{ext} (see Table 4.7). However, this trend reverses at the flame extinction limit where $u'/u'_{ext} \approx$ unity). The flame lengths of all the dilution levels (20%, 40% and 60%) with Ar- and He-diluted flames at the smallest and the greatest u'/u'_{ext} are tabulated in Table 4.7. In Table 4.7, it can be seen that the difference of the flame lengths at the smallest value of u'/u'_{ext} (i.e. onset of fluctuation of flow) change their value from negative to positive as the u'/u'_{ext} increases until the greatest value of u'/u'_{ext} except that in the 20% dilution case at 10 and 100Hz and in the 60% dilution at 100Hz (remains unchanged in a sign negative to negative). Furthermore, in Table 4.7, it was found that the difference of the flame lengths of the 20%, 40% and 60% dilution for 10Hz at u'/u'_{ext} = unity showed that it decreased monotonically (0.7, 0.45 and 0.15) compared to the difference of the flame lengths of the same dilutions for 100Hz, which do not increase or decrease rather oscillate (-0.15, 0.2 and -0.1). In other words, the He-diluted flames are more readily bulged out by acoustic pulsation at the highest amplitude of velocity fluctuation where u'/u'_{ext} = unity than the Ar-diluted flames for all the dilution at 10Hz. In addition, the change of the L_f which is related to reaction zone volume is sensitive to the increase of the degree of dilution. In the case of the unsteady flames at 100Hz, the similar crossing-tendency of the flame lengths for the 40% and 60% dilution were observed in Figures 4.15 and 4.16. In Table 4.7, the difference of the flame lengths of the Ar- and He-diluted flames at 100Hz is negative (i.e. when L_f for He-diluted flame is shorter than that of Ar-diluted flame) in the cases for the 20% and 60% dilution

Table 4.7: Flame length of unsteady H_2-Ar and H_2-He diluted flames measured at the smallest and the greatest values of u'/u'_{ext} for 10 and 100Hz

20% dilution		H_2-He flame	H_2-Ar flame	
Frequency	u'/u'_{ext}	$L_{f,He}$ (cm)	$L_{f,Ar}$ (cm)	$L_{f,He} - L_{f,Ar}$ (cm)
10Hz	0.250	1.45	1.35	0.1
	1.000	2.75	2.05	0.7
100Hz	0.125	1.3	1.3	0
	1.000	1.8	1.95	-0.15
40% dilution		H_2-He flame	H_2-Ar flame	
Frequency	u'/u'_{ext}	$L_{f,He}$ (cm)	$L_{f,Ar}$ (cm)	$L_{f,He} - L_{f,Ar}$ (cm)
10Hz	0.286	0.95	1.05	-0.1
	1.000	1.8	1.35	0.45
100Hz	0.143	1.05	1.1	-0.05
	1.000	1.65	1.45	0.2
60% dilution		H_2-He flame	H_2-Ar flame	
Frequency	u'/u'_{ext}	$L_{f,He}$ (cm)	$L_{f,Ar}$ (cm)	$L_{f,He} - L_{f,Ar}$ (cm)
10Hz	0.333	0.8	0.85	-0.05
	1.000	1.25	1.1	0.15
100Hz	0.143	0.85	0.95	-0.1
	1.000	1.25	1.35	-0.1

at u'/u'_{ext} = unity. This is opposite to trend observed in the case of the same dilutions for 10Hz at u'/u'_{ext} = unity in Table 4.7.

From Figure 4.14 and Figure 4.16, it is remarkable that as the amplitude of velocity fluctuation increases, the He-diluted flame shows a tendency for a decline in its L_f as u'/u'_{ext} approaches the extinction limit where u'/u'_{ext} = unity. This tendency was not observed any cases in all the flames of the low frequency 10Hz. This can be attributable to the fact that at the high u' regime more mixing of He-diluted flame (entrainment of surplus oxidizer into a flame zone) with coflowing air due to its higher mass diffusivity, lower density and lighter molecular weight caused more strain. This may lead to local flame extinction which affects a flame maximum temperature. Moreover, the tendency of a decrease of L_f of He-diluted flames at 100Hz can be further supported by the fact that since a He-diluted flame has higher mass diffusivity and more unstable against momentum transferred by speaker pulsation, the He-diluted flame has more incoming reactants flowing into the flame zone, and flame residence time becomes smaller than time required for chemical reaction. This may cause fuel leakage (i.e. escape of unburned fuel) to downstream leading flame extinction.

4.5 NO_x Emission Levels of Unsteady State H_2-Ar and H_2-He Flames

First of all, like the cases of the unsteady L_f at the smallest values of u'/u'_{ext}, NO_x emission levels for the unsteady flames of all the dilution levels at the smallest values of

u'/u'_{ext} are always higher than those for the steady state flames for all the dilution studied. For example, the NO_x emission levels for the 20% dilution are 4.21ppm and 4.02ppm for Ar- and He-diluted unsteady flames for 10Hz at $u'/u'_{ext} = 0.250$ and 4.46ppm and 4.05ppm for 100Hz at $u'/u'_{ext} = 0.125$ while those of NO_x emission levels from the steady state were 4.13ppm and 3.64ppm for Ar- and He-diluted flames at the jet velocity 30 cm/s. This trend was also observed in the 40% and 60% unsteady Ar and He flames. From Table 4.8, it is noticed that like the case of the steady state Ar- and He-diluted flames for all the dilution levels, the NO_x emission level for Ar-diluted flame was always higher than that of He-diluted flame at the smallest value of u'/u'_{ext} with each dilution for 10 and 100Hz. This is noticeable because in the steady case, greater L_f may cause a higher NO_x level for Ar-diluted flame case with all the dilution levels, as discussed in Section 4.3. However, in the unsteady case, the L_f of the 20% He-diluted flame at u'/u'_{ext} =0.250 for 10Hz was higher than that of the 20% Ar-diluted flame (see Figure 4.11). This implies that the relationship of L_f and NO_x emission level in an unsteady flame is relatively less significant than in a steady case.

Once a flame is acoustically excited for both Ar- and He-diluted flames, it should have a volumetric expansion of a flame zone, where more reactants can react with air (i.e. the flame bulges out). Then, due to the characteristic of NO_x formation, which is an integrated effect of the surface flame temperature, the readings from the NO_x analyzer are likely to be higher than those from the steady data unless the acoustic excitation causes excessive supply of reactants (more likely to happen for He-diluted flame). Prior to the discussion regarding NO_x levels for the unsteady flames, it should be noted that for the

low frequency 10Hz in this study, NO_x emission levels with an increase of u'/u'_{ext} never decrease below the values of the steady state Ar- and He-diluted flames presented in Figures 4.17 through 4.19. This observation implies that the acoustic excitation plays a role in varying the NO_x level (however, not lowering the levels below that of the steady case) within the given range (i.e. 0 to 1 of u'/u'_{ext}). Contrary to this, for the high frequency 100Hz, as u'/u'_{ext} reaches to unity, NO_x levels of the He-diluted flames have a tendency to decrease below the steady value. Nevertheless, the Ar-diluted flames with the high frequency (except the 20% case at 100Hz) do not show such trend similar to the He-diluted flame case. Apparently, this implies how a He-diluted flame with all the dilution levels responds more readily to the acoustic pulsation by the loudspeaker than an Ar-diluted flame--due to higher mass diffusivity, density and partly kinematic viscosity of H_2-He diluted mixture (see Table 3.6). For the high frequency 100Hz case, there was no crossing- tendency shown for the Ar and He flames with any degree of dilutions. It was, however, found that NO_x emission levels of the He-diluted flames for all the dilution cases decreased as u'/u'_{ext} increased and approached to the flame extinction limit for 100Hz. Table 4.8 shows the NO_x emission levels of all the dilution levels at the smallest and the greatest values of u'/u'_{ext} for 10 and 100Hz and it can be seen that the ratio of the NO_x emission levels of Ar- and He-diluted flames (i.e. $NO_{x,Ar}/NO_{x,He}$) at each of the smallest values of u'/u'_{ext} for 10 and 100Hz is around unity in the most cases of all the dilutions (except somewhat higher than unity in 60% case). However, at $u'/u'_{ext} = 1$, for the high frequency 100Hz, the ratio of the NO_x emission levels of the flames vary about 2.405, 3.593 and 2.203 with 20% to 60%, while on the other hand, the ratio remains

around 1.1 at $u'/u'_{ext} = 1$ for 10Hz. By this fact, with the relatively unchanged Le_f for He-diluted flames (Recall 0.998, 1.012 and 1.035 for 20%, 40%, 60% dilution) for 100Hz at $u'/u'_{ext} = 1$, it is noted that the unsteadiness effect by the intensity of velocity fluctuation is maximized for the dilution level where Ar- and He-diluted flames have the same Le_f (=1.012) although it is expected to occur in the 60% dilution case if coupled with Le_f effect.

Le_f effect on the unsteady flames studied here has tendency on NO_x emission level similar to that in the steady state case. As shown in Section 4.2, in the 20% dilution of the steady case, the values of the maximum flame temperature for Ar ($Le_f = 1.389$) and He ($Le_f = 0.998$) diluted flames were close (2,206K for Ar-diluted flame and 2,174K for He-diluted flame). However, the maximum flame temperatures for Ar flames were always higher than those of He flames in all the dilution cases regardless of Le_f (refer to Table 4.1). It was found that the ratios of the NO_x levels of Ar and He unsteady flames at the smallest u'/u'_{ext} in Table 4.8 were close to one another for both 10 and 100Hz (1.048 vs 1.101, 1.094 vs 1.145 and 1.203 vs 1.270 for 10 and 100Hz with 20%, 40% and 60% dilutions, respectively). Therefore, at each of the smallest u'/u'_{ext}, the difference of the NO_x levels should be mainly due to the Le_f effect (similar to the steady case) since the intensity of velocity fluctuation is the minimal, and its effect may be attenuate. However, for the case of 100Hz, at the highest u'/u'_{ext}, the ratios of the NO_x levels of Ar- and He-diluted unsteady flames increased about 2.405, 3.593 and 2.203 (20%, 40% and 60%, respectively) whereas this increase of the ratios was not observed for the 10Hz case at the highest u'/u'_{ext} (remains around unity 1.008, 1.134 and 1.161 for 20%, 40% and 60% in

Table 4.8: NO_x emission level of unsteady H_2-Ar and H_2-He diluted flames measured at the smallest and the greatest values of u'/u'_{ext} for 10 and 100Hz

20% dilution		H_2-He flame	H_2-Ar flame		
Frequency	u'/u'_{ext}	$NO_{x,He}$ (ppm)	$NO_{x,Ar}$ (ppm)	$NO_{x,Ar}$ - $NO_{x,He}$ (ppm)	$NO_{x,Ar}$ / $NO_{x,He}$
10Hz	0.250	4.02	4.21	0.19	1.048
	1.000	5.00	5.04	0.04	1.008
100Hz	0.125	4.05	4.46	0.41	1.101
	1.000	1.57	3.78	2.21	2.405
40% dilution		H_2-He flame	H_2-Ar flame		
Frequency	u'/u'_{ext}	$NO_{x,He}$ (ppm)	$NO_{x,Ar}$ (ppm)	$NO_{x,Ar}$ - $NO_{x,He}$ (ppm)	$NO_{x,Ar}$ / $NO_{x,He}$
10Hz	0.286	1.44	1.57	0.13	1.094
	1.000	1.45	1.64	0.19	1.134
100Hz	0.143	1.42	1.62	0.21	1.145
	1.000	0.50	1.79	1.29	3.593
60% dilution		H_2-He flame	H_2-Ar flame		
Frequency	u'/u'_{ext}	$NO_{x,He}$ (ppm)	$NO_{x,Ar}$ (ppm)	$NO_{x,Ar}$ - $NO_{x,He}$ (ppm)	$NO_{x,Ar}$ / $NO_{x,He}$
10Hz	0.333	0.41	0.49	0.08	1.203
	1.000	0.42	0.48	0.07	1.161
100Hz	0.143	0.40	0.51	0.11	1.270
	1.000	0.24	0.54	0.29	2.203

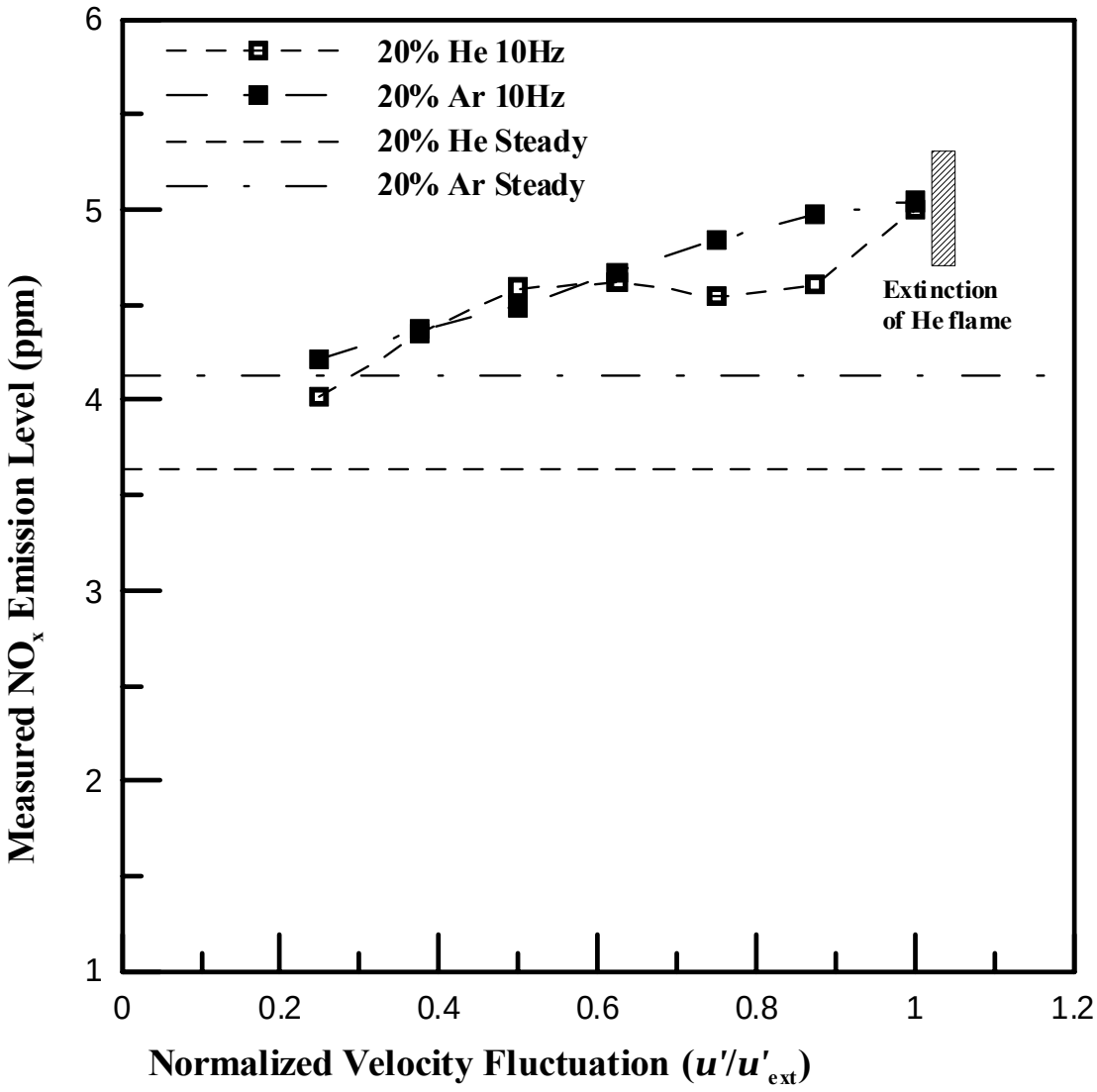

Figure 4.17: NO_x level vs u'/u'_{ext} of 20% Ar- and He-diluted flames pulsed at 10Hz.

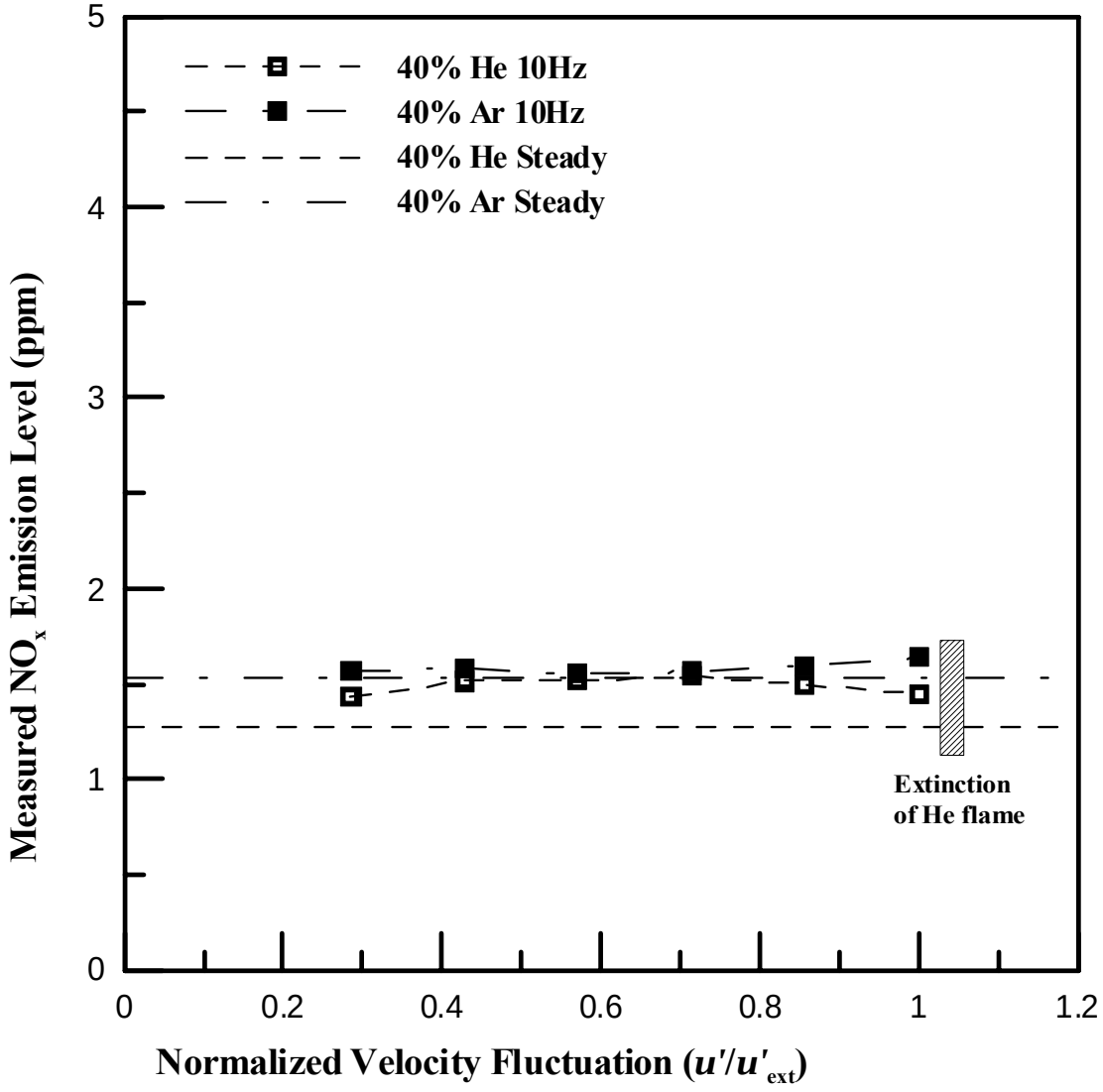

Figure 4.18: NO_x level vs u'/u'_{ext} of 40% Ar- and He-diluted flames pulsed at 10Hz.

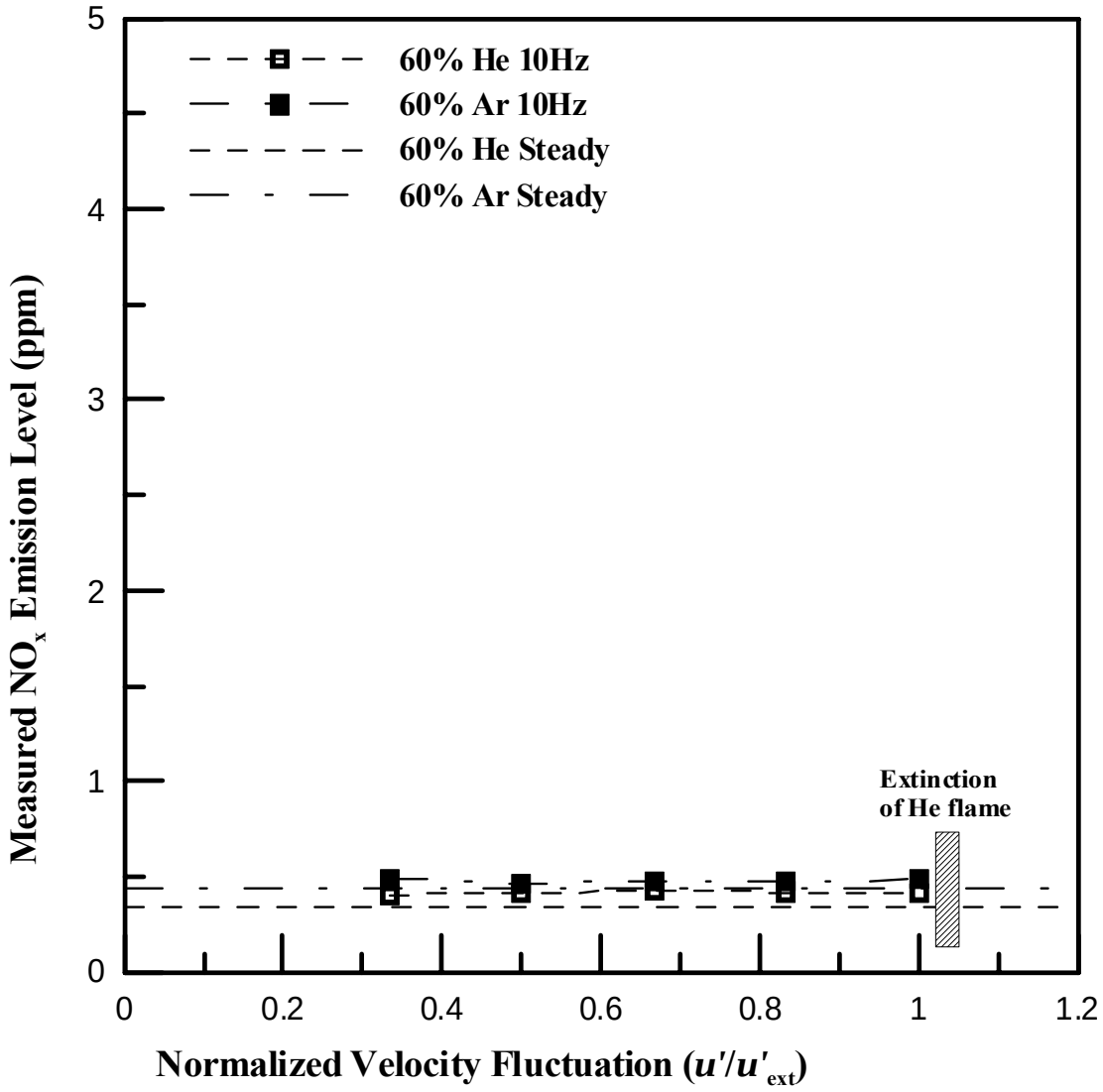

Figure 4.19: NO_x level vs u'/u'_{ext} of 60% Ar- and He-diluted flames pulsed at 10Hz.

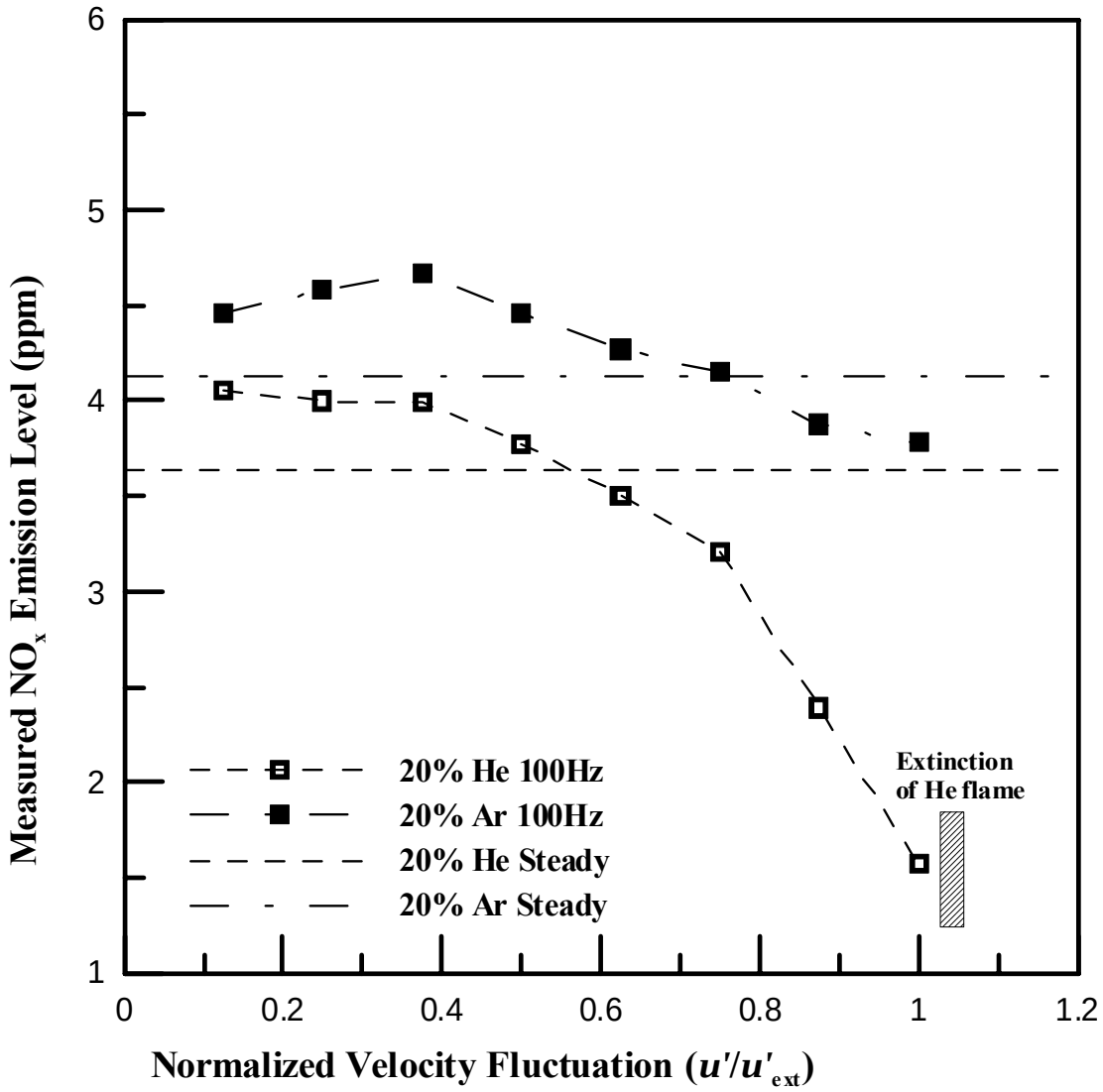

Figure 4.20: NO_x level vs u'/u'_{ext} of 20% Ar- and He-diluted flames pulsed at 100Hz.

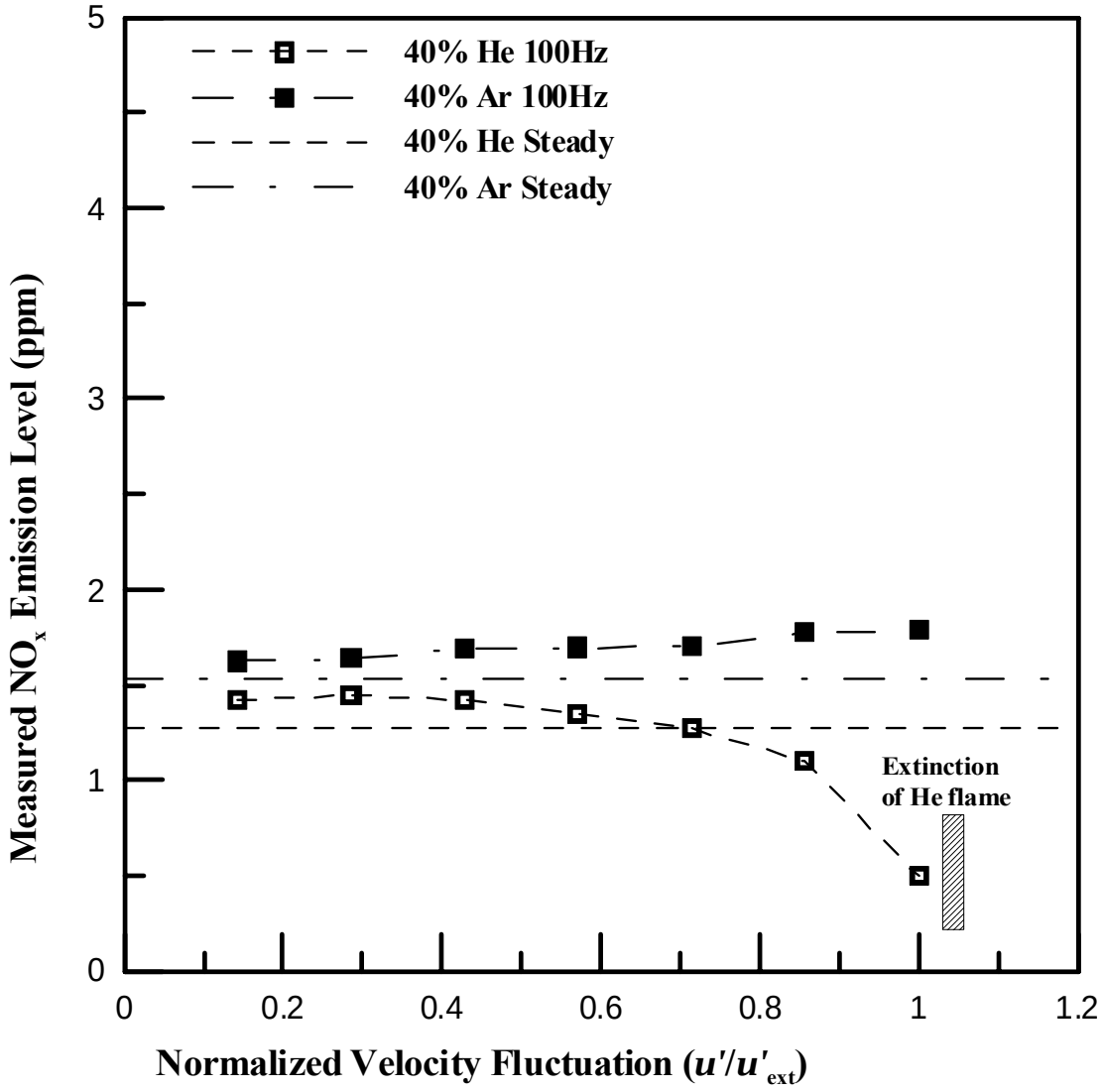

Figure 4.21: NO_x level vs u'/u'_{ext} of 40% Ar- and He-diluted flames pulsed at 100Hz.

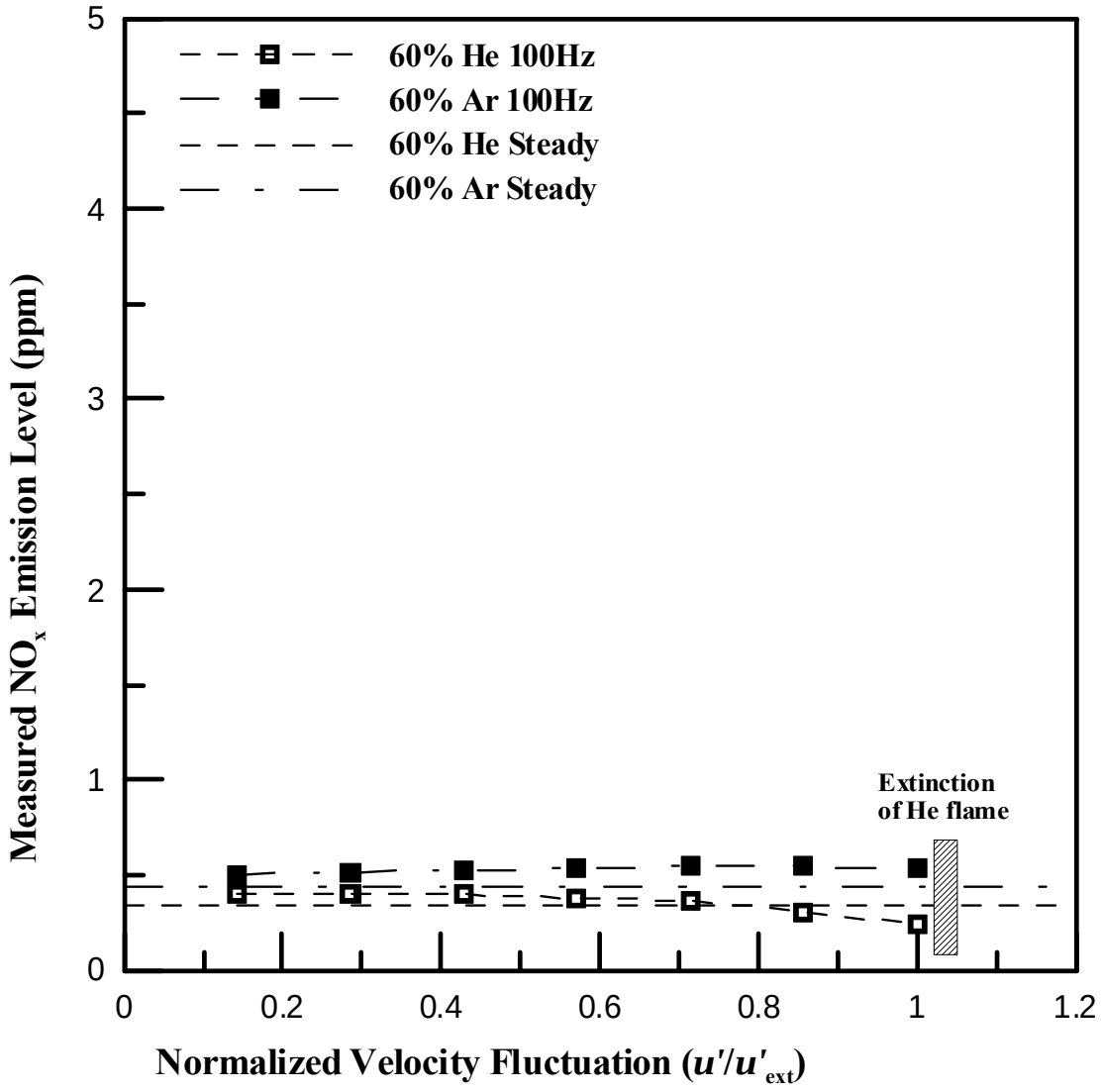

Figure 4.22: NO_x level vs u'/u'_{ext} of 60% Ar- and He-diluted flames pulsed at 100Hz.

Table 4.8). This observation implies that there is obviously an unsteady effect which contributes to dramatic temperature drop during the acoustic pulsation and is likely to dominate Le_f effect at that point as the velocity fluctuation increases and becomes maximized to quench the flame.

In Chaos (2003), it was mentioned that Ar- and He-diluted flames at low frequency (10Hz), have structures of flame zones similar to the steady Ar- and He-diluted flames and the flames have relatively thicker reaction zone (called the flame thickness) than those of the Ar- and He-diluted flames at high frequency (100Hz). Contrary to the structure of the low frequency, at the high frequency, it was found that a great amount of curvature was observed through PLIF measurement. Chaos (2003) further reported that regardless of the values of Le_f, He-diluted flames always produce a higher maximum temperature at some point during the sinusoidal cycle of pulsation than Ar-diluted flames for the same dilution level, the same pulsing frequency (10 or 100Hz) and the same amplitude (see Table 3.3 in Chaos, 2003). However, even if He-diluted flames exhibit the higher maximum temperature during the cycle, it is not necessary that they will yield more NO_x emission than Ar-diluted flames. During the sinusoidal cycle, after the flame is "pushed up" at a phase angle φ, ranging from 0° to 90°, it is possible to consider that the amount of H_2 flux into the flame increases and, consequently, more mass of the fuel burns intensively. With high amplitudes of his study, when the angle exceeds 90° (i.e. flame is "pulled down"), the images for OH intensity show the intermittent absence of a flame through some phases until 360°. This may be due to partial extinction of the flame which is likely to play an important role in an effort to understand NO_x formation

between the flames with the two diluents.

For the sake of understanding the unsteady effect of pulsation on NO_x emission trend, it is necessary to introduce the plots of the temperature data based upon the phase angles in Chaos (2003) for the flames pulsed at 10 and 100Hz (no data available for 5 and 50Hz). Figures 4.23 through 4.28 show how the maximum flame temperatures throughout Ar- and He-diluted flames fluctuate differently during the cycle. Prior to the discussion with the data, Chaos (2003) notes that "high" amplitude (a speaker voltage and not velocity fluctuation) means the value close to flame extinction limit of all the He-diluted flames while "low" amplitude corresponds a half value of high amplitude.

For the 40% dilution cases of Ar- and He-diluted flames, in Figure 4.25, it can be seen that regardless of the low or high amplitudes (i.e. speaker strength, Chaos, 2003), the maximum flame temperature always occurs when φ varies from 0° to 90° (i.e. during the "pushed up" phase) for Ar- and He-diluted flames. However, the sinusoidal behavior of the temperature values at all the phase angles for He-diluted flame show relatively wider range of temperature oscillation than for Ar-diluted flame as the phase angle increases until one cycle is completed. For 40% Ar dilution case at 10Hz, Chaos (2003) notes that the maximum temperatures along the phase angle do not deviate much from the temperature line of the steady state of Ar-diluted flame presented in Figure 4.25. With this consideration, the trend of NO_x level in the 40% dilution case in Figure 4.18 shows an agreement with the plot of maximum temperature along the phase angles. With the same values of Le_f(=1.012) for the 40% dilution of H_2-Ar and H_2-He flames at $V/V_{ext} = u'/u'_{ext} \approx 0.5$, the NO_x emission levels of He- and Ar-diluted flames become relatively

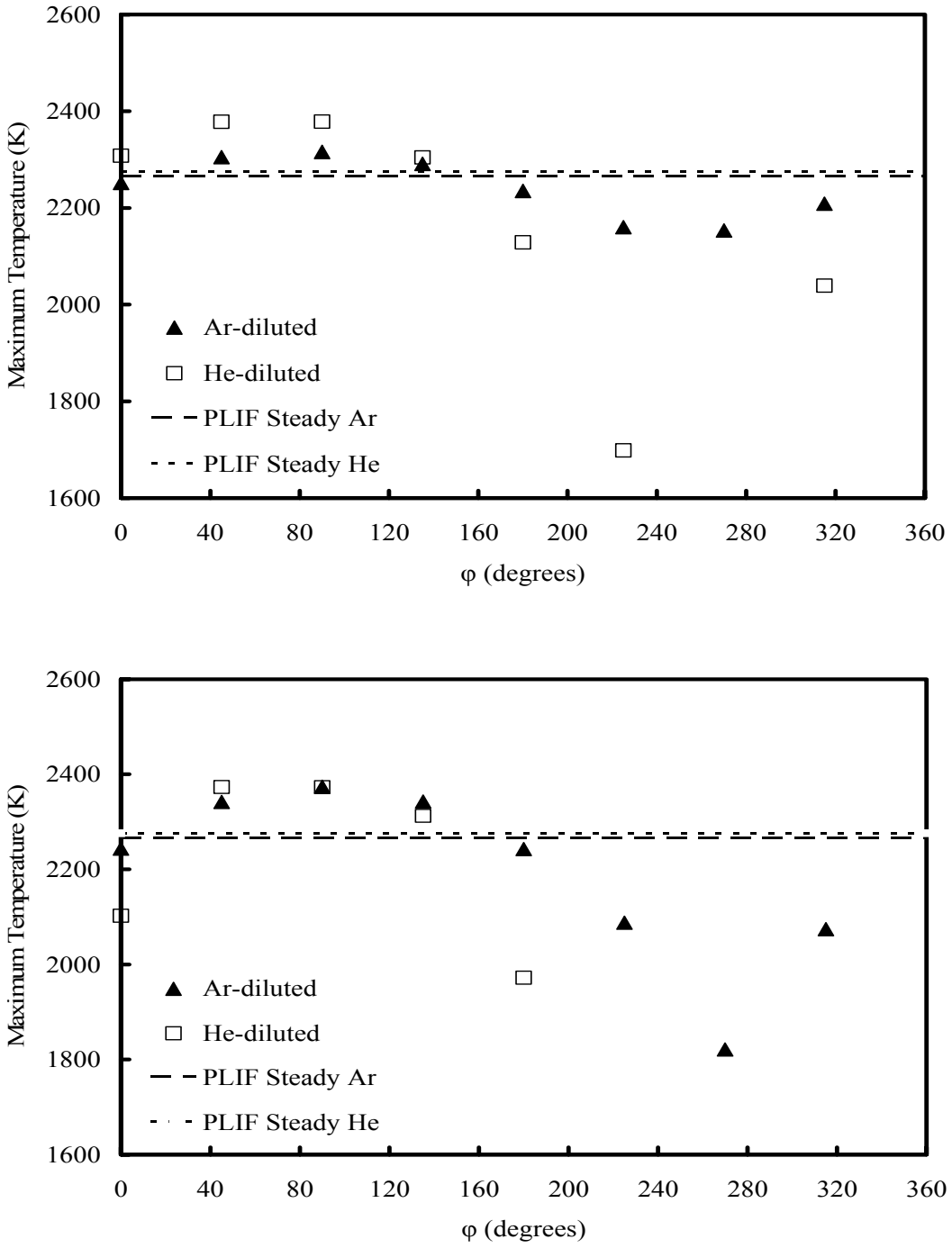

Figure 4.23: Maximum temperature for 20% fuel dilution at 10Hz, top and bottom plots are for low and high amplitudes ($u'/ u'_{ext} \approx 0.5$ and ≈ 1, respectively) from Chaos (2003).

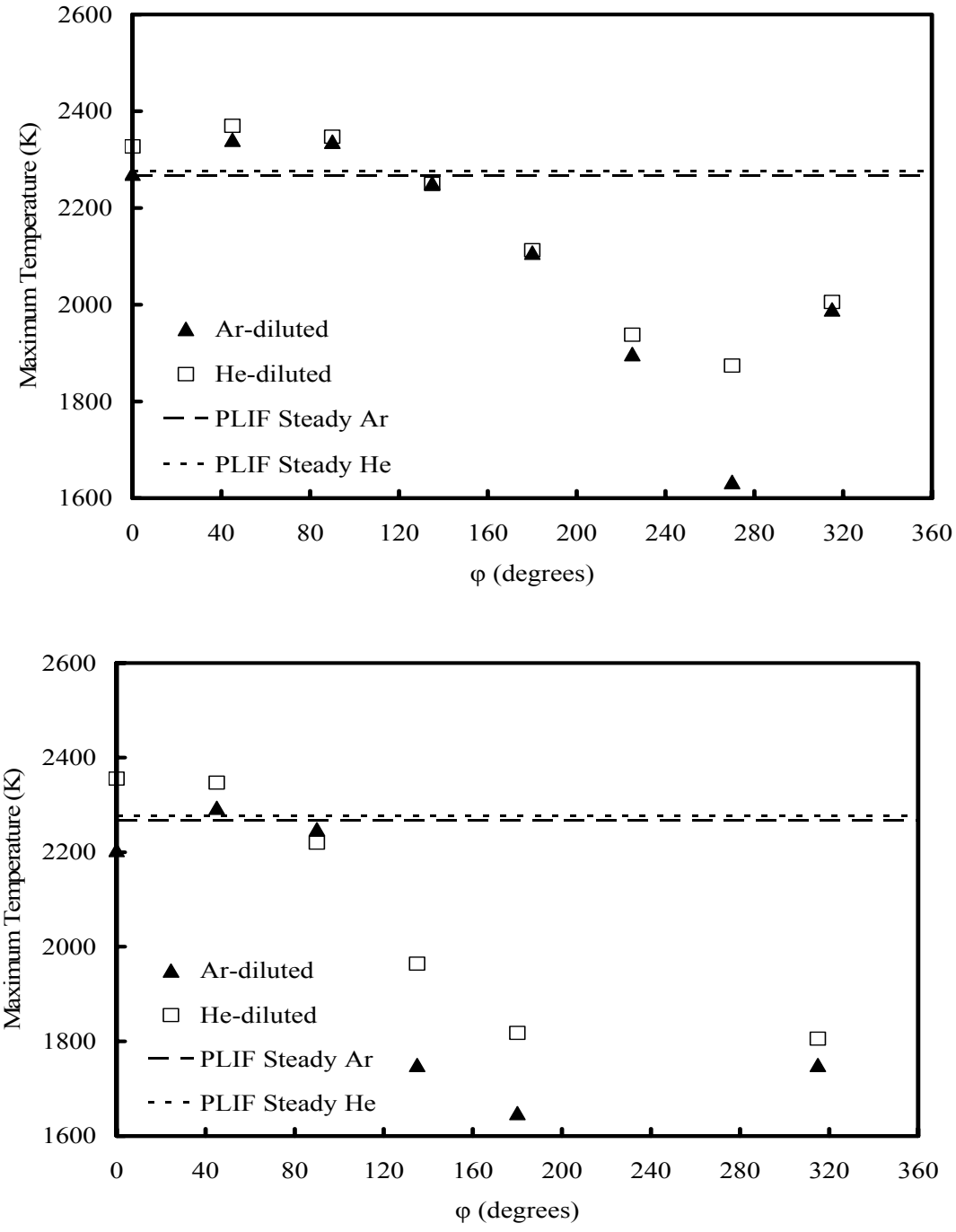

Figure 4.24: Maximum temperature for 20% fuel dilution at 100Hz, top and bottom plots are for low and high amplitudes ($u'/u'_{ext} \approx 0.5$ and ≈ 1, respectively) from Chaos (2003).

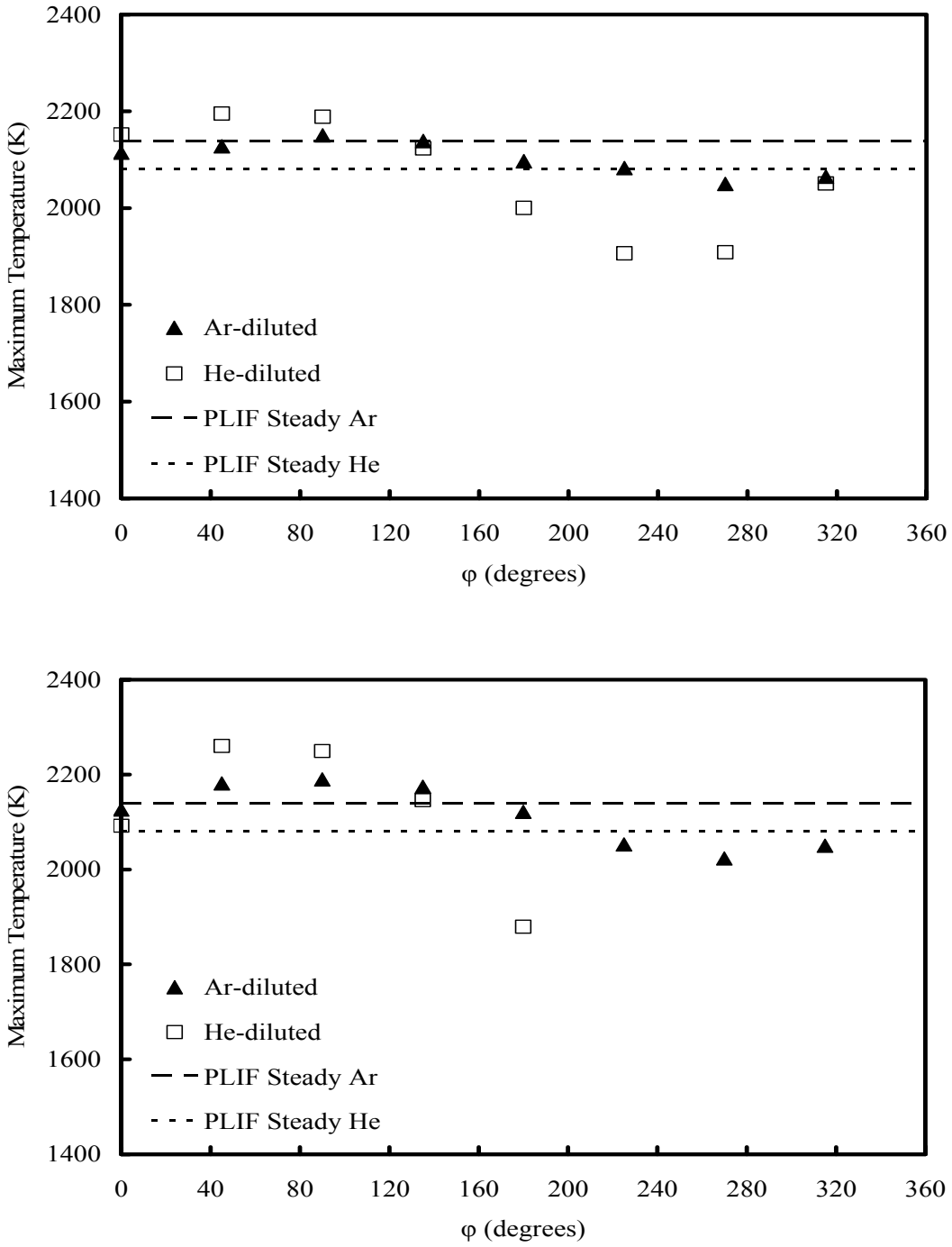

Figure 4.25: Maximum temperature for 40% fuel dilution at 10Hz, top and bottom plots are for low and high amplitudes ($u'/u'_{ext} \approx 0.5$ and ≈ 1, respectively) from Chaos (2003).

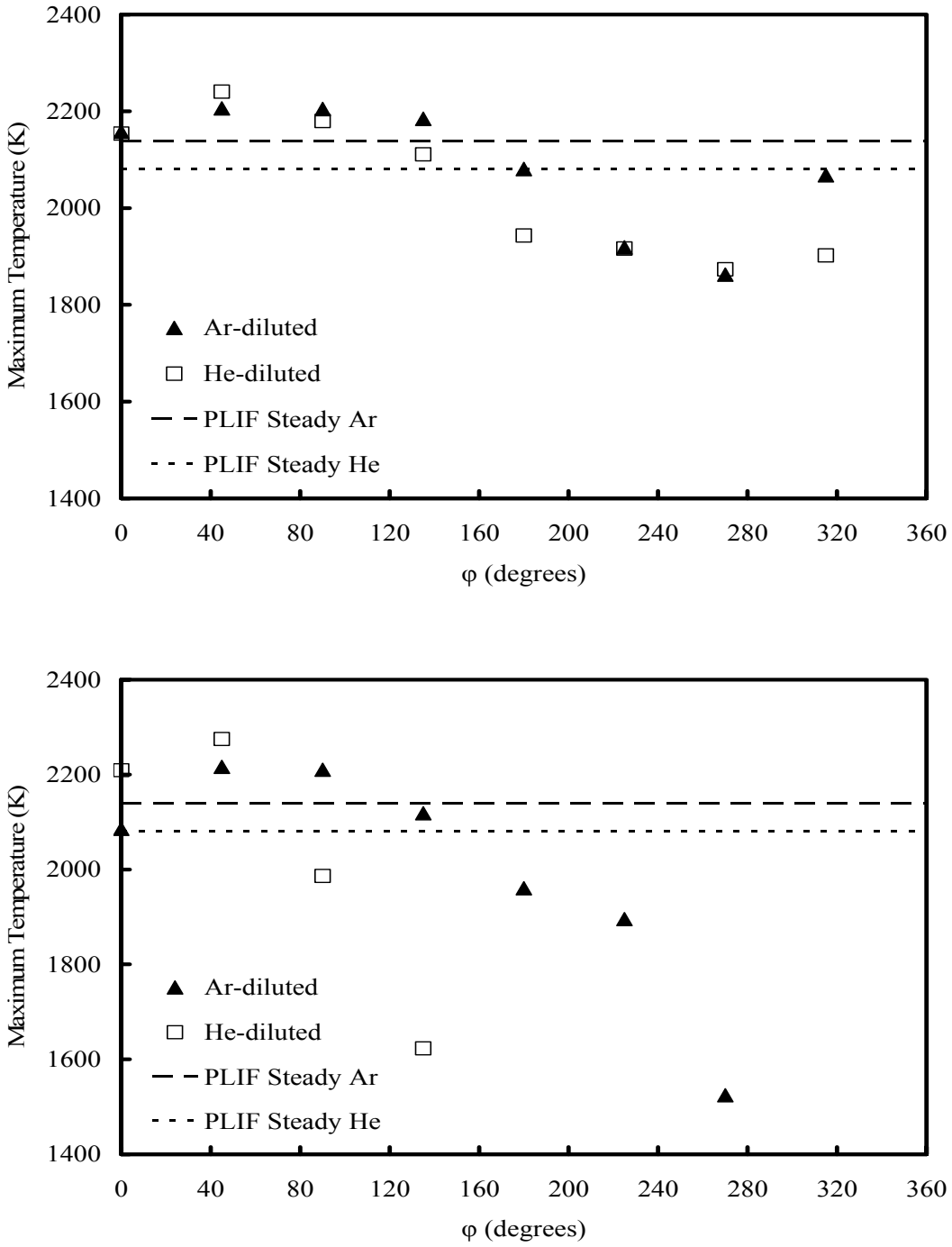

Figure 4.26: Maximum temperature for 40% fuel dilution at 100Hz, top and bottom plots are for low and high amplitudes ($u'/ u'_{ext} \approx 0.5$ and ≈ 1, respectively) from Chaos (2003).

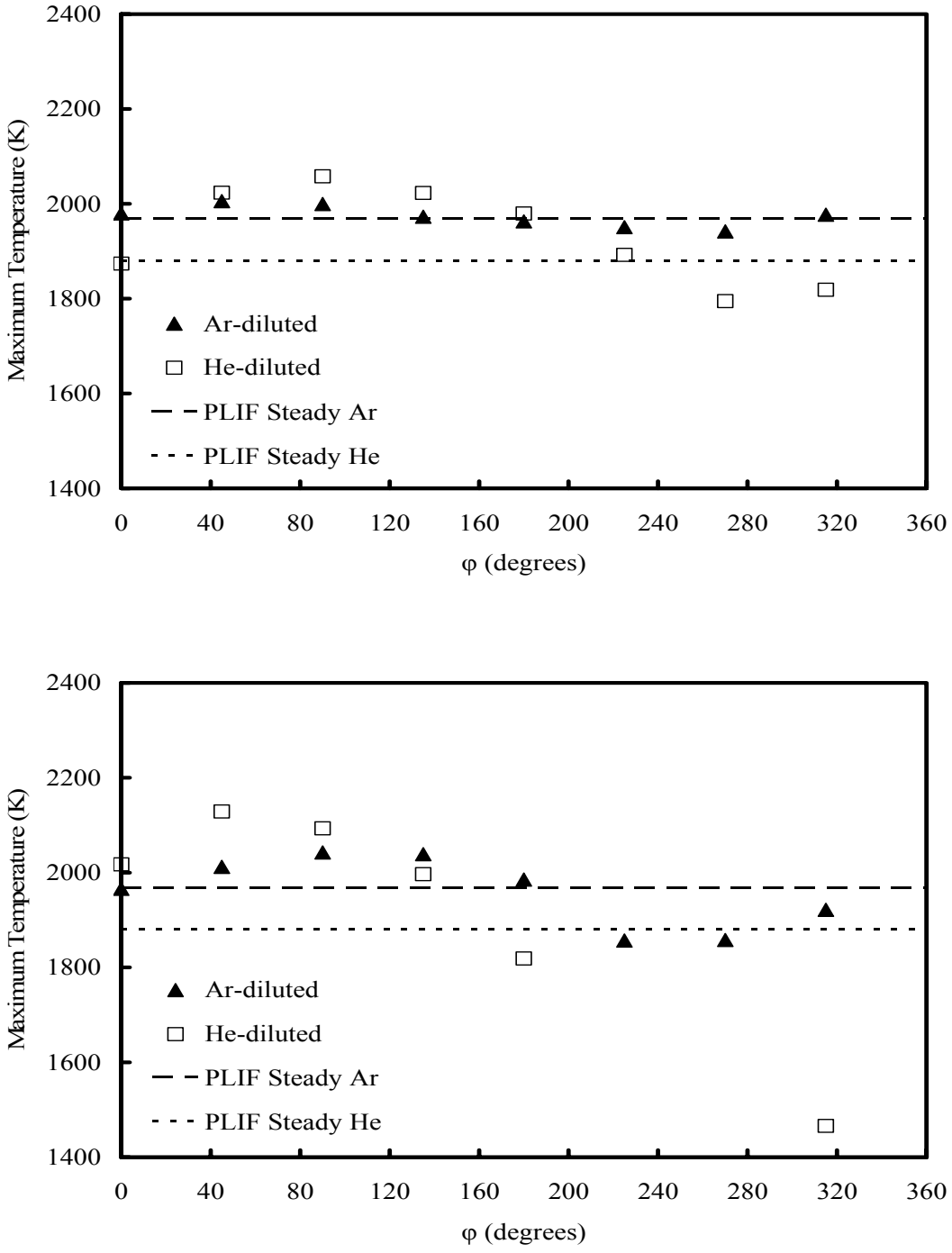

Figure 4.27: Maximum temperature for 60% fuel dilution at 10Hz, top and bottom plots are for low and high amplitudes ($u'/u'_{ext} \approx 0.5$ and ≈ 1, respectively) from Chaos (2003).

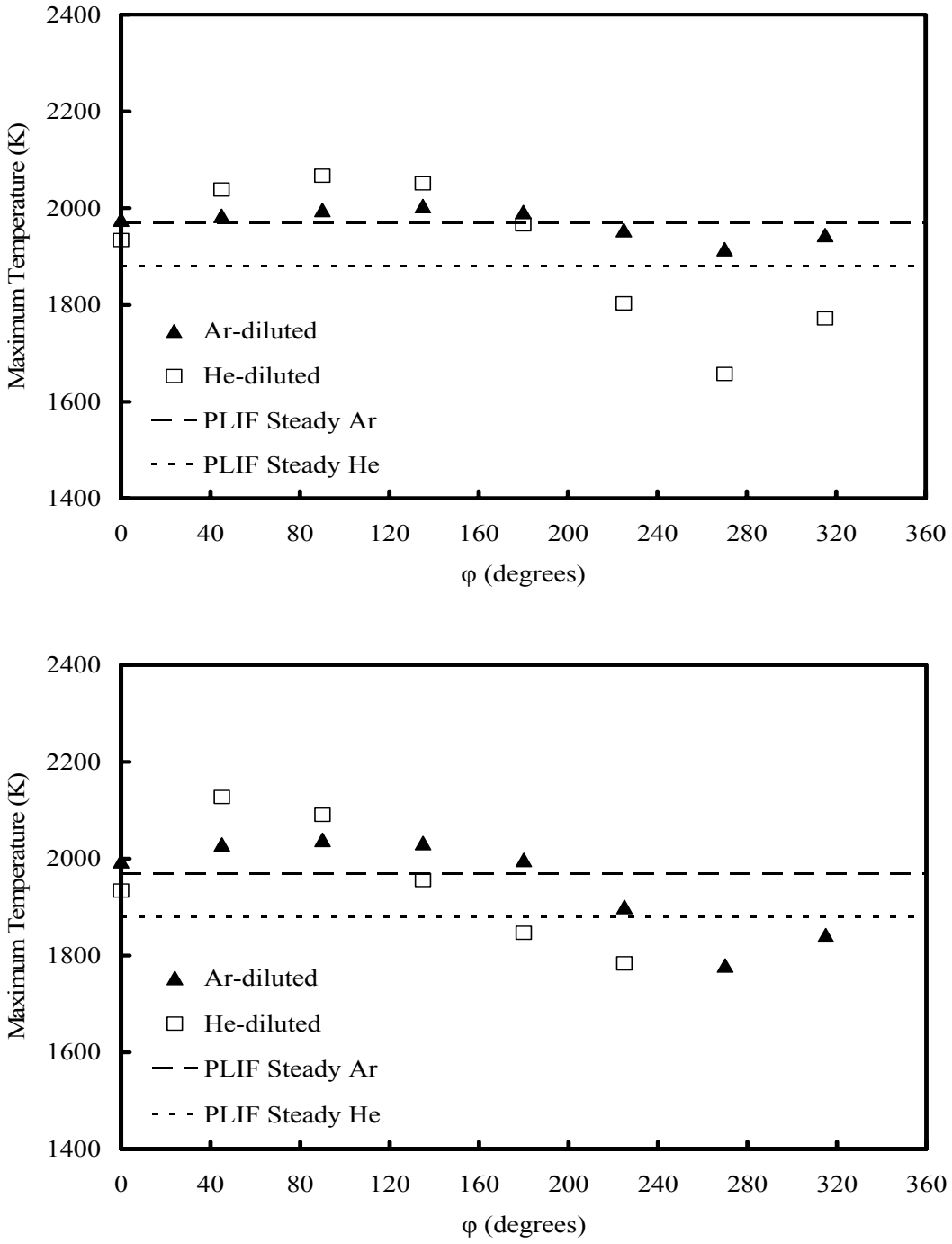

Figure 4.28: Maximum temperature for 60% fuel dilution at 100Hz, top and bottom plots are for low and high amplitudes ($u'/ u'_{ext} \approx 0.5$ and ≈ 1, respectively) from Chaos (2003).

converged. However, as the u'/u'_{ext} further increases, NO_x emission levels of the Ar- and He-diluted flames diverge. As mentioned earlier, this is primarily due to the fact that after "pushed up" the region, the He-diluted flame shows dramatic temperature drop during φ varying from 135° to 315° (i.e. "pulled down" region). Moreover, in Figure 4.25, the four temperature data for φ ranging from 225° to 315° are below 1,400K where flame partial extinction may occur. This temperature drop becomes prominent as the amplitude of velocity fluctuation increases, and this drastic temperature drop may not be compensated by the superiority of the maximum flame temperatures of He-diluted flames observed at the "pushed up" region for both the low and high amplitudes in Figure 4.25. In other words, the discussion above, the difference of NO_x levels at the smallest value of u'/u'_{ext} for the 40% Ar- and He-diluted unsteady flames is similar to the difference of the steady state where Ar-diluted flame has a larger NO_x level and a maximum flame temperature. However, as the amplitude of velocity fluctuation increases, the burning of H_2-He diluted flame becomes intensive due to its relatively more enhanced H_2 mass flux with He dilution than with Ar dilution by acoustic pulsation. Therefore, as the amplitude of velocity fluctuation increases from the smallest value (=0.286) of u'/u'_{ext} to $u'/u'_{ext} \approx 0.5$, a larger amount of reactants for H_2-He mixture should flow into the reaction zone. As the reaction zone is expanded by the speaker pulsation, more intensive burning is expected. As a result, the maximum temperature by intensive burning during the cycle should increase which should cause more NO_x formation close to that of Ar-diluted flame (see the top plot in Figure 4.25 with Figure 4.18). However, at $u'/u'_{ext} \approx$ unity, it can be presumed that the increased amount of reactants is excessively sufficient and therefore,

the flame residence time may become significantly shorter than the time required for a chemical reaction. As a consequence, Damkohler number (defined as the ratio of mixing time to chemical reaction time) decreases in order to cause a local flame extinction of the 40% He-diluted flame.

In the case of 60% dilution, it is believed that the Le_f effect (for Ar 0.718 and for He 1.035) coupled with the unsteady effect should be evident in the maximum flame temperature reduction. Although not obvious, orifice-shaped trend (i.e. converging and diverging with the increase of velocity fluctuation) of NO_x emission levels for 40% Ar- and He-diluted flames for 10Hz shown in Figure 4.18 is also present in the Figure 4.19 for 60% Ar- and He-diluted flames for 10Hz. As u'/u'_{ext} increases and reaches around 0.5, the NO_x level for the unsteady 60% Ar- and He-diluted flames shows trend like slight convergence. In Figure 4.27, the top plot shows that all the temperatures for both the 60% Ar and He flames at the low amplitude ($u'/u'_{ext} \approx 0.6$) for 10Hz become relatively closer as φ increases and the corresponding NO_x levels for Ar- and He-diluted flames differ by 0.05ppm (0.47ppm for Ar and 0.42ppm for He). Nevertheless, the values of NO_x levels for the two flames at $u'/u'_{ext} \approx$ unity become slightly higher (0.49ppm for Ar and 0.41ppm for He). This is possibly due to the absence (partial extinction) of a flame at the range of φ from 225° to 270° according to OH images of Chaos (2003). In addition, this may be directly related to reduction of NO_x formation owing to the integrated effect of NO_x emission over the entire flame zone. Contrary to the observations in the case of He-diluted flame, the partial extinction was not observed in the case of 60% Ar-diluted flame for the same degree of amplitude at the same angles (Refer to the OH image of 60%

dilution flame at 10Hz in Chaos, 2003).

It was shown earlier that the Le_f effect on the 20% dilution of the steady flame is ambiguous when comparing the flames of other dilutions in the steady state. In Figure 4.23, a similar trend of the temperature drop for the 20% He-diluted flame after the "pushed up" region is shown. The NO_x level of the 20% He-diluted flame at 10Hz increases as u'/u'_{ext} increases; after $u'/u'_{ext} = 0.5$, it starts decreasing although not much. At the extinction limit where u'/u'_{ext} = unity, the NO_x level increases and becomes close to that of the 20% Ar-diluted flame (5.04ppm for Ar and 5.00ppm for He). This tendency (double crossing) is never seen in the other NO_x plots of this study. As the intensity of velocity fluctuation increases, at the region slightly above the $u'/u'_{ext} \geq 0.5$, the NO_x levels for both the 20% Ar- and He-diluted flames for 10Hz have relatively close values (4.58ppm vs 4.48ppm at $u'/u'_{ext} = 0.500$ and 4.61ppm vs 4.66ppm at $u'/u'_{ext} = 0.625$ for He and Ar, respectively). The drop of the maximum temperatures between the range of φ from 180° to 315° (i.e. the intermittent flame extinction) may reduce the overall flame temperature profile of the 20% He-diluted flame for 10Hz. However, the OH images of Chaos (2003) indicate that, for 10Hz, the flame zone volume of the 20% He-diluted flame by speaker pulsation is larger and wider than that of the 20% Ar-diluted flame. This would possibly offset the temperature loss caused by the drop of the maximum flame temperature presented in the top plot of Figure 4.23. This can be attributed to the close values of NO_x emission levels around $u'/u'_{ext} \approx 0.5$. Furthermore, the OH image of Chaos (2003) reveals that the intensive burning in the thickened reaction zone due to the increased incoming fuel mass flux (H_2) by the acoustic pulsation indeed exists. At u'/u'_{ext}

≈ unity, the NO_x level of the 20% He-diluted flame for 10Hz is lower than that of the Ar-diluted flame due to the temperature drop along the φ ranging from 225° to 315°.

For the 40% dilution case at 100Hz, in the top plot of Figure 4.26, the maximum flame temperatures of Ar- and He-diluted flames are close along φ from 0° to 360° However, all the values of NO_x levels of the 40% He-diluted flame for 100Hz in Figure 4.21 are lower than those of the Ar-diluted flame despite of the relative vicinity of the maximum temperatures along the increase of φ. This is to be expected when investigating the intermittent partial extinction of the He-diluted flame according to the OH image of 40% dilution case for 100Hz in Chaos (2003). The trend of the temperature drop for He-diluted flame occurs most severely in the 40% He-diluted flame case at the high amplitude where u'/u'_{ext} is nearly unity pulsed at 100Hz. In the bottom plot of Figure 4.26, the temperature drop begins from even at φ = 90° (which is never observed in the other cases) and furthermore, after 135°, there was no measured maximum temperature which can be observed above 1,400K. With regard to this result, the OH image in Chaos (2003) corresponds favorably to the observed phenomenon. The OH image in the 40% He-diluted flame shows that a rollup of the flame zone at φ = 45° is present and after which the flame zone almost vanishes until φ, 315°. For the 40% He-diluted flame at 100Hz, this rollup phenomenon may be primarily responsible for the reduction of the temperatures since it can lead to an increase of heat release which is ensued by a local flame extinction due to a large strain and curvature induced by the vortex of a fuel stream. As a result, the value of the NO_x level according to the maximum flame temperature for the 40% He-diluted flame severely collapses by 64.8% from the emission value

(1.42ppm) at $u'/u'_{ext} = 0.143$ to the emission value (0.50ppm) at u'/u'_{ext} = unity. Compared to 60.8% in the case of the 20% He-diluted flame at 100Hz (4.05ppm at $u'/u'_{ext} = 0.125$ and 1.57ppm at u'/u'_{ext} = unity) and 61.2% in the case of the 60% He-diluted flame at 100Hz (0.40ppm at $u'/u'_{ext} = 0.143$ and 0.24ppm at u'/u'_{ext} = unity), it is evident the effect of presence of a rollup lowers a flame temperature. In the 60% dilution case at 100Hz, the values of Le_f for the Ar- and He-diluted flames are 0.718 and 1.035 respectively. As mentioned in Section 4.2, in the 60% dilution case, the Le_f effect is present in the maximum temperature response in the steady state as well as the unsteady state during the cycle of the pulsation. In this regard, a decrease of NO_x level is attributable solely to the Le_f effect where the amplitude of velocity fluctuation is relatively low (at $u'/u'_{ext} = 0.143$) and NO_x level linearly diminishes as u'/u'_{ext} is approaching unity where the coupled effect of Le_f and flame unsteadiness dominate the flame temperature behavior. The OH images for low and high amplitudes in Chaos (2003) also support the reason of the decrease of NO_x emission level based upon the evident extinction of the presence of the 60% He-diluted flames in both the images.

Figure 4.20 notes for 20% diluted flame cases pulsed at 100Hz, the value of the NO_x level for the Ar-diluted flames slightly increases from $u'/u'_{ext} = 0.125$ to $u'/u'_{ext} = 0.375$ (4.45ppm, 4.57ppm and 4.67ppm at $u'/u'_{ext} = 0.125$, 0.250 and 0.375, respectively). On the other hand, the NO_x value of He-diluted flames remains approximately unchanged until $u'/u'_{ext} = 0.375$ (4.05ppm, 4..00ppm and 3.98ppm at $u'/u'_{ext} = 0.125$, 0.250 and 0.375, respectively). It is interesting that although both the coupled or the sole effect of Le_f and/or unsteadiness play a role in varying a maximum flame temperature during a

sinusoidal cycle for the other dilution cases mentioned earlier, in the case of the 20% dilution at 100Hz around the low velocity fluctuation (i.e. $u'/u'_{ext} \leq 0.5$), the effect of Le_f is relatively ambiguous. Not only the effect of Le_f, but also the effect of flame unsteadiness on the NO_x emission seems to have almost the same contribution in varying NO_x emission levels when considering the differences of NO_x values in the steady case and the unsteady case from $u'/u'_{ext} = 0.143$ to 0.375 in Figure 4.20. The difference of NO_x levels for the 20% Ar and He flames at 100Hz from $u'/u'_{ext} = 0.143$ to 0.500 is not precisely parallel but rather slightly diverges beyond the point at $u'/u'_{ext} = 0.5$. However, assuming the difference of NO_x levels between the 20% Ar- and He-diluted flames for 100Hz to be approximately parallel, it can be implied that only diluent effect alone (different thermodynamic properties using two different diluents) is attributable to the difference of NO_x levels of Ar and He flames within the region. This tendency was also observed in the case of the steady 20% dilution in Section 4.2 due to the close maximum temperatures (2,174K for the 20% He and 2,206K for the 20% Ar) caused by present but less pronounced effect of Le_f. In Figure 4.20, as u'/u'_{ext} reaches nearly unity, the NO_x level for the 20% He-diluted flame diminishes drastically compared to that of the 20% Ar-diluted flame. Near the flame extinction limit where $u'/u'_{ext} \approx$ unity, the unsteadiness effect of the 20% He-diluted flame for 100Hz becomes more pronounced possibly due to the preferable diffusivity of H_2 in He than in Ar which leads to surplus of reactants relevant to flame extinction.

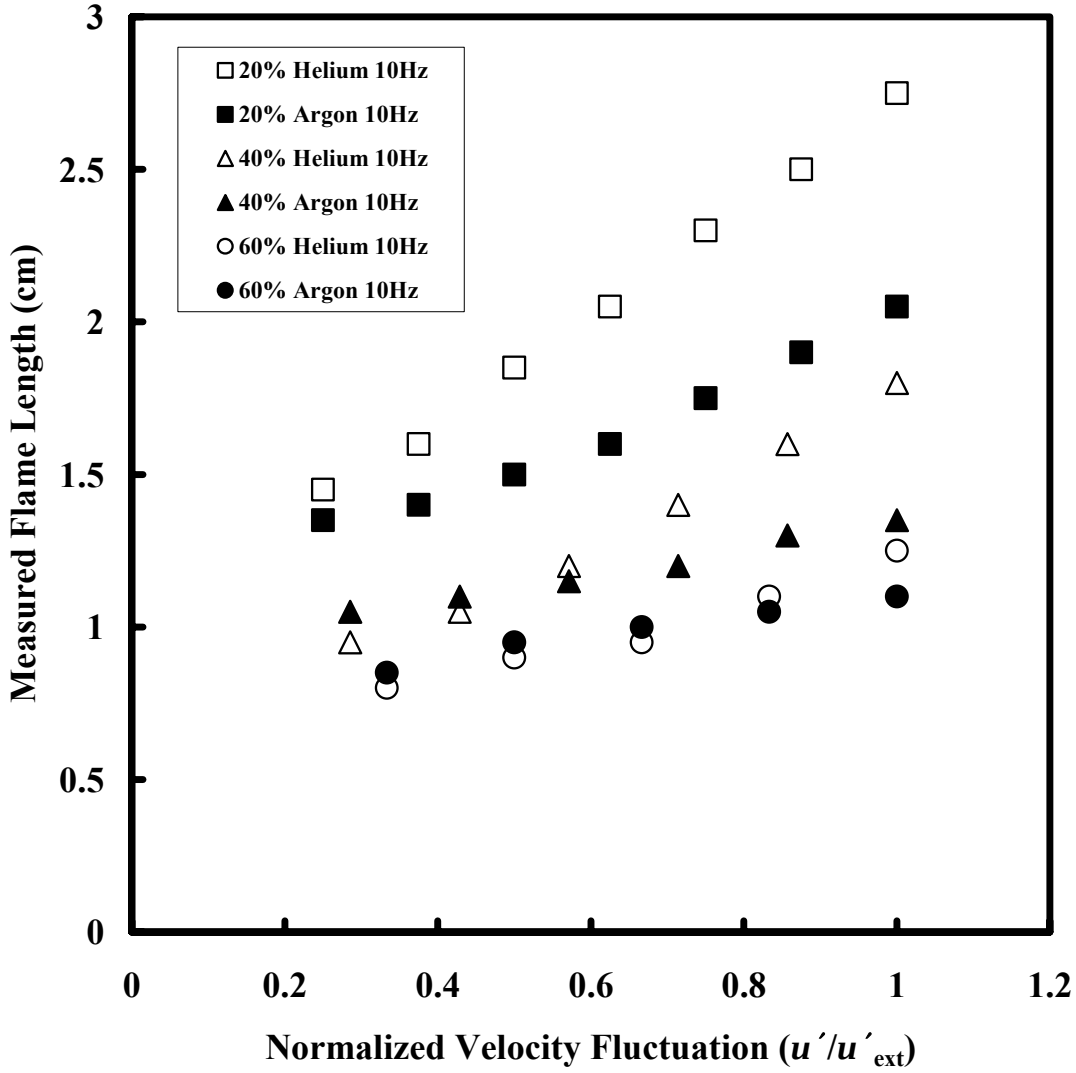

Figure 4.29: Flame length vs u'/u'_{ext} of 20%, 40% and 60% Ar- and He-diluted flames pulsed at 10Hz.

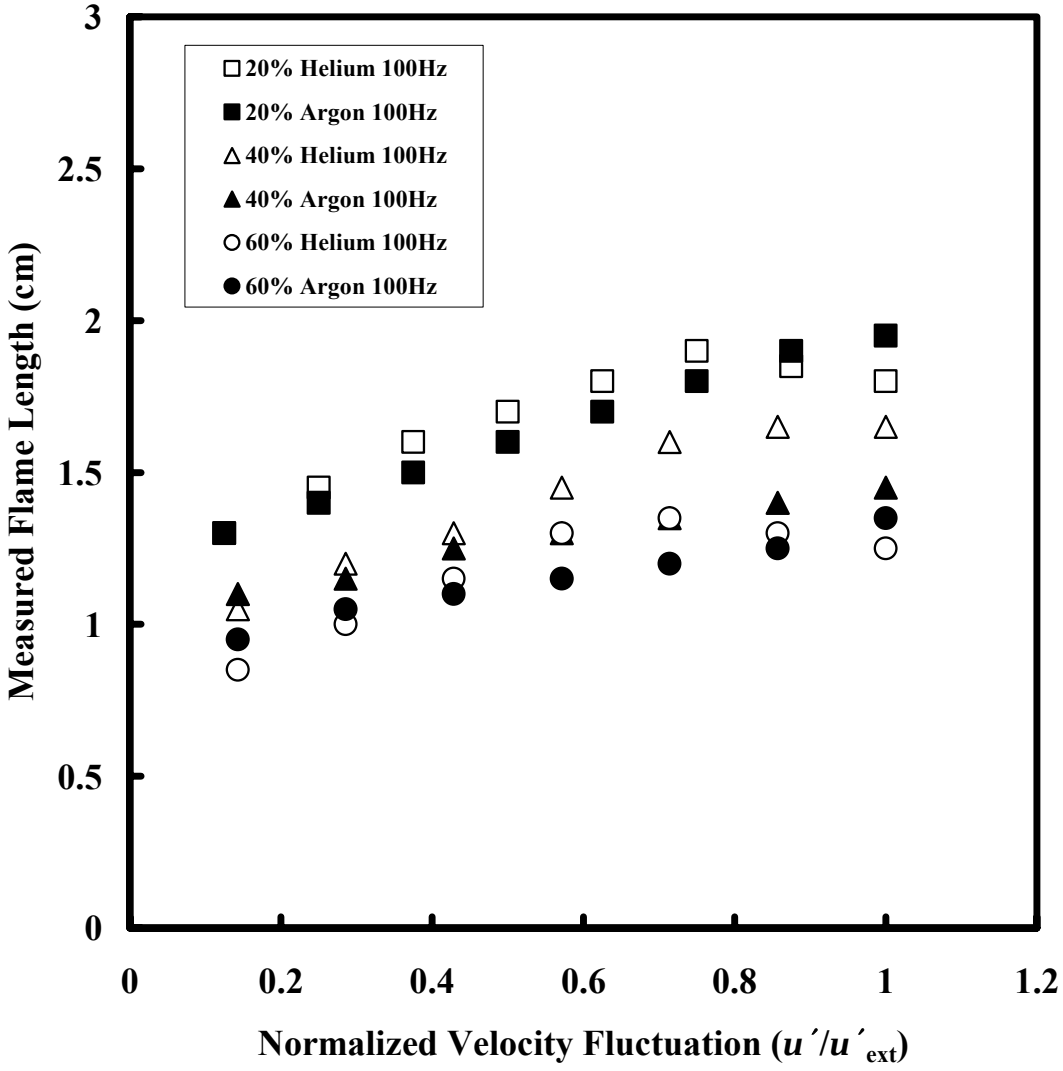

Figure 4.30: Flame length vs u'/u'_{ext} of 20%, 40% and 60% Ar- and He-diluted flames pulsed at 100Hz.

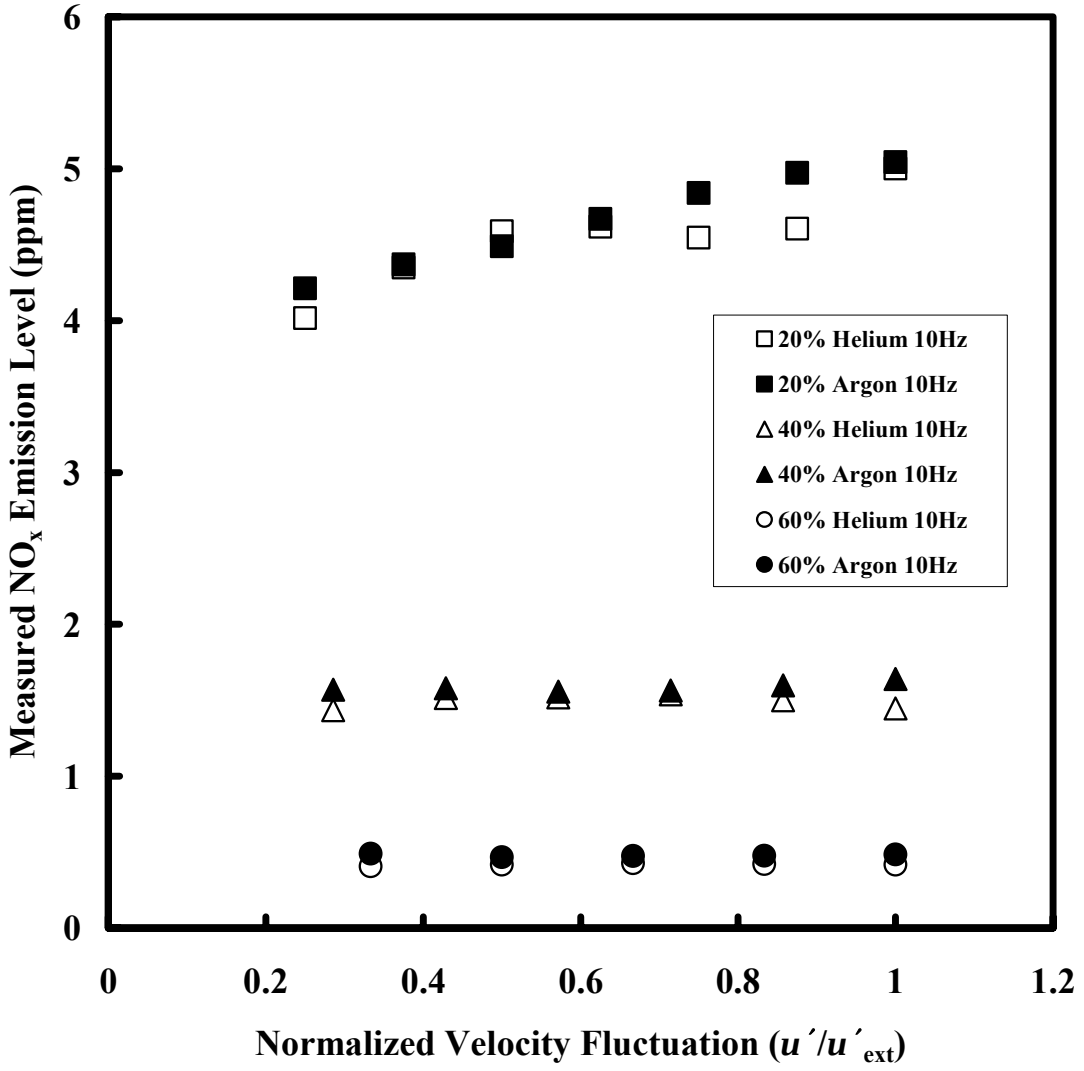

Figure 4.31: NO_x level vs u'/u'_{ext} of 20%, 40% and 60% Ar- and He-diluted flames pulsed at 10Hz.

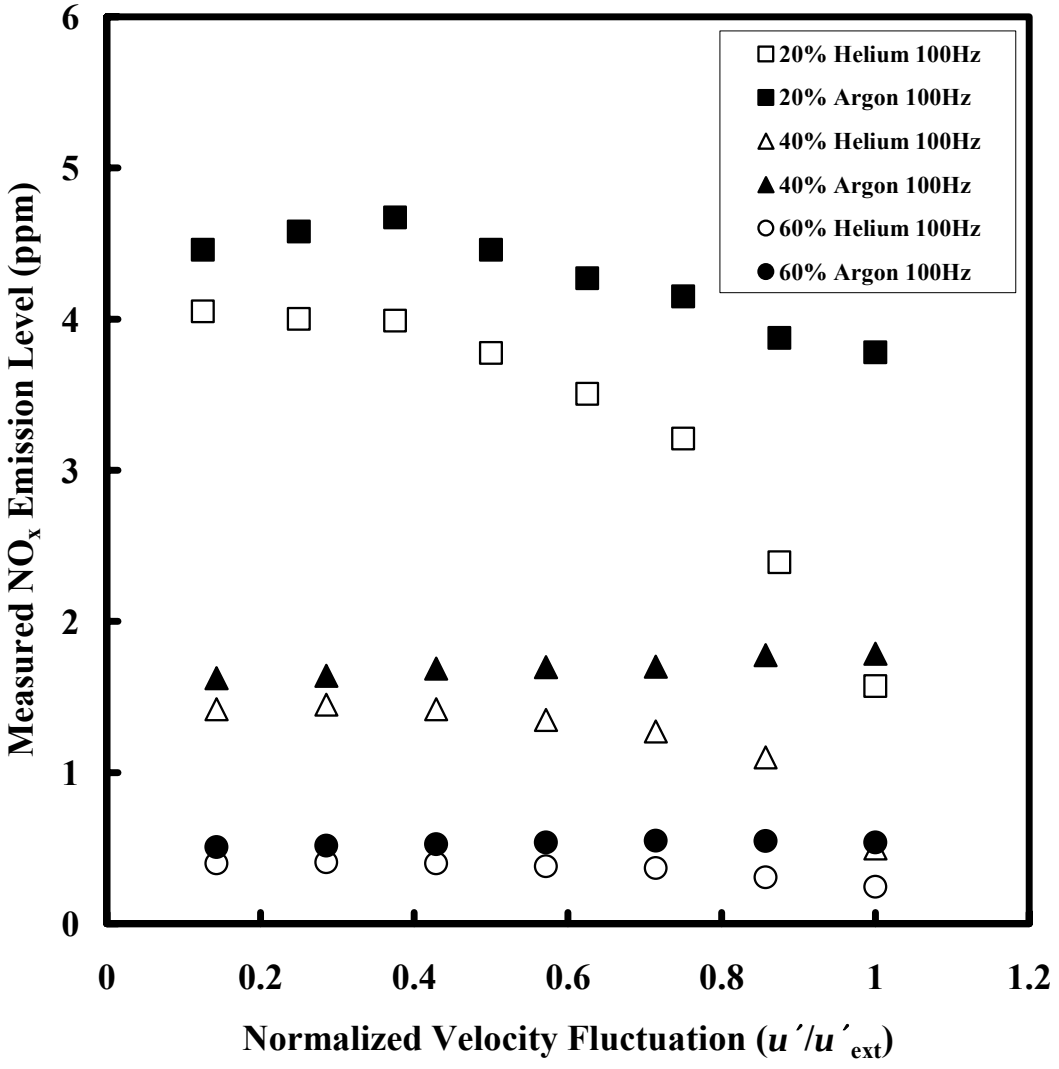

Figure 4.32: NO_x level vs u'/u'_{ext} of 20%, 40% and 60% Ar- and He-diluted flames pulsed at 100Hz.

CHAPTER 5: CONCLUSION

Hydrogen is the lightest and most abundant gas in the universe. To reduce environmental pollution produced by hydrocarbon fuels, hydrogen is preferred as the main energy source in the future. However, although many researchers have investigated the complexity and behavior of a diffusion flame, they still remain difficult to be completely understood. In an effort to reduce NO_x emission effectively, the hydrogen flames with two different diluents (Ar and He) have been investigated in the steady and unsteady flames and a summary of the results is presented:

A. In the steady flame, flame lengths of the Ar-diluted flames for all the dilution levels (20%, 40% and 60%) are larger than those of the He-diluted flames which do not exhibit Le_f effect on L_f previously discussed in Chen *et. al*. (1997).

B. Comparison of the maximum flame temperatures among all the studies presented in Table 4.1 show good qualitative agreement for the steady 40% and 60% diluted flames. However, for the 20% dilution in the steady case, Le_f effect may be present. Nevertheless, it appears to be seemingly suppressed by other effects such as diluent effect and, partly, thermodynamic properties.

C. In the NO_x emission levels in the steady state flame, the trend of NO_x formation corresponds to that of the maximum flame temperatures for all the degrees of dilutions levels (i.e. higher temperature vs higher NO_x level). In the velocity range studied, it was found that NO_x levels increase proportionally to the increase of the fuel jet velocity due to the increase of flame residence time, including buoyancy acceleration.

D. In the unsteady flames, the flame lengths for acoustically pulsed Ar- and He-diluted flames for all dilution levels showed a linear increase until the flame extinction limit for the low frequency (10Hz). However, for the high frequency (100Hz), this was not observed for the He-diluted flame for all dilution levels. This can be due to the different density and molecular weight of the Ar- and He-diluted flames against the speaker pulsation.

E. In an effort to reduce NO_x emission, this study suggests that it is more effective to utilize high frequency pulsation (100Hz) rather than low frequency (10Hz). Finally, it is recommended to introduce He diluent instead of Ar diluent in a fuel stream with the degrees of the dilution levels studied to reduce a flame temperature more effectively in both steady and unsteady (100Hz) cases.

REFERENCES

Bradley, D. and Matthews, K. J. "Measurement of High Gas Temperatures with Fine Wire Thermocouples." *Journal of Mechanical Engineering* 10 (1968): 299-305.

Burke, S. P., and Schumann, T. F. W. "Diffusion Flames." *Industrial and Engineering Chemistry* 20 (1928): 998-1004.

Chaos, M. "A Planar Laser-Induced Fluorescence Study on the Effects of Unsteadiness and Fuel Lewis Number in Hydrogen Laminar Diffusion Flames." Dissertation. University of Central Florida at Orlando, 2003.

Chen, R.-H., and Driscoll, J. F. "Nitric Oxide Levels of Jet Diffusion Flames: Effects of Coaxial Air and Other Mixing Parameters." *Proceedings of the Twenty-Third Symposium (International) on Combustion*, Orlans, France (1990): 281-288.

Chen, R.-H., Navedo, J. E., and Chew, L. "Effect of Fuel Lewis Number on and Damköhler Number Scaling of Nitric Oxide Emission Level of Burke-Schumann Type Flames." *Combustion Science and Technology* 127 (1997): 293-318.

Chung, S. H., and Law, C. K. "Burke-Schumann Flame with Streamwise and Preferential Diffusion." *Combustion Science and Technology* 37 (1984): 21-46.

Churchill, S. W. and Bernstein, M. "A Correlating Equation for Forced Convection from Gases and Liquids to a Circular Cylinder in Crossflow." *Journal of Heat Transfer, Transactions ASME* 99 (1977): 300-306.

Dandy, D. S. *Software Tools*. 29 Jul. 2003. 20 Apr. 2003. http://navier.engr.colostate.edu/tools/diffus.html

Drake, M. C., and Blint, R. J. "Relative Importance of Nitric Oxide Formation Mechanisms in Laminar Opposed-Flow Diffusion Flames." *Combustion and Flame* 83 (1991): 185-203.

Drake, M. C., Correa, S. M., Pitz, R. W., Shyy, W., and Fenimore, C. P. "Superequilibrium and Thermal Nitric Oxide Formation in Turbulent Diffusion Flames." *Combustion and Flame* 69 (1987): 347-365.

Driscoll, J. F., Chen, R.-H., and Yoon, Y. "Nitric Oxide Levels of Turbulent Jet Diffusion Flames: Effects of Residence Time and Damköhler Number." *Combustion and Flame* 88 (1992): 37-49.

Feese, J. J., and Turns, S. R. "Nitric Oxide Emissions from Laminar Diffusion Flames: Effects of Air-Side versus Fuel-Side Diluent Addition." *Combustion and Flame* 113 (1998): 66-78.

Fenimore, C. P. "Formation of Nitric Oxide in Premixed Hydrocarbon Flames." *Proceedings of the Thirteenth Symposium (International) on Combustion*, The Combustion Institute, Pittsburgh, PA (1971): 373-379.

Gabriel, R., Navedo, J. E., and Chen, R.-H. "Effects of Fuel Lewis Number on Nitric Oxide Emission of Diluted H_2 Turbulent Jet Diffusion Flames." *Combustion and Flame* 121 (2000): 525-534.

Glassman, I. *Combustion*. 3rd ed. San Diego: Academic Press, 1996.

Glawe, G. E., and Shepard, C. E. *Some Effects of Exposure to Exhaust-Gas Streams on Emittance and Thermoelectric Power of Bare-Wire Platinum Rhodium – Platinum Thermocouples*. NACA Technical Note 3253. Washington, 1954.

Hori, M. "Experimental Study of Nitrogen Dioxide Formation in Combustion Systems." *Proceedings of the Twenty-First Symposium (International) on Combustion*, Munich, Germany (1986): 1181-1188.

Im, H. G., and Chen, J. H., and Chen, J.-Y. "Chemical Response of Methane/Air Diffusion Flames to Unsteady Strain Rate." *Combustion and Flame* 118 (1999): 204-212.

Kothawala, A. "The Effects of Transport Properties on Blow-off Velocities, Life-off Characteristics and Maximum Temperatures of Laminar Diffusion Flames." Thesis. University of Central Florida at Orlando, 2003.

Kee, R. J., Rupley F. M., Miller, J. A, Coltrin, M. E., Grcar, J. F., Meeks, E., Moffat, H. K., Lutz, A. E., Dixon-Lewis, G., Smooke, M. D., Warnatz, J., Evans, G. H., Larson, R. S., Mitchell, R. E., Petzold, L. R., Reynolds, W. C., Caracotsios, M., Stewart, W. E., Glarborg, P., Wang, C., and Adigun, O. *CHEMKIN Collection, Release 3.6*. San Diego, CA: Reaction Design, Inc.,.2000.

Law, C. K., and Chung, S. H. "Steady State Diffusion Flame Structure with Lewis Number Variations." *Combustion Science and Technology* 29 (1982): 129-145.

Lewis, G. S., Cantwell, B. J., Vandsburger, U., and Bowman, C. T. "An Investigation of the Structure of a Laminar Non-premixed Flame in an Unsteady Vortical Flow." *Proceedings of the Twenty-Second Symposium (International) on Combustion*, Seattle, Washington (1988): 515-522.

Li, S. C., and Williams, F. A. "NO_x Formation in Two-Stage Methane-Air Flames." *Combustion and Flame* 118 (1999): 399-414.

Nishioka, M., Nakagawa, S., Ishikawa, Y., and Takeno, T. "NO Emission Characteristics of Methane-Air Double Flame." *Combustion and Flame* 98 (1994): 127-138.

Roper, F. G. "The Prediction of Laminar Jet Diffusion Flame Sizes: Part I. Theoretical Model." *Combustion and Flame* 29 (1977): 219-226.

Roper, F. G., Smith, C., and Cunningham, A. C. "The Prediction of Laminar Jet Diffusion Flame Sizes: Part II. Experimental Verification." *Combustion and Flame* 29 (1977): 227-234.

Rørtveit, G. J., Hustad, J. E., Li, S.-C., and Williams, F. A. "Effects of Diluents on NO_x Formation in Hydrogen Counterflow Flames." *Combustion and Flame* 130 (2002): 48-61.

Samaniego, J.-M., Labegorre, B., Egolfopoulos, F. N., and Ditaranto, M. "Mechanism of Nitric Oxide Formation in Oxygen-Natural Gas Combustion." *Proceedings of the Twenty-Seventh Symposium (International) on Combustion*, Naples, Italy (1998): 1385-1392.

Santoro V. S., Kyritsis, D. C., Smooke, M. D., and Gomez, A. "Nitric Oxide Formation During Flame/Vortex Interaction." *Proceedings of the Combustion Institute* 29 (2002): 2227-2233.

Takeno, T., and Nishioka, M. "Species Conservation and Emission Indices for Flames Described by Similarity Solutions." *Combustion and Flame* 92 (1993): 465-468.

Turns, S. R. "Understanding NO_x Formation in Nonpremixed Flames: Experiments and Modeling." *Progress in Energy and Combustion Science* 21 (1995): 361-385.

Turns, S. R. An Introduction to Combustion. International ed. New York: McGraw Hill, Inc., 1996.